National Library of Canada

Acquisitions and Bibliographic Services Branch

395 Wellington Street
Ottawa, Ontario
K1A 0N4

Bibliothèque nationale du Canada

Direction des acquisitions et des services bibliographiques

395, rue Wellington
Ottawa (Ontario)
K1A 0N4

Your file *Votre référence*

Our file *Notre référence*

NOTICE

The quality of this microform is heavily dependent upon the quality of the original thesis submitted for microfilming. Every effort has been made to ensure the highest quality of reproduction possible.

If pages are missing, contact the university which granted the degree.

Some pages may have indistinct print especially if the original pages were typed with a poor typewriter ribbon or if the university sent us an inferior photocopy.

Reproduction in full or in part of this microform is governed by the Canadian Copyright Act, R.S.C. 1970, c. C-30, and subsequent amendments.

AVIS

La qualité de cette microforme dépend grandement de la qualité de la thèse soumise au microfilmage. Nous avons tout fait pour assurer une qualité supérieure de reproduction.

S'il manque des pages, veuillez communiquer avec l'université qui a conféré le grade.

La qualité d'impression de certaines pages peut laisser à désirer, surtout si les pages originales ont été dactylographiées à l'aide d'un ruban usé ou si l'université nous a fait parvenir une photocopie de qualité inférieure.

La reproduction, même partielle, de cette microforme est soumise à la Loi canadienne sur le droit d'auteur, SRC 1970, c. C-30, et ses amendements subséquents.

Canada

A Brownian Dynamics Algorithm for the Simulation of Polymers in Confined Media

by

Grant Ian Nixon

Thesis presented to the School of Graduate Studies of the
University of Ottawa
in fulfilment of the thesis requirement for the degree of

Master of Science
in Physics

Department of Physics
Faculty of Science
University of Ottawa

ISBN 0-612-07893-0

Canada

UNIVERSITÉ D'OTTAWA
UNIVERSITY OF OTTAWA

Abstract

The techniques of electrophoresis have undergone rapid developments in recent years. The problem of predicting and explaining results of electrophoretic experiments requires a well designed dynamical model that reproduces the proper dynamics under well-understood conditions.

The challenge is to design a model which can predict complex dynamics in a variety of situations of interest and yet, be efficient enough to run on common workstations. We believe that we have been successful in achieving these goals. Our Brownian Dynamics model is sufficiently general for the investigation of a wide variety of problems (as we will demonstrate), moreover, it implements a simulation innovation, a dynamically self-regulating time increment which varies in accordance with the stresses in the system. This permits for reasonably long simulation times with good averaging statistics.

After benchmarking the model with the well understood Rouse regime in isotropic and confined media, the model was applied to two case studies of particular interest: (i) electrophoretic collisions and stacking (chain pinning), and (ii), the onset of the entropic trapping regimes for low fields.

We have found that, as far as simple isolated collisions are concerned, our model predicts a widening of electrophoretic molecular bands with an accompanying loss in spatial resolution. The onset of entropic regimes for low fields is demonstratedly counter-productive due to the wide variance of trapping times. Both these results are in accord with recent experimental observations. A more complete study is planned for a supercomputer to elaborate on these findings as well as to investigate kink-formations in pulsed-field gel electrophoresis (PFGE).

Acknowledgements

I would like to take this opportunity to express my sincere gratitude to my research supervisor, Dr. Gary W. Slater, for his continued support guidance during the entire course of this research. His guidance and example have always been, for me, a great source of inspiration.

May I also take this opportunity to thank all without whom university life would just not be same: Dr. Cyril Benson, Bei Wah ("The Joker") Chan, Hélène Lacasse, and Roger Chagnon for their gestures of good will and their assistance with the undergraduate teaching labs; Dr. Serge Desgreniers and Bruno Riel for the good times while teaching 3rd & 4th year laboratories; Drs. Béla Joos and Brian Logan for their open and honest discussions, you are most appreciated; to the transient people in the department: Dr. Riccardo ("Mexican Whistler") Brun del Re, always a man with a mission, and Dr. Robert ("Tough-Guy") Blanchard, the great fisherman: may your head always diffract neutrons and may your stomach always digest catfish; Dave Leblanc and Daniel Racicot, for their provisions of organic solvents of the barley kind: may you both live long and prosper (just don't multiply!); to Gary's lot of students, my friends: Song Yan ("Tanchi-deren") Wu, Hong ("Gung Ho") Guo, Sylvain Hubert, and Claude ("I'm a rebel") Desruisseaux; you make all days enjoyable; to Robert Parent for many enjoyable discussions and to my good friend, Saeed ("WWF Wrestler") Hadjifaradji, for his Ghandi-like good-nature and continued friendship.

And finally, to my wife Dee for her endless support, patience, and enduring love; my deepest thanks.

Dedicated to my wife Dee who makes it all worthwhile and dedicated also to my in-laws Harold and Rita Gregory to whom I am eternally grateful; all this would not be possible were it not for you. Also in loving memory of my dear grandmother Margaret (McGuinney) Nixon and John ("Unca Jack") Gregory who have touched me deeper than I can possibly know; you are most sorrily missed.

Table of Contents

Chapter 4. Case Studies

Chapter 1.

Introduction

1.1 Electrophoresis

It can be said, without exaggeration, that the largest collective project in the history of biological sciences is the Human Genome Project. This project has as its main goal nothing less than to sequence the entire human genome. It need hardly be mentioned the enormous benefits, to mankind as a whole, which arise as a direct outgrowth of this endeavour, none the least of which are the prospects of treating or even eliminating many genetic diseases.

At the heart of this most ambitious project, lies the main sequencing technology which is *based on electrophoresis*. This method exploits the fact that DNA is a polyelectrolyte, that is to say, it is, in solution, a charged polymer composed of (negative) ions with its cloud of disassociated (positive) ions. Restriction enzymes are often used to break-up the DNA strands at specific sites along the backbone. An electric field is then applied as a driving force which migrates the DNA through some convenient separation medium; this could be a gel (as in gel electrophoresis), microporous media[1], etc. The goal is to make these fragments migrate with different velocities through the separation medium in such a way as to form distinctive bands containing species of uniform molecular weight. Moreover, one requires that these bands have

[1]Harrington et al. (1994).

enough spatial *resolution*[2], that is, the band width w.r.t. the distance between bands should be small enough so that the bands do not overlap.

1.2 Algorithms

In the quest for new sequencing methods and technologies, separation scientists have sought computer simulations as both a laboratory for exploration, and as a springboard for launching new ideas and innovations. The track record is most impressive. In fact, my supervisor, G. W. Slater as well as his collaborators (G. Drouin and P. Mayer) are working on various patentable inventions, based, in part, on evidence supplied directly through computer simulations.

One such simulation program is presented herein; it is a Brownian Dynamics-based algorithm which employs some key innovations which render it efficient enough for use on common workstations. But first, we will briefly outline other simulation methods, each having their own particular strengths and weaknesses, as they apply to the simulation of polymers.

Of those methods of simulation science that are of a stochastic nature, by far the most common technique is the so-called Monte Carlo method. It has found widespread application because of its inherent simplicity, elegance, and efficiency. In particular, the method generally does not require floating-point operations, a factor which usually provides great advantages since integer arithmetic is faster on binary computers. Most of the MC methods, as applied to polymers, utilize some type of *kink-jump* algorithm whereby the chain dynamics is governed by the motion of kink formations along the chain.

---

[2]Luckey and Smith (1993).

Edwards[3] was one of the first to attempt a MC approach; the resulting statistics were, however, unphysical. The kink-jump model of Muthukumar (1991) and the usual short-range MC algorithms do not apply to highly stretched chains; artificial potential barriers are produced due to a characteristic of the algorithmic method. Newer MC algorithms, like the non-local MC methods of Deutsch and Reger (1991) and Duke and Viovy (1992), employ non-local moves to avoid such problems. Also noteworthy is the repton algorithm of Duke (1990).

Tube-reptation (TR)-based models (Lumpkin et al. (1985); Slater and Noolandi (1985)) are limited since they apply mostly to the simulation of dense polymer solutions. For example, the reptation model requires the motion to be confined within a hypothetically-defined tube which is, in effect, a mean-field like approach. However, if one wishes to study problems such as collisions or the onset of entropic regimes, these methods are not directly applicable. The extension of the reptation theory to cases where a uniform external field is applied (such as in the case of gel electrophoresis) have been met with some success. However, good quantitative agreement with experiment are still needed. For instance, Deutsch and Madden (1989) found that, in the case of flexible chains in strong fields, an instability produced by the applied field causes frequent contractions of the chain onto itself which is inconsistent with the tube picture.

The Molecular-Dynamics (MD) methods, unlike the MC method, are limited to simulations of physically short times and are often used to simulate the individual monomers of very small chains. For simulating polymers such as DNA, where there could be millions of such monomers and where the relaxation times can be enormous (days, weeks, etc.), the application of the MD approach is very limited indeed. The equations of motion are much more complicated

---

[3]Olvera de la Cruz et al. (1986).

than those of MC since they may include internal degrees of freedom (e.g., bond vibration and rotation). Moreover, these internal modes relax at very different time scales from those of molecular collisions which dominate global translational and rotational motion. This, of course, requires enormous computing power, unattainable to all but those with access to super-computers. The method can yield, however, very accurate dynamics over relatively small time scales.

The Brownian Dynamics (BD), or, more precisely, the position Langevin equation[4] approach, offers an inexpensive alternative to molecular dynamics. The method utilizes a bead-spring model where the dynamics is determined by the *long time evolution* of the position Langevin equation of motion. One uses this model with the full realization that the short-time dynamics are known to be unrealistic since inertial effects are ignored.

The effects of thermal forces, viscous drag forces, entropic spring forces, applied field forces and, in some cases, obstacle forces are included. Not included in our implementation is the Coulombic repulsion between the beads of the chain. The real deficiency of the method is the omission of hydrodynamic effects. These two omissions are, to some extent, physically offset by a screening effect of the counter-ions which get dragged-along with the chain in solution.

Shaffer and Olvera de la Cruz (1989), used a BD algorithm with Hookean springs and dimensionless point obstacles. Their system does not port well to situations involving large electric fields due to the use of Hookean springs (unphysical stretching results). Moreover, the model does not allow the springs to rotate around the obstacles (e.g., entanglements in the gel) with any ease; the resulting dynamics may then tend to reflect the model, especially in the high field and/or large molecular size regimes. Moreover, the model requires very short time

---

[4]See, for example, Allen and Tildesley (1992), p.263.

increments and the use of a CRAY X-MP supercomputer. Judging by the small number of runs used in their paper (ensemble size=10), this approach appeared discouraging.

Our approach consists of a two-dimensional BD algorithm, for simplicity and efficiency, and makes use of anharmonic springs; consequently, the algorithm ports well to high-field conditions and suffers none of the (field-induced) overstretching problems. Hard-core potentials are used in the place of obstacles as well as sharp soft-cores extending beyond the obstacles for a small (user-defined) distance. In this way, the simulation implements excluded volume interactions as a repulsion between the obstacle and the polymer which is more efficient than recourse to solving merely hard-core collision problems during time steps. Also, the simulations were all performed on standard workstations. In fact, some trials can be performed over a few days on a standard AT class PC with ensemble sizes in the hundreds. The reason for this is that our time increment is dynamically self-regulating and increases, boundary conditions permitting, up to some user-defined maximum value which can be set quite large. This affords much in the way of computing efficiency since we need not venture a guess as to how small the time increment must be. Moreover, under extreme conditions (such as high electric fields, confined media, *U-Shaped* conformations resulting from collisions, etc.), it may not even be possible to speculate on such a figure, especially in view of the use of (sharp) soft-core potentials. This may explain the large absence of the BD approach as applied to such problems in the literature. Our algorithm thus permits a BD study of a wide range of problems which were previously in a domain open but to a few of the newer MC algorithms.

1.3 Interesting Problems

Problems of interest include collision problems and the study of the related U-shaped conformations observed during gel-electrophoresis experiments (Volkmuth et al. (1994)). The newly "discovered" entropic trapping regime is a rich area for development and shows promise for exploitation by separation scientists (Hoagland and Muthukumar (1992); Mayer, Drouin, Slater (1993)). Filters are in common use and there remains much work in quantifying the dynamics within filters of differing specifications (such as the mean pore size). The use of porous media (Harrington et al. (1994)) has recently come onto the scene as a way to avoid convective currents and yield stability during the separation process. Within the area of gel-electrophoresis, the study of the initial entry into the gel, which causes stacking, is of special interest since it appears to reduce the band widths.

Our algorithm was designed to permit the BD approach to chart this new territory. The physics of electrophoretic collision, stacking, and entropic regimes will be addressed within the Case Studies portion of the thesis, Chapter 4.

Chapter 2.

A Rouse-like model

2.1 The bead-spring (Rouse) model

The Rouse model[5] describes a polymer chain as a succession of M "beads" (Fig. 2.1) at positions $\boldsymbol{R}_1, \boldsymbol{R}_2, ..., \boldsymbol{R}_M$ separated by M-1 "springs" along the vectors $\Delta\boldsymbol{R}_1, \Delta\boldsymbol{R}_2, ..., \Delta\boldsymbol{R}_{M-1}$. Each spring represents a sequence of N Kuhn statistical segments[6] which are designated by the (uncorrelated) Kuhn vectors $\boldsymbol{a}_i$. Moreover, the springs embody the entropic properties of the monomers that they are meant to replace. The dynamics of the polymer is governed by the Brownian motion of the coupled beads. The entropic (or elastic) energy stored within springs results in a contractive force which will be examined in Sect. 2.2.

Physically, a chain cannot cross itself. This phenomena is the ubiquitous *excluded volume* effect and it plays a dominant role in the conformational statistics of a real polymer chain. In our two dimensional model, we do not take this effect into account (not between the Kuhn segments making-up the springs, nor between the beads or springs themselves). To do so would severely impede the computational efficiency of the program. Moreover, self-excluded volume effects put

---

[5]See, for example, Doi and Edwards (1986), Chapter 4.

[6]Here, we use the term loosely to be any uncorrelated segment length (which we are relatively free to scale as desired). In the strict sense, the Kuhn statistical length is defined by $b_K \equiv \langle (R_M - R_1)^2 \rangle / |R_M - R_1|_{max}$ where $|R_M - R_1|_{max}$ is the maximum length of the end-to-end vector (see, for example, the footnote in Doi and Edwards (1986) on p.11).

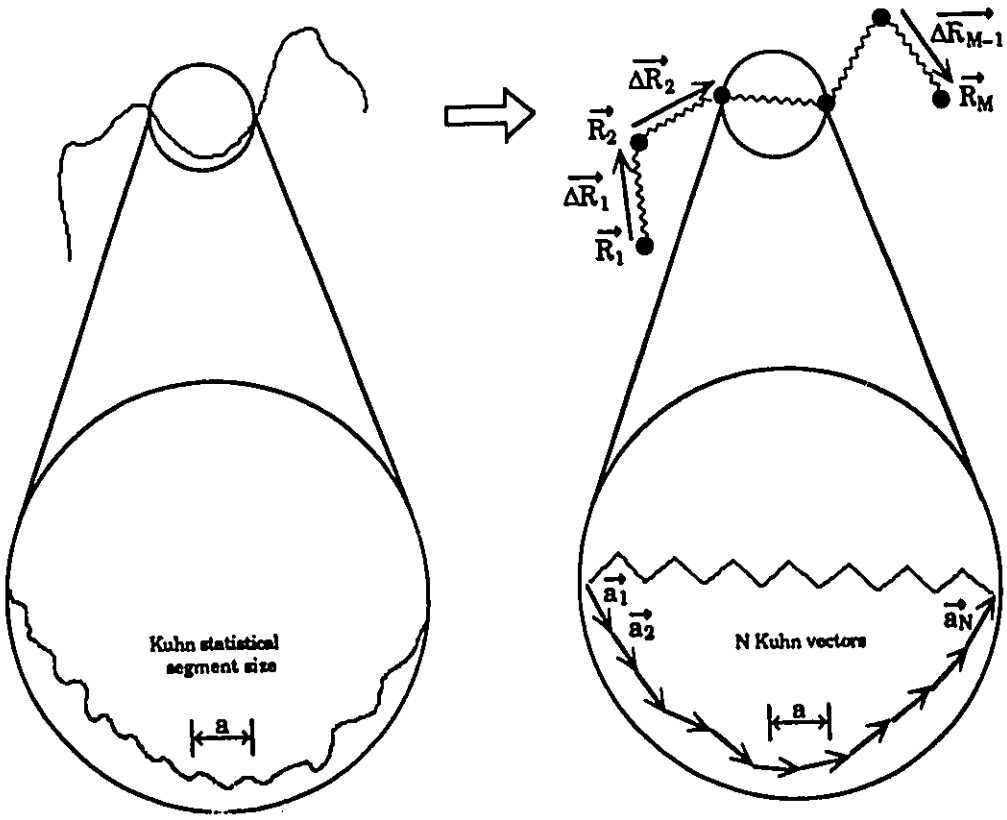

Fig. 2.1 - The linear polymer chain and its representation in the Rouse model as a succession of beads joined by entropic springs. The polymer chain is comprised of monomers as base units. We simply rescale the chain in terms of independent Kuhn statistical segments of length *a*.

extreme constraints on the motion in two dimensions, so much so that the study of very confined polymers would be, in our case, useless if we are to seek any qualitative agreement with three dimensional systems where those constraints appear, comparatively speaking, relaxed to some extent. We therefore must deal with so-called *phantom chains* in that the chain segments are permitted to move freely through one another, i.e., we use random-walk (RW) polymers. We also neglect hydrodynamic effects since polyelectrolytes (e.g., DNA) drag along counter-ions which tend to screen out these effects[7]. Finally, the choice of a two-dimensional model was made based on two criteria: i) we wanted a simple system where the analysis would be much simpler and easily visualized; and (ii), we required a model that could port itself easily to common workstations which are (at the time of this writing) of somewhat limited computing power (i.e., ~ 4 to 10 MFLOPS) w.r.t. three-dimensional dynamics.

In polymer solutions, the time scale over which the velocities of the beads approach their equilibrium values (relaxation time of the bead velocities) is much shorter than the positional relaxation time of the beads. This scenario is commonly known as the *strong-damping limit*[8] of Brownian Dynamics (BD) and the time evolution can be written as a generalized Langevin equation of motion[9] describing the dynamics of a polymer chain bead n (n=1, 2, ..., M):

---

[7]See, for example, Munk (1989), Sect. 3.3.5.

[8]See, for example, Johnson (1987).

[9] See, for example, Doi and Edwards (1986), Eq. (4.10). This is, perhaps, more precisely called the position Langevin equation (see Allen and Tidesley (1992) p. 263). Alternatively, it may also be called the "diffusive displacement equation" in the absence of hydrodynamic interactions (see Ermak and McCammon (1978)).

$$\zeta\frac{d\vec{R}_n}{dt} \approx \zeta\frac{[\vec{R}_n(t+\Delta t) - \vec{R}_n(t)]}{\Delta t} \tag{1}$$
$$= \vec{F}_s(n+1,n) + \vec{F}_s(n-1,n) + \sum_{obst} \vec{F}_{obst}(\vec{R}_n(t)-\vec{R}_{obst}) + q\vec{E} + \vec{f}_n(t)$$

where ζ is the friction coefficient of a single bead, $\vec{R}_n$ is the bead position, $\vec{F}_s(m,n)$ is the entropic spring force on bead n due to bead m, $\vec{F}_{obst}$ is the force on bead n due to some obstacle at position $\vec{R}_{obst}$, $q\vec{E}$ is the force due to the electric field $\vec{E}$ acting on the charge q of the bead, and $\vec{f}_n$ is the stochastic force acting on bead n. The stochastic (Langevin) force $\vec{f}_n$ is characterized by the moments:

$$\langle f_{n\alpha}(t)\rangle = 0 \tag{2}$$
$$\langle f_{n\alpha}(t)\, f_{m\beta}(t')\rangle = 2\,\zeta\, k_B T\, \delta_{nm}\, \delta_{\alpha\beta}\, \delta(t-t')$$

where

$$\alpha,\beta=(1, 2, \ldots, d). \tag{3}$$

are dimensional labels denoting each of the orthogonal coordinate axes. Of course, if we are to discretize our equations of motion, one must render these moments into computational form. From Eq. (2), it is not difficult to establish the relation

$$\langle f^2_{n\alpha}(t)\rangle = \frac{2\zeta k_B T}{\Delta t} \tag{4}$$

where Δt is the correlation time of the stochastic force. The derivation proceeds as follows:

$$\int_0^{\infty} dt' \, \langle f_{n\alpha}(t) f_{n\alpha}(t') \rangle = 2\zeta k_B T \int_0^{\infty} dt' \, \delta(t - t') = 2\zeta k_B T$$

$$\begin{aligned} \textit{Now, lhs} &= \int_0^{\infty} dt' \, \langle f_{n\alpha}(t) f_{n\alpha}(t') \rangle \\ &\approx \sum_{j=0}^{\infty} \Delta t \, \langle f_{n\alpha}(i*\Delta t) f_{n\alpha}(j*\Delta t) \rangle \\ &= \sum_{j=0}^{\infty} \Delta t \, \langle f_{n\alpha}^2(t) \rangle \, \delta_{ij} = \Delta t \, \langle f_{n\alpha}^2(t) \rangle \end{aligned} \tag{5}$$

$$\textit{Thus, } \langle f_{n\alpha}^2(t) \rangle = \frac{2\zeta k_B T}{\Delta t} \quad \textit{Q.E.D.}$$

The stochastic force $f_{n\alpha}$ is chosen such as to obey the Gaussian probability distribution[10]:

$$P(f_{n\alpha}) \, df_{n\alpha} = \frac{1}{\sqrt{2\pi \langle f_{n\alpha}^2 \rangle}} \exp\left(-\frac{f_{n\alpha}^2}{2\langle f_{n\alpha}^2 \rangle} \right) df_{n\alpha} \tag{6}$$

For simulation purposes, and also to make the problem more general, it is necessary to use dimensionless variables. To this end, we introduce the d-dimensional stochastic vector $\eta_n=(\eta_{n1}, \eta_{n2}, \ldots, \eta_{nd})$ via the following relation

$$f_{n\alpha} = \sqrt{\frac{2\zeta k_B T}{\Delta t}} \, \eta_{n\alpha}(t) \tag{7}$$

where $\eta_{n\alpha}$ is Gaussian distributed, as is $f_{n\alpha}$, and has zero mean and unit variance

[10] This is to conform with the Smoluchowski equation. See, for example, Doi and Edwards (1986), Eq. (3.11.18).

$$\langle \eta_{n\alpha}(t) \rangle = 0 \ , \ \langle \eta^2_{n\alpha}(t) \rangle = 1 \tag{8}$$

If we now define the following natural units

$$f_L = \frac{2k_BT}{L} \tag{9}$$

$$\tau_L = \frac{\zeta L^2}{2k_BT} \tag{10}$$

$$L = Na \tag{11}$$

for force, time and length ($L=Na$ is the maximum spring length and N is the number of Kuhn statistical segments of size a per spring) respectively, we may express our equation of motion Eq. (1), making use of Eq. (7), in the scaled form

$$\begin{aligned} \Delta\vec{r}_n(\tau) &= \vec{r}_n(\tau+\Delta\tau) - \vec{r}_n(\tau) \\ &= \Delta\tau \left[\vec{f}_s(n+1,n) + \vec{f}_s(n-1,n) + \sum_{obst} \vec{f}_{obst}(\vec{r}_n(\tau)-\vec{r}_{obst}) + \vec{\epsilon} \right] + \sqrt{\Delta\tau} \sum_{\alpha=1}^{d} \eta_{n\alpha}(\tau)\, \hat{x}_\alpha \end{aligned} \tag{12}$$

where $\mathbf{x}_\alpha$ is a unit vector along the coordinate axis α. We have also implicitly defined several scaled variables, namely

$$\frac{\vec{R}_n(t)}{L} \rightarrow \vec{r}_n(\tau); \quad \frac{\vec{F}_s}{f_L} \rightarrow \vec{f}_s; \quad \frac{\vec{F}_{obst}}{f_L} \rightarrow \vec{f}_{obst}; \quad \frac{q\vec{E}}{f_L} \rightarrow \vec{\epsilon}; \quad \frac{t}{\tau_L} \rightarrow \tau; \quad \frac{\Delta t}{\tau_L} \rightarrow \Delta\tau. \tag{13}$$

Equation (12) is in the form needed for computational purposes; all the variables are scaled and thus rendered dimensionless. The time variable is also discretized and the noise has an average

second moment of unity. We note that normal Rouse behaviour[11] results for ε=0 and f_{obst}=0 as will be examined in Sections 2.3, 2.4, and 4.1. The nature of the obstacle forces will be described later on in this chapter. We will now describe the origin of the (scaled) spring force and derive all pertinent relations.

2.2 The entropic spring force

Let us imagine that a sub-portion of a chain (subchain), represented by a spring, consists of N Kuhn segments, each having a length a called the *Kuhn length* (see Fig. 2.1). The segments are pictured as forming a freely-jointed subchain, i.e., the Kuhn vectors $\boldsymbol{a}_i$ are free of constraints. We can derive a relation for the *effective contractile force* $-\boldsymbol{F}_s$ acting between the ends of the d-dimensional subchain when the ends are separated by a *mean distance* ΔR. Vibrational and other forms of energy are assumed to be independent of the shape of the chain (or subchain). If the subchain is subject to a constant external force $\boldsymbol{F}_s$ pulling anti-parallel on each end, there is, in the steady state, a resulting contractile force, equal and opposite in magnitude. This contractile force pulling on the subchain ends is referred to as the entropic spring force since the effect of increasing ΔR results in a loss of entropy in the system of Kuhn segments forming the subchain (or spring). We introduce a spherical coordinate system with polar axis in the direction of $\boldsymbol{F}_s$. The Kuhn vectors are independent and therefore,

[11]We are referring to the usual scaling laws, not quantitative agreement since, unlike in the Rouse model, our springs will be anharmonic.

$$\Delta R = Na \langle \cos\theta \rangle \qquad or \qquad \Delta r = \frac{\Delta R}{Na} = \langle \cos\theta \rangle \tag{14}$$

The problem is thus reduced to calculating the mean component of each Kuhn vector in the direction of the external force, i.e., $a \langle cos\ \theta \rangle$. We may express the single-segment probability distribution function by the usual Boltzmann factor

$$p(\theta) = \frac{1}{Z_1} \exp\left[\frac{\vec{F}_s \cdot \vec{a}}{k_B T}\right] = \frac{1}{Z_1} \exp\left[f_a \cos\theta\right], \tag{15}$$

where

$$f_a = \frac{F_s a}{k_B T} = \frac{2 f_s}{N} \tag{16}$$

and Z_1 is the d-dimensional partition function for a single segment. The N-segment partition function in d-dimensions can be calculated using hyper-spherical coordinates where the volume element is given by

$$(dV)_{d\geq 2} = r^{d-1} (\sin\theta_1)^{d-2} (\sin\theta_2)^{d-3} \ldots (\sin\theta_{d-2})\, dr\, d\theta_1 \ldots d\theta_{d-2}\, d\phi \tag{17}$$

from which[12]

[12]See Gradshteyn and Ryzhik (1980), Eq. (3.915.4) for the solution to the integral.

$$Z_N = Z_1^N \propto \left[\int_0^{\pi} d\theta \; e^{f_a \cos\theta} \sin^{d-2}\theta \right]^N = \left[C \, f_a^{-(d/2-1)} \, I_{d/2-1}(f_a) \right]^N \tag{18}$$

where C is a constant, θ denotes the angle θ_i of Eq. (17), and I_υ is the modified Bessel function of the first kind of order υ. The average end-to-end spring extension on the force axis, ΔR, is easily related to the partition function Z_N using Eqs. (14) and (15)

$$\Delta R = k_B T \frac{\partial}{\partial F_s} \left(\ln Z_1^N \right) = Na \frac{\partial}{\partial f_a} \left(\ln Z_1 \right) \tag{19}$$

It is readily shown that the above expression reduces to

$$\Delta r = \frac{\Delta R}{Na} = \frac{\partial}{\partial f_a} \ln(Z_1) = \frac{\partial Z_1 / \partial f_a}{Z_1} = \frac{I_{\frac{d}{2}}(f_a)}{I_{\frac{d}{2}-1}(f_a)} \tag{20}$$

where we have used the identity[13]

$$\frac{\partial}{\partial x}\left[x^{-\nu} I_\nu(x) \right] = x^{-\nu} I_{\nu+1}(x) \tag{21}$$

Thus, for d=1, the rhs of Eq. (20) reduces to the hyperbolic tangent function $tanh(f_a)$, and for d=3, the Langevin function $L(f_a) = coth(f_a) - 1/f_a$. Inverting the Taylor series expansion of Eq. (20), using Mathematica™, yields the general force relation expansion

[13]See Abramowitz, M. and Stegun, I. A. (1972), Eq. (9.6.28) for the identity in its general form.

$$f_s = \frac{Nd}{2}\,\Delta r\left[\,1+\frac{d}{(2+d)}(\Delta r)^2+\frac{d^2(8+d)}{(2+d)^2(4+d)}(\Delta r)^4+\frac{d^3(120+14d+d^2)}{(2+d)^3(4+d)(6+d)}(\Delta r)^6+\ldots.\right] \tag{22}$$

from which the general form of the harmonic spring constant (as it would appear in a linear force relation like $F_s=k_h\Delta R$) is shown to be

$$k_h = \frac{Nd}{2}\frac{f_L}{L} = d\,\frac{k_BT}{Na^2} \tag{23}$$

where we have reintroduced the proper units. Although Eq. (22) provides an interesting expansion, its usefulness is limited due to slow convergence. As $\Delta r\rightarrow 1$, the force must diverge as this implies a spring (i.e., a system of monomers) subject to thermal agitation while retaining maximal alignment (minimum entropy); clearly, this requires an, albeit unphysical, infinite force. In order to avoid a truncated series (which does not yield the correct asymptotic behaviour), we can try to approximate the expansion using a "modified Padé approximant" such as[14]

$$f_a = \frac{2f_s}{N} \approx \frac{\Delta r\,[\,d-(\Delta r)^2\,]}{1-(\Delta r)^2} \tag{24}$$

which proves remarkably accurate (the error is less than 6.5% over the whole range of spring extensions for dimensionality d=2) and possesses the correct asymptotic behaviour. An even better approximation is provided by the relation

[14]We developed this approach for this research. The results and techniques are to be found in Appendix A as it appeared in Slater, Hubert, and Nixon (1994).

$$f_a = \frac{2f_s}{N} \approx d \times \Delta r \times \left(\frac{1 + \frac{(1-12/d)(\Delta r)^2 + (14/d^2-24/d^3)(\Delta r)^6}{(1+6/d)(1+2/d)}}{1 - \frac{(18/d)(\Delta r)^2 + (1-10/d+12/d^2)(\Delta r)^4}{(1+6/d)(1+2/d)}} \right) \qquad (25)$$

which is accurate to within 1.25% error over the whole range of spring extensions ($0 \leq \Delta r < 1$) for d=2. For most analytical work, Eq. (24) is all that is required (see Fig. 2.2). For even the most exacting calculations, Eq. (25) is readily integrable and proves accurate beyond what is usually required of Rouse Dynamics. We have improved the usefulness of the theory and extended its range of applicability by taking into account the anharmonicity of the spring force. Thus, attempting to improve further upon the accuracy and to go beyond Eq. (25) for simulation purposes would, in our situation, prove to be overkill. Moreover, Eqs. (24) and (25) possess the correct asymptotic behaviour (which is demanded by their construction) thus ensuring their predictive power and usefulness for analytical work. We will examine the overall effects of anharmonic springs in a later section using these relations. Next, we review the predictions of the Rouse model using the harmonic approximation (viz. Eq. (23)).

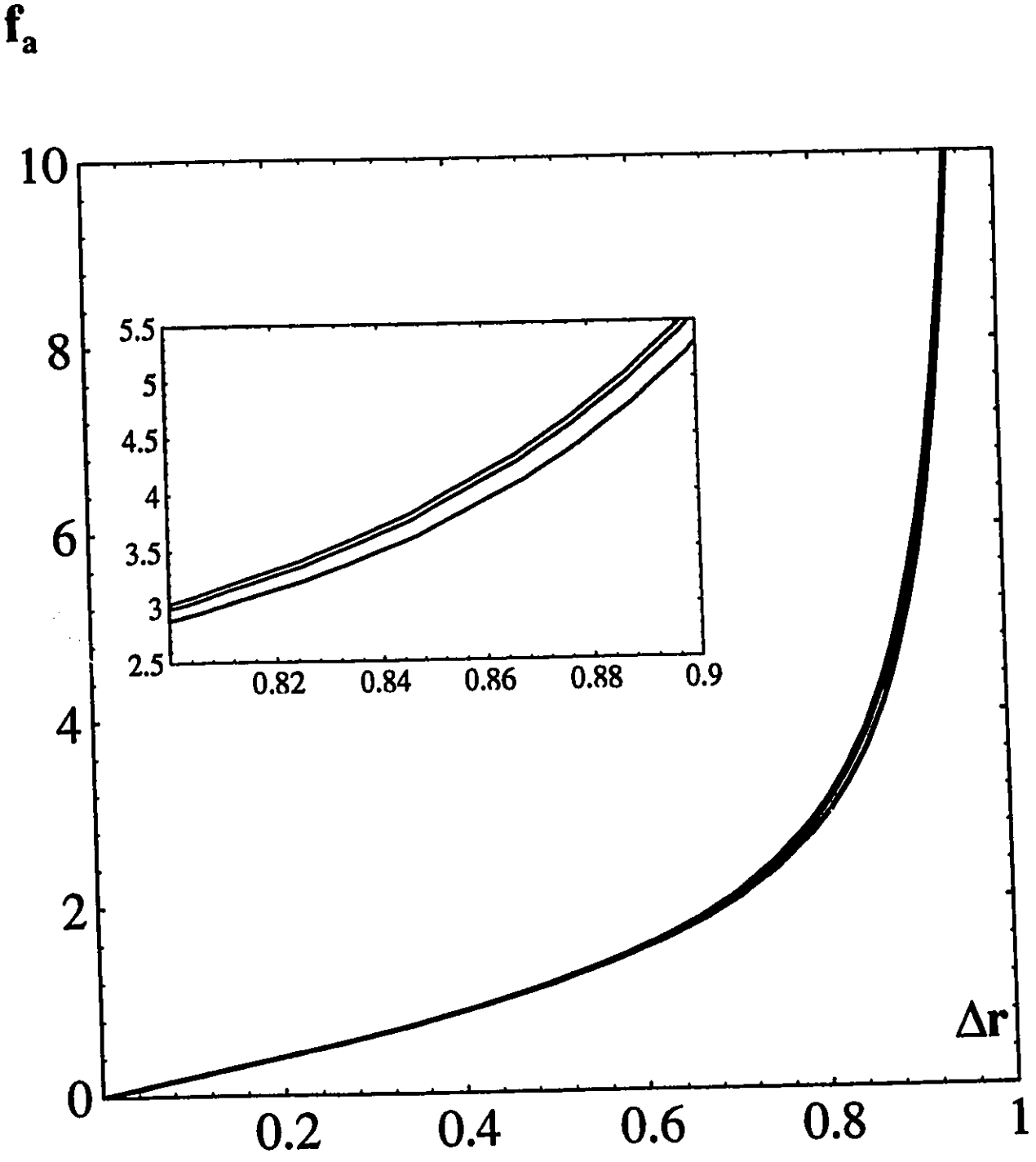

Fig. 2.2 - The anharmonic spring force $f_a(\Delta r)$ and two "modified Padé approximants" are compared. From top to bottom, we have the *inverse* of Eq. (20) followed by Eqs. (25) and (24), respectively. Note the high degree of accuracy provided by these approximations.

2.3 Predictions of the Rouse model (harmonic springs)

The consequences of the Rouse model are best studied using normal coordinates[15] using only the harmonic term of the entropic force (Eq. (23)). We will forego any development along these lines and merely summarize the salient features.

2.3.1 The average spring extension

The spring vector for spring i is defined as the difference between the position vectors of the terminal beads (see Fig. 2.1)

$$\Delta \boldsymbol{R}_i \equiv \boldsymbol{R}_{i+1} - \boldsymbol{R}_i \tag{26}$$

As mentioned in Section 2.1, $\Delta \boldsymbol{R}_i$ is given by the sum over all the statistically independent and randomly-oriented Kuhn vectors $\boldsymbol{a}_i$ making up spring i. Hence, the *mean square spring extension* will be given by the random-walk result

$$\langle (\Delta \boldsymbol{R})^2 \rangle_0 = Na^2 \tag{27}$$

for all springs. The subscript of zero is used to denote that we are dealing with harmonic springs. In scaled units this becomes

$$\langle (\Delta \boldsymbol{r})^2 \rangle_0 = \frac{\langle (\Delta \boldsymbol{R})^2 \rangle_0}{L^2} = \frac{1}{N} \tag{28}$$

Also noteworthy is the higher moment[16]

---

[15]See, for example, Doi and Edwards (1986), Appendix 3.II.

[16]See, for example, Flory (1969) Eq.(VIII3.32).

$$\langle(\Delta R)^4\rangle_0 = N\left[\frac{5}{3}(N-1)+1\right]a^4 = \frac{5N-2}{3N}\langle(\Delta R)^2\rangle_0^2 \tag{29}$$

which can be used to calculate the dispersion of Eq. (28) from which we can compute the mean-square uncertainty

$$\langle[\Delta(\Delta R)^2]^2\rangle_0 = \langle(\Delta R)^4\rangle_0 - \langle(\Delta R)^2\rangle_0^2 = \frac{2(N-1)}{3N}\langle(\Delta R)^2\rangle_0^2 \tag{30}$$

It is a trivial matter to scale these equations. The fourth moment of the spring extension becomes

$$\langle(\Delta r)^4\rangle_0 = \frac{5N-2}{3N}\langle(\Delta r)^2\rangle_0^2 \tag{31}$$

and we can express the *relative mean square uncertainty* as

$$\frac{\sqrt{\langle[\Delta(\Delta r)^2]^2\rangle_0}}{\langle(\Delta r)^2\rangle_0} = \sqrt{\frac{2(N-1)}{3N}} \tag{32}$$

We see that the *relative mean square uncertainty* is of the order of unity which indicates that large fluctuations of this quantity are intrinsic; only by increasing the ensemble size may we reduce the relative uncertainty[17]. This is an example of *lack of self-averaging* [18].

2.3.2 The average end-to-end distance of a linear polymer

The end-to-end vector of a linear polymer chain

---

[17]Of course, N=1 corresponds to a single Kuhn segment of length a, hence, no fluctuations in the spring extension are then possible since the "spring" is then merely a rigid rod.

[18]See Binder and Heermann (1992), Section 2.3.8.

$$\boldsymbol{P}(t) = \boldsymbol{R}_M(t) - \boldsymbol{R}_1(t) \tag{33}$$

has a (random-walk) *mean-square end-to-end distance*

$$\langle \boldsymbol{P}^2 \rangle = (M-1)\,\langle (\Delta \boldsymbol{R})^2 \rangle \tag{34}$$

This was to be expected, even for anharmonic springs (this is why we dropped the zero subscript), because the Kuhn vectors making up a spring are mutually independent, so must be the spring vectors making up the chain. We can compute the fourth moment[19]

$$\langle \boldsymbol{P}^4 \rangle = \frac{(5M-7)}{3(M-1)}\,\langle \boldsymbol{P}^2 \rangle^2 = \frac{1}{3}(M-1)(5M-7)\,\langle (\Delta \boldsymbol{R})^2 \rangle^2 \tag{35}$$

of the end-to-end vector. Scaling these using our natural units, we have

$$\langle p^2 \rangle = (M-1)\,\langle (\Delta r)^2 \rangle \tag{36}$$

for the *mean-square end-to-end distance*, and for the *relative mean-square uncertainty*

$$\frac{\sqrt{\langle [\Delta (p^2)]^2 \rangle}}{\langle p^2 \rangle} = \sqrt{\frac{2(M-2)}{3(M-1)}} \tag{37}$$

from which it is evident that the relative mean uncertainty will be, even for large molecular sizes $M \to \infty$, limited to a minimum value of the order of unity. As in the case of Eq. (32), this is known as the *lack of self averaging* of random-walks.

2.3.3 The centre-of-mass and the radius of gyration

The position of the centre-of-mass of a polymer is defined as

[19] See, for example, Flory (1969), Eq. (VIII.3.32).

$$R_{cm} \equiv \frac{1}{M} \sum_{n=1}^{M} R_n \tag{38}$$

where the sum extends over all bead positions. The mean-square radius of gyration is defined as

$$\langle R_g^2 \rangle \equiv \left\langle \frac{1}{M} \sum_{n=1}^{M} (R_n - R_{cm})^2 \right\rangle \tag{39}$$

which can be rewritten[20], for a RW, as

$$\langle R_g^2 \rangle = \frac{M^2 - 1}{6M} \langle (\Delta R)^2 \rangle = \frac{M + 1}{6M} \langle P^2 \rangle \tag{40}$$

By methods applicable in the limit $M \to \infty$, the two first (even) moments of the radius of gyration can be evaluated[21]:

$$\begin{aligned} \langle r_g^2 \rangle_{M\to\infty} &= \frac{1}{6} M \langle (\Delta r)^2 \rangle \\ \langle r_g^4 \rangle_{M\to\infty} &= \frac{19}{540} M^2 \langle (\Delta r)^2 \rangle^2 = \frac{19}{15} \langle r_g^2 \rangle_{M\to\infty}^2 \end{aligned} \tag{41}$$

(in scaled units) from which follows

$$\left(\frac{\sqrt{\langle [\Delta (r_g^2)]^2 \rangle}}{\langle r_g^2 \rangle} \right)_{M\to\infty} = \sqrt{\frac{4}{15}} \tag{42}$$

again of the order of unity. In fact, $\langle (\Delta r)^2 \rangle$, $\langle p^2 \rangle$, and $\langle r_g^2 \rangle$ are themselves fluctuations. This explains why the Central Limit Theorem, $\langle (\Delta A)^2 \rangle / \langle A \rangle^2 \sim 1/N \to 0$ as $N \to \infty$, of (strong) self-

---

[20]See, for example, Flory (1969), Eq. (I.5.15).

[21]Ibid, Eq.(VIII7.77,78)

averaging for an extensive thermodynamic variable A, does not apply to these quantities (although it would in the case of a biased random walk).

2.3.4 The self-diffusion constant of the centre-of-mass

The self-diffusion constant of the centre-of-mass is defined by the relation

$$D_{cm} = \lim_{t\to\infty} \frac{1}{2d} \frac{\langle [\vec{R}_{cm}(t) - \vec{R}_{cm}(0)]^2 \rangle}{t} \tag{43}$$

from which, the Rouse model (for d=2 dimensions) yields[22]

$$D_{cm} = \frac{k_B T}{M\zeta} \tag{44}$$

which, in scaled units, is

$$d_{cm} = \frac{1}{2M} \tag{45}$$

since the time is measured in units of τ_L and distances in units of L=Na.

2.3.5 The Rouse time

The motion of the end-to-end vector $\vec{p}$ is characterized by the time auto-correlation function of the end-to-end distance[23]

[22]See Doi and Edwards (1986), Sect. 4.1.2 and Appendix 4.II.

[23]See Doi and Edwards (1986), Eq. (4.35)

$$\langle \vec{P}(t)*\vec{P}(0)\rangle_0 = (M-1)\,\langle(\Delta R)^2\rangle_0 \sum_{k=1,3,\ldots}\left[\frac{8}{k^2\pi^2}\exp\left(\frac{-k^2 t}{t_{R_0}}\right)\right] \qquad (46)$$

The Rouse time, defined as the longest (terminal) relaxation time of the above auto-correlation function, is given by

$$t_{R_0} = \frac{\zeta M^2\langle(\Delta R)^2\rangle}{d\pi^2 k_B T} = \frac{\zeta M^2 N a^2}{2\pi^2 k_B T} \qquad (47)$$

for d=2 dimensions. In scaled units, the Rouse time is given by

$$\tau_{R_0} = \frac{t_{R_0}}{\tau_L} = \frac{2}{d}\left(\frac{M}{\pi}\right)^2 \langle(\Delta r)^2\rangle_0 = \frac{1}{N}\left(\frac{M}{\pi}\right)^2 \qquad (48)$$

Hence, for $\tau > \tau_{R0}$, the logarithm of the time auto-correlation function of the end-to-end vector should decrease linearly with time as $-\tau/\tau_{R0}$ (in our scaled units), that is,

$$\ln\left[\frac{\langle\vec{p}(\tau)*\vec{p}(0)\rangle_0}{\langle[p(0)]^2\rangle_0}\right] = -\frac{\tau}{\tau_{R_0}} - constant\,, \quad \tau \geq \tau_{R_0} \qquad (49)$$

We will now examine the expected effects due to the anharmonicity of the springs with respect to the above parameters.

2.4 The effects of the anharmonic springs

2.4.1 The average spring extension

In a recent paper[24], we derived an approximate form for the spring force from which we can yield the distribution function for the extension of a d-dimensional anharmonic spring (as derived from Eq. 24) comprised of N Kuhn segments

$$p(d,N,\Delta r) = C(N)\ (\Delta r)^{d-1}\ [1-(\Delta r)^2]^{N(d-1)/2}\ \exp[-N\ (\Delta r)^2/2] \tag{50}$$

Drawing on these results, the mean squared extension of an entropic anharmonic spring can be approximated by

$$\langle(\Delta r)^2\rangle = \int_0^1 d(\Delta r)\ (\Delta r)^2\ p(d,N,\Delta r) \tag{51}$$

In our simulations, d=2 and we set N=5; therefore, our expectation value is

$$\langle(\Delta r)^2\rangle_{\substack{d=2\\N=5}} = 0.1590 \tag{52}$$

in scaled units. This can be contrasted with the exact result obtained by numerical integration of the exact expression[25], to four-figures, using Mathematica™

---

[24]See Appendix A (i.e., Slater, Hubert, and Nixon (1994)).

[25]Ibid.

$$\langle(\Delta r)^2\rangle_{\substack{d=2\\N=5}} = 0.1610 \qquad (num.\ int.) \tag{53}$$

We note that the results are in close agreement, as required. These results are to be compared with the harmonic approximation

$$\langle(\Delta r)^2\rangle_{\substack{d=2\\N=5}} = \frac{1}{5} \qquad harmonic \tag{54}$$

which is greater by 25% due to a smaller restoring force. Noteworthy is the higher moment

$$\langle(\Delta r)^4\rangle_{\substack{d=2\\N=5}} = 1.7858\ \langle(\Delta r)^2\rangle^2_{\substack{d=2\\N=5}} \tag{55}$$

which was evaluated using the same distribution function. From which the relative dispersion of $\langle(\Delta r)^2\rangle$ is

$$\left(\frac{\sqrt{\langle[\Delta(\Delta r)^2]^2\rangle}}{\langle(\Delta r)^2\rangle}\right)_{\substack{d=2\\N=5}} = 0.8865 \tag{56}$$

We note that the ratio is again of the order of unity.

2.4.2 The average end-to-end distance

The mean square end-to-end distance

$$\langle p^2\rangle_{\substack{d=2\\N=5}} = (M-1)\ \langle(\Delta r)^2\rangle_{\substack{d=2\\N=5}} = 0.1590\ (M-1) \tag{57}$$

does not change in its dependence on the mean-square spring extension, only its numeric value changes. The same is true for the fourth moment

$$\langle p^4 \rangle_{\substack{d=2 \\ N=5}} = \frac{5M-7}{3(M-1)} \langle p^2 \rangle^2_{\substack{d=2 \\ N=5}} \tag{58}$$

The dispersion

$$\langle [\Delta(p^2)]^2 \rangle = \frac{2(M-2)}{3(M-1)} \langle p^2 \rangle^2 \tag{59}$$

as well as the relative mean uncertainty

$$\left(\frac{\sqrt{\langle [\Delta(p^2)]^2 \rangle}}{\langle p^2 \rangle} \right) = \sqrt{\frac{2(M-2)}{3(M-1)}} \tag{60}$$

retain their original format.

2.4.3 The radius of gyration

The radius of gyration of the polymer does not change its linear dependence on the mean-square spring extension and its dependence on the number of beads is given by (for d=2 and N=5 Kuhn segments)

$$\langle r_g^2 \rangle_{\substack{d=2 \\ N=5}} = \frac{M^2-1}{6M} \langle (\Delta r)^2 \rangle_{\substack{d=2 \\ N=5}} \tag{61}$$

All other pertinent relations follow similarly.

2.4.4 The self-diffusion constant of the centre-of-mass

The self diffusion constant of the centre-of-mass is independent of the force linking the constituent beads in the polymer chain and so Eqs. (43) - (45) remain valid.

2.4.5 The Rouse time

The relaxation of the polymer chain vector $p(\tau)$ is governed by the nature of the interaction existing between constituent beads and, as a result, the time auto-correlation function may change (due to the anharmonic terms). We will examine this effect in Chapter 3.

2.5 The obstacle force

There exists a number of ways to implement obstacles in a simulation. What is needed is a general, consistent, and yet simple method of handling these bead-obstacle excluded volume interactions. Let Δr be the distance between the obstacle surface and the bead (the beads are points). Thus, when calculating the force due to a wall, the distance Δr is the separation of the bead from the wall. In the case of a spherical obstacle of radius ρ centred at $\mathbf{r}_{obst}$, we have $\Delta r = |r_{bead} - r_{obst}| - \rho$. Let us denote the extent of the soft core *by* σ ; beyond which, the force goes to zero (Fig. 2.3). In our implementation, we make the substitution $\Delta r' = \Delta r + \sigma$ and adopt a Lennard-Jones-like force, directed perpendicular to the surface, viz.

$$f_{obst}(\Delta r') \to \infty , \qquad (\Delta r' < \sigma) \tag{62}$$

$$f_{obst}(\Delta r') = A \times \Delta r' \times \left[\frac{1}{(\Delta r')^2 - \sigma^2} - \frac{1}{3\sigma^2} \right]^2 , \qquad (\sigma < \Delta r' < 2\sigma) \tag{63}$$

$$f_{obst}(\Delta r') = 0 , \qquad (\Delta r' > 2\sigma) \tag{64}$$

We ensure against the possibility of entering within the hard core region where the force is undefined: this is described in Section 4.1. The skin depth σ can be chosen as small as required (for example, to make it negligible w.r.t. the extent ρ of the hard-core of an obstacle).

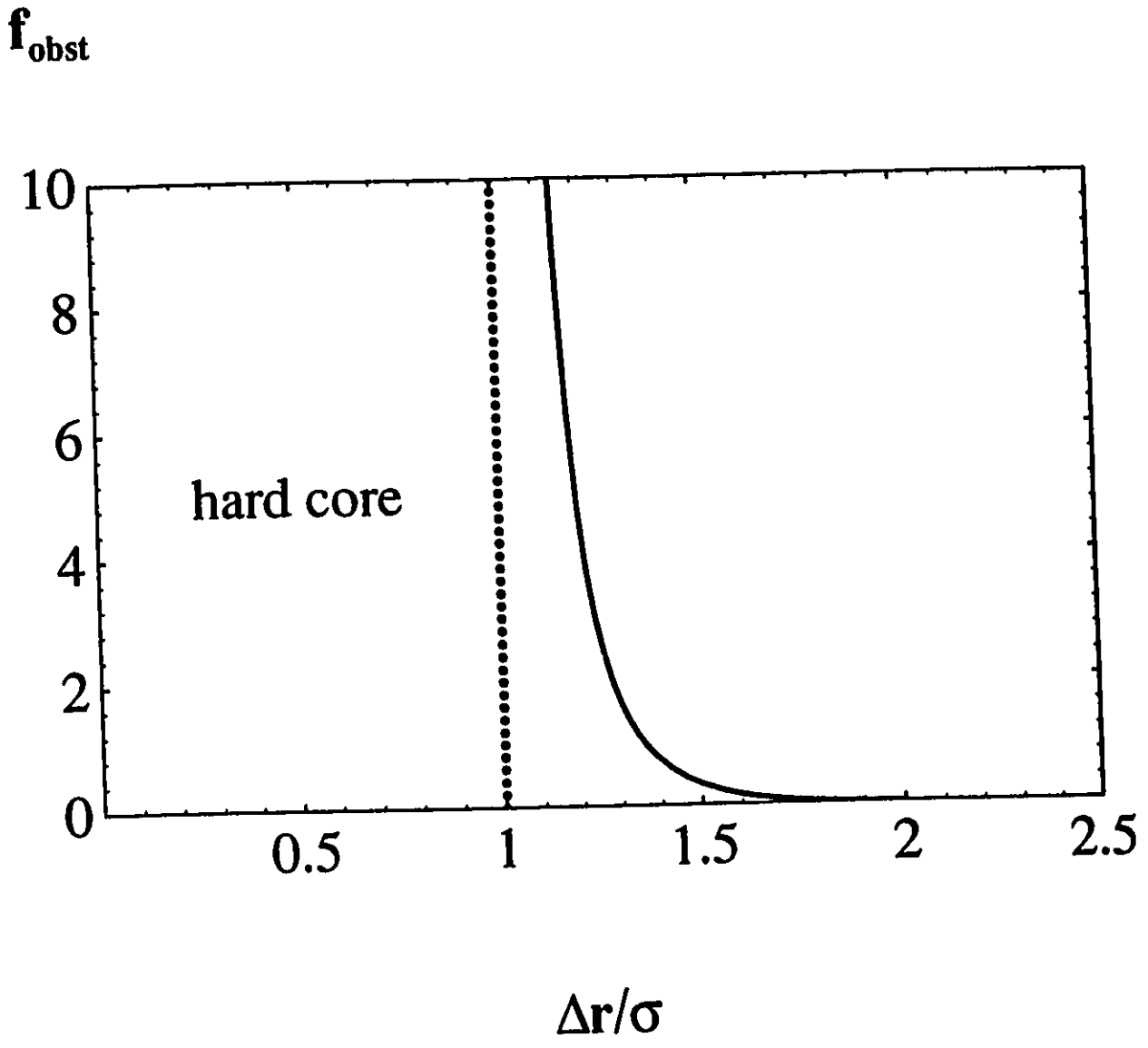

Fig. 2.3 - The soft-core potential f_{obst} used for representing bead-obstacle repulsive interactions.

Chapter 3.

Algorithm Implementation

3.1 Introduction

It should be re-emphasized that no self-excluded volume interactions nor any hydrodynamic effects are considered. We're dealing with "ghost chains" with the particular feature of being interacting with their environment.

The implementation of the integration scheme proceeds as follows: (1) All forces on individual beads are computed and the system beads making up the chain are all moved simultaneously in time. (2) The system integrity is checked against all constraints: (3a) If there are no violations, the moves are accepted. (3b) Should a violation of integrity occur (e.g., maximum spring extension violation), the beads are returned to their original positions, $\Delta\tau$ is divided (by 4 in our implementation), and the move is re-attempted. This last series of steps is repeated as necessary until a move is accepted. (4) After a legally performed move, the time counter is incremented by the current time increment $\Delta\tau$ and the latter is also increased but according to Eq. (65); we will discuss the time increment in Section 3.8.

The above integration scheme was designed so as to optimize the CPU time when integrating the equations of motion. The justification of this scheme and accounts of some

excluded-volume interactions are presented in this chapter along with analysis of the pertinent parameters.

3.2 Spring forces / Maximum spring extension

An important feature of the algorithm is the elimination of unphysical molecular stretching which has been shown to be characteristic of systems with harmonic springs (Shaffer and Olvera de la Cruz (1989)) in situations of high stress such as U-shape (pinned) conformations as in Fig. 3.1. In our system, we use anharmonic springs, which possess a maximum spring extension (Δr_{max}=1 according to our computer units); a spring must not and cannot (in the mathematical sense) exceed the length of its constituent Kuhn segments once these are aligned end-to-end[26]. The anharmonic spring force is the embodiment of this constraint (see Section 2.2). For small extensions, we see that the force-extension behaviour is more or less linear; this is the harmonic limit. For large extensions, the nonlinear terms in Eq. (22) become more prominent and the spring force then diverges (see Fig. 2.2). The spring extension constraint ($\Delta r < 1$) must be checked after each attempted move (simulation step) due to the discrete nature of the simulation process. Should this constraint be violated for any given spring, the time increment $\Delta\tau$ is reduced and the time step is repeated for the chain as a whole (the method is outlined in Section 3.8). We already described several (Eqs. (24) and (25)) accurate approximations to the force-spring extension relation (Eq. 20), and one of these relations (Eq. 24) was used for the simulations.

[26]Lest, of course, the polymer ruptures. We do not permit this in the present implementation.

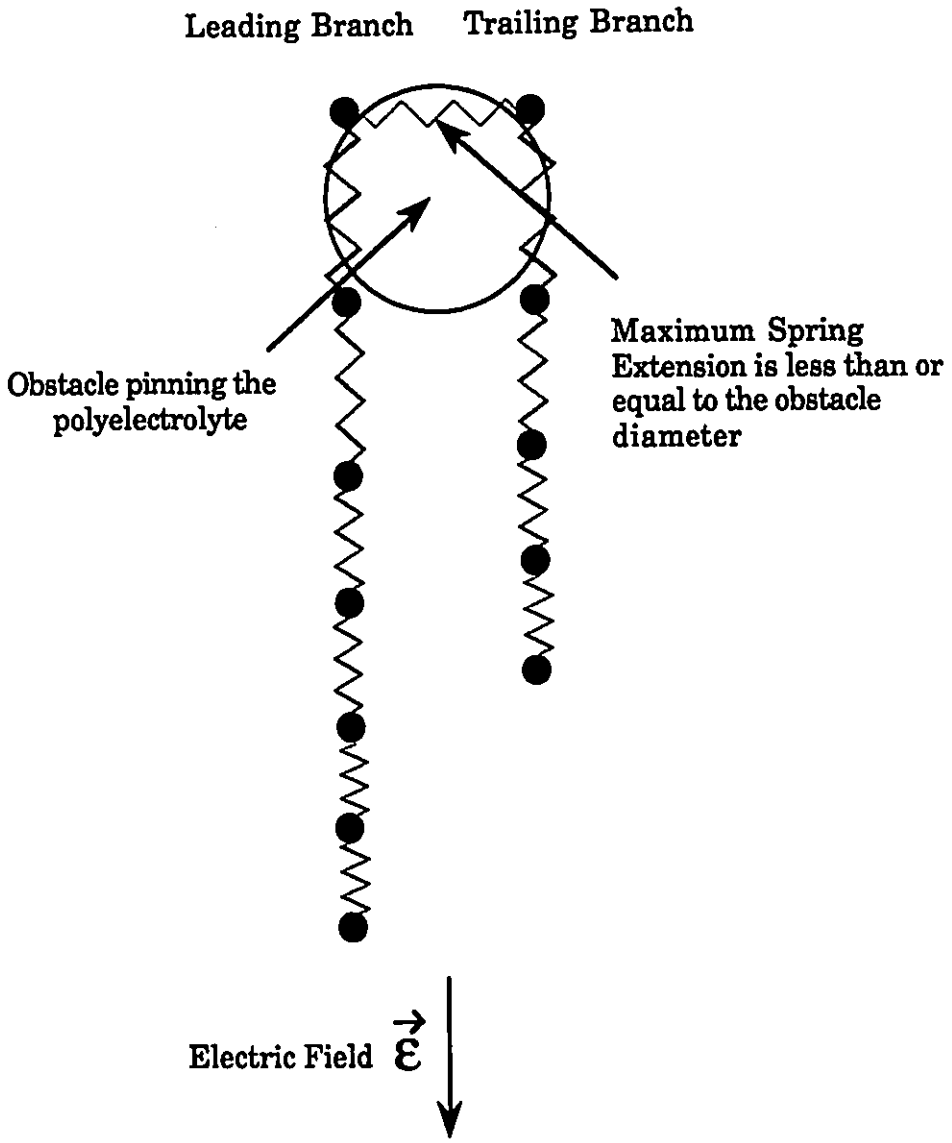

Fig. 3.1 - Depiction of a chain pinning process. A polyelectrolyte migrates through a matrix of obstacles under the influence of an electric field ε. The chain is then pinned against an obstacle and assumes a U-shape conformation before finally unravelling.

3.3 Obstacles

As we have seen in Section 2.5, we chose to adopt a Lennard-Jones-like force that is purely repulsive and directed perpendicularly to the obstacle's surface. The skin depth σ (which is dimensionless with $0<\sigma<1$) of the soft-core can be chosen as small as required (as a user input) in order to render its extent negligible with respect to the length scales of interest. We must ensure that there is no possibility of entering within the hard-core region where the force is undefined. Should a bead jump within the hard-core of some obstacle, $\Delta\tau$ is reduced and the time step repeated as discussed in Section 3.8. Also, we must not permit a bead to jump over (through) some obstacle and hence the need for a maximum jump length λ (see Section 3.6).

3.4 Stochastic forces (Thermal noise)

Equation (6) indicates that the distribution function of the Langevin term is assumed Gaussian. In our dimensionless implementation of the Langevin force η_α, we use normal distributions of mean zero and standard deviation one for both η_x and η_y separately. These Langevin components are generated using the polar method[27] for normal deviates which is due to G. E. P. Box, M. E. Muller, and G. Marsaglia[28].

Since large values of the Langevin force will increase the frequency of attempted breaches of spatial constraints (spring extension violations and maximum jump size violations), we elect to reject all computed values over a certain cut-off value which was chosen to be 5 standard

---

[27]See Knuth (1982), Algorithm 3.4.1P or Heermann (1990), Algorithm A1.5.

[28] As it turns out, the source code for this simple method can be found in Press, Flannery, Teukolsky, and Vetterling (1988) Section 7.2 under the moniker of the Box-Muller method.

deviations: we accept only $|\eta_\alpha|<5$. This amounts to removing the tails of the distribution. The inherent error in simulation accuracy due to a cut-off of 5 standard deviations, relative to the other uncertainties in the simulation, is negligible ($\approx -1.544 \times 10^{-3}$ %).

3.5 Use of tables for Langevin forces

The computations of the Langevin forces are replaced with the efficient use of look-up tables. The stochastic force table is *balanced*, that is to say, each (positive) force generated by the normal distribution generating function is placed in the table along with its negative counterpart. This helps to ensure that the time averaged value of the random force is zero and thus eliminates directional bias (i.e., the first moment will be zero) due to the finite size of the table. Of course, one could pick a random sign at every iteration and need only store the positive values. This however would reduce the computational efficiency. As for the second moment (the mean-squared Langevin term), it will be of the order of unity provided that enough unique Langevin terms are sampled (we thus need a large table or, at least, a rapidly regenerating table) and provided that we select a cut-off value that is high enough (several standard deviations). Our table was chosen to be 10000 entry pairs long and we renew these entries at a rate of one pair per completed step.

3.6 The need for a maximum jump length λ

A bead jump size constraint, $|r_\alpha(\tau+\Delta\tau) - r_\alpha(\tau)| < \lambda$, is necessary for smooth integration of the equations of motion, especially in regions where a bead might jump over some obstacle.

We must fine-grain the motion in these regions so that the bead experiences the corresponding potentials (force fields) for long enough times such that enough work is performed on the bead thus limiting "attempts" to violate excluded volume effects to a minimum. This is especially important when the external force (e.g., due to an electric field ε) is high. For example, since all beads move at each time step, the average distance covered by any given bead is approximately $\varepsilon\Delta\tau$ where ε is the scaled electric field and $\Delta\tau$ is the scaled time increment. Consider the case of a bead moving towards some obstacle. Should the product $\varepsilon\Delta\tau$ exceed the diameter $2\rho_{obst}$ (twice the obstacle's radius) of the given obstacle, the bead can emerge on the other side of the obstacle, in effect, passing straight through the obstacle. A sufficient constraint would be $|\varepsilon\Delta\tau| < \lambda$ where $\lambda < \rho_{obst}$, preferably, $\lambda < \sigma$ where σ is the "skin-depth" of the obstacle. We typically adopt $\lambda = \sigma/4$ in practice, the skin-depth being set to approximately 5% of ρ_{obst}. If the jump size exceeds λ, the time increment $\Delta\tau$ is cut and the move is reattempted (see Fig. 3.2).

3.7 Having a variable time increment (time cutting)

There surely exist suitably small time increments $\Delta\tau$ for any given simulation which would permit well behaved motions of all chains and avoid any violation of spatial constraint or boundary condition. The potentials, corresponding to the constraints and boundary conditions, will thus be allowed to perform enough mechanical work upon the polymer beads in order to avoid any breach in the integrity of the simulation. The question naturally arises as to how one can foresee all scenarios and pick a sufficiently low (optimum) time increment. Picking a time increment that is too low may well extend the simulation indefinitely. We cannot even begin to guess as to what the largest such time increment is. Also desirable is to be able to handle large

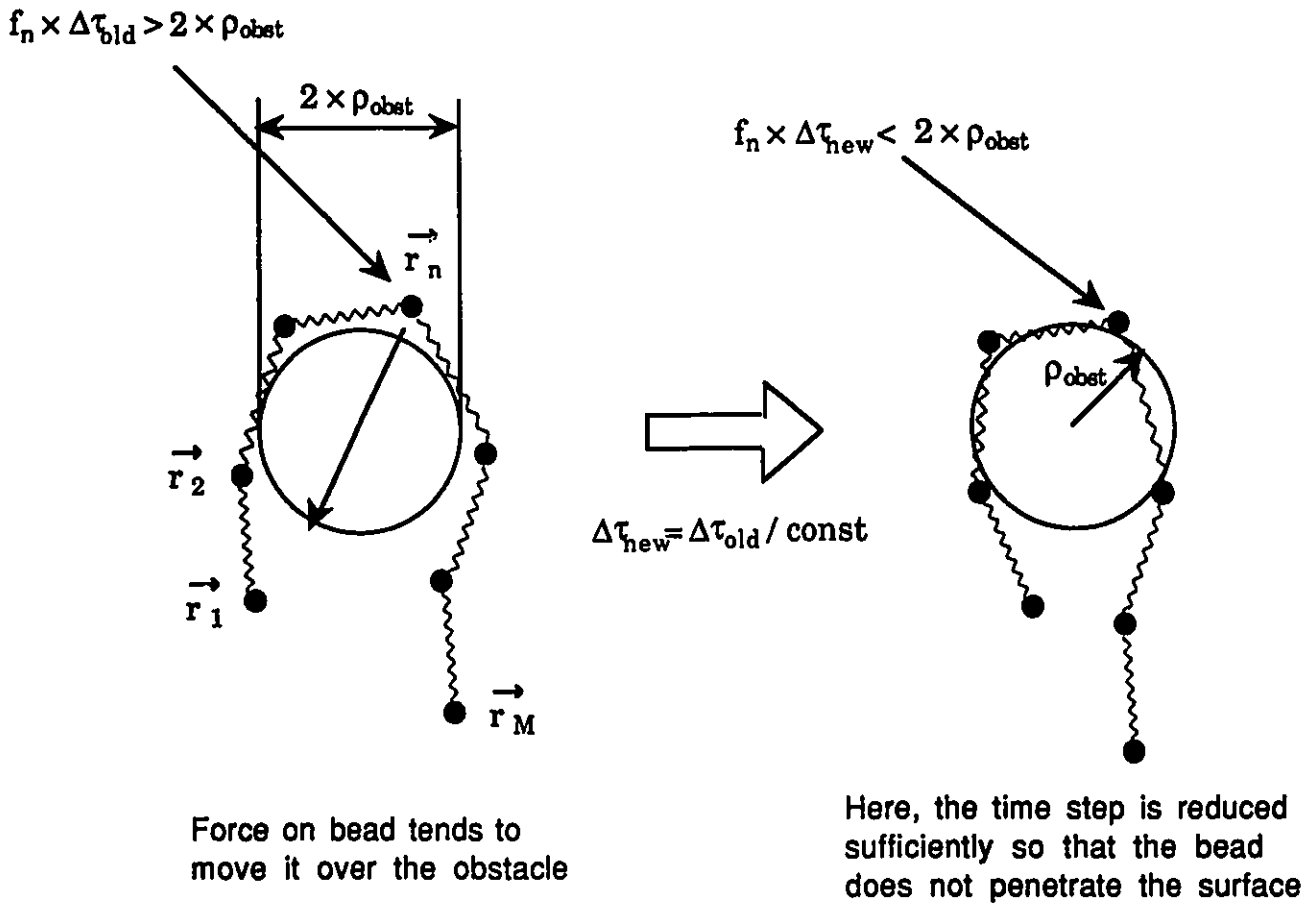

Fig. 3.2 - Beads must not be permitted to enter or cross over hard core potentials.

fields with few attempted breaches of system integrity. Some sort of scheme is thus needed to deal with this computational dilemma.

What is needed is a time increment that varies in accordance with states which compromise simulation integrity. In fact, the mere fact that we wish to limit the integration of the equations of motion by imposing a maximum jump size λ requires the ability to modify the time increment dynamically.

3.7.1 Reducing $\Delta\tau$ solely for the time step following a time cut

The modification of the time increment alludes to the need for caution in how to handle the stochastic term. One must avoid putting bias on any chosen Langevin force.

In the development phase, a scheme was adopted whereby the Langevin force for each bead is renewed after each time step (see Fig. 3.3). The time increment was only decreased (e.g., divided by 4) subsequent to a breach in system integrity; the time increment $\Delta\tau$ being reset to its default value $\Delta\tau_0$ immediately upon completion of the time step.

But there are predicaments to this scheme. For example, we will have, in a probabilistic sense, a bias for longer time increments when the stochastic terms are small. The reason being that larger forces have a tendency to cause beads to violate spatial boundary conditions more readily than do smaller forces. To be more precise we should specify that the *force and time increment* and the *stochastic force and square root of time increment* products have a tendency to compromise system integrity when the forces are appreciable and the time increment is not too small. We therefore are giving "more weight" (bias) to smaller forces (in the way of integrated time). The net result is that the distribution of integrated time with respect to stochastic

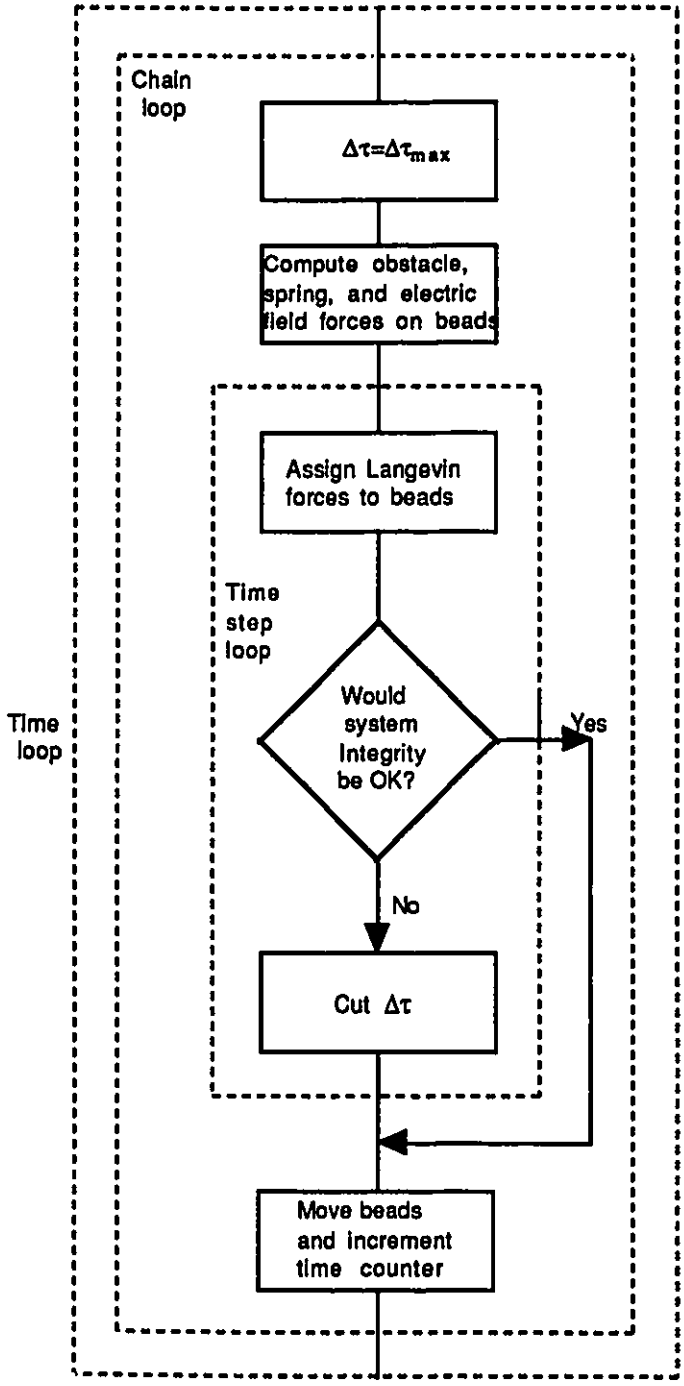

Fig. 3.3 - A time cutting scheme that leads to stochastic "cooling".

force will no longer be equivalent to that of the (Gaussian) probability distribution of the stochastic force: the distribution will be more strongly peaked (about smaller stochastic forces) and the standard deviation would therefore be smaller. This biasing poses a problem for many reasons. Firstly, the relaxation time for the springs (and hence the chain as a whole) may not be correct as a result. Secondly, this leads to a diffusion coefficient that is too small which is the physical equivalent of having a *cooler* system in that the mean temperature is smaller than it should otherwise be.

Identifying and surmounting these fundamental computational problems proved to be the most important issues of the project and required a considerable time investment.

3.7.2 Keeping stochastic forces over several time steps

To avoid the cooling bias as previously described, it would be sufficient to keep stochastic forces over equal intervals of time (i.e., equal weights). These time intervals can be chosen to be, say, the default (maximum) time increment, $\Delta\tau_{max}$, for convenience sake. Unfortunately, this new scheme leads to new repercussions.

The problem with this scheme is that, in many cases, we will need to keep the same stochastic forces (for all beads) for several consecutive (reduced) time steps. A curious situation was found to occur on occasion: one of the chain's beads gets caught in a resonance-like situation where the bead is made to oscillate back and forth utilising very small time increments $\Delta\tau$, and, consequently, requiring much CPU time before the cycle is broken. For example, take the case a chain bead n (referring to Fig. 3.4) that finds itself being propelled towards a wall under the influence of a Langevin force, as in (1), for some small time increment $\Delta\tau$. The

stochastic (Langevin) force $\mathbf{f}_n$ acting on bead n effectively drives the bead a step towards the wall. At position (2), the repulsive force due to the wall's sharp soft-core potential has increased enough to allow the product $\mathbf{f}_{wall} \times \Delta\tau$ to dominate over the product of $\mathbf{f}_n \times \sqrt{\Delta\tau}$ (i.e., the wall's repulsive force now dominates) and the bead is repelled from the wall. The bead finds itself, more or less, back at its starting point (1), and the process is re-iterated until enough integrated time τ_{int} has been simulated before arriving at that part in the algorithm which requires the selection of a new Langevin force $\mathbf{f}_n$. These metastable oscillatory states can indeed take a long time to dissipate and, being the situation can be quite common, this problem can effectively stall a simulation for good.

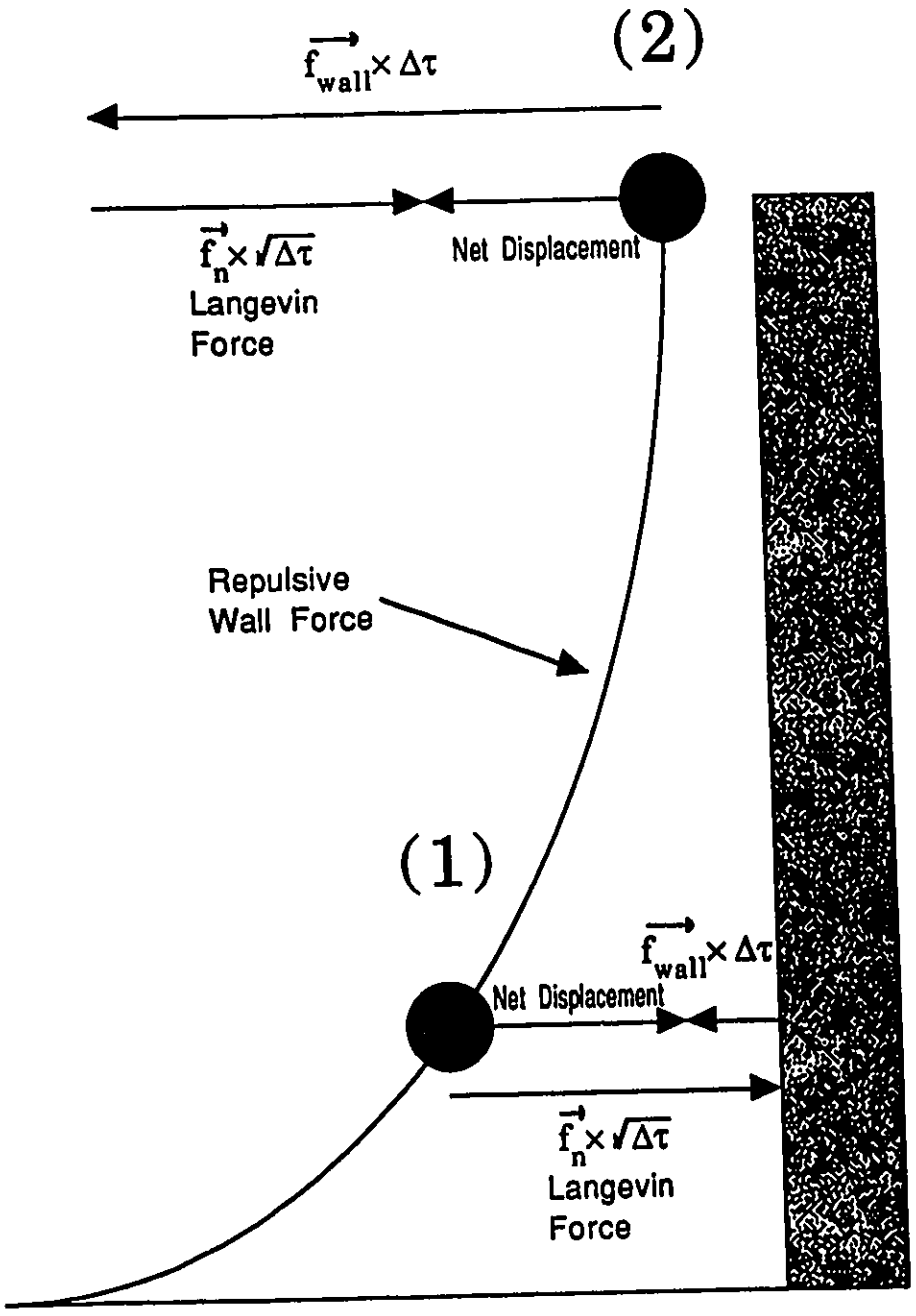

Fig. 3.4 - A metastable state is set-up as a resonance-like situation of a bead which is forced to move between two points where one of either force (the wall's repulsive force or the Langevin force) dominates.

3.8 Our approach: time cutting with damped evolution

3.8.1 Time cutting

At each iteration in the program, the before-mentioned boundary conditions and constraints are strictly adhered to before the move is accepted and the time counter is increased. Any system integrity violation will result in the time increment being divided (cut) by four and the step repeated.

Thus, the time increment is not static but is reduced in accordance with the stresses built up in the chain. This is important for many other reasons. This allows for better integration of the equations of motion, being that the force on any given bead varies widely as a function of time. It also allows us to scale the motion to suit the dimensions of the system simulated, that is, it enables the incorporation of a maximum step size λ (see Sect. 3.6).

However, if $\Delta\tau$ is not increased following the time cut, the simulation becomes very inefficient, especially if the large stresses are dissipated (e.g., the molecule has moved away from a wall). Section 3.7 presented two schemes (for varying $\Delta\tau$) which fail. Convenient methods for readjusting $\Delta\tau$ in situations of reduced stress are now presented.

3.8.2 Damping the evolution of the time increment

If we relax our requirement that every stochastic term receive the same *a priori* time increment and simply demand that each receive *approximately* the same time increment *on average* only, then the implementation dependent problems (namely cooling described in Section 3.7.1 and metastable states described in Section 3.7.2) can be averted.

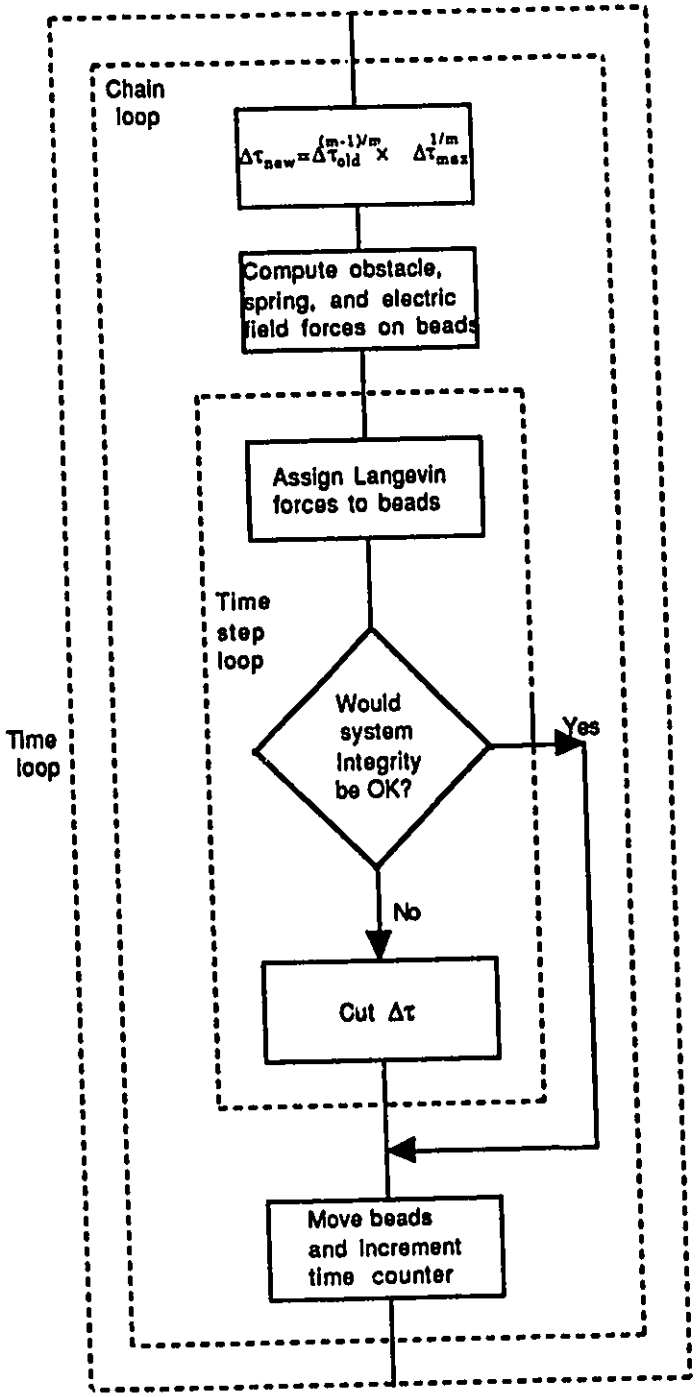

Fig. 3.5 - The time cutting sequence used in our simulation algorithm.

There exist a number of ways of accomplishing these requirements. Referring to Fig. 3.6a, we might simply employ a step-like method whereby the time increment $\Delta\tau$ is cut to some suitable size and thereafter, for a user specified duration, the same reduced time increment is maintained before finally returning to its default value. Although the method would constitute an improvement, it would be inefficient because the time increment is not allowed to increase until such time as the user-specified delay has elapsed and then, $\Delta\tau$ would jump abruptly ,possibly too abruptly, and require a time cut and, therefore, the process to be reiterated.

One might try an interesting approach: taking the geometric mean. In this case, the time increment can be made slowly varying (by increasing the damping parameter m) and thereby giving a large number of succeeding Langevin terms (randomly chosen) the same amount of integrated time (more-or-less). Let's say that $\Delta\tau$ has just been cut and that the new time increment allows the system to perform a time step. The next time increment can be chosen to be the geometric mean (see Fig. 3.6b)

$$\Delta\tau_{new} = (\Delta\tau_{old})^{\frac{m-1}{m}} \times (\Delta\tau_{max})^{\frac{1}{m}} \tag{65}$$

of the maximum time increment with that of the time increment previously used.

This scheme can be made to approximate the ideal situation, namely equal time increments on average for each stochastic force chosen. The damping parameter m used in the geometric mean calculation can be chosen big enough so that the time increment function increases very slowly during the course of the simulation. This is important; we want ergodicity in the sense that we want each chosen Langevin (stochastic) force to get approximately the same mean time increment over the course of the entire simulation (i.e., we want the normalized

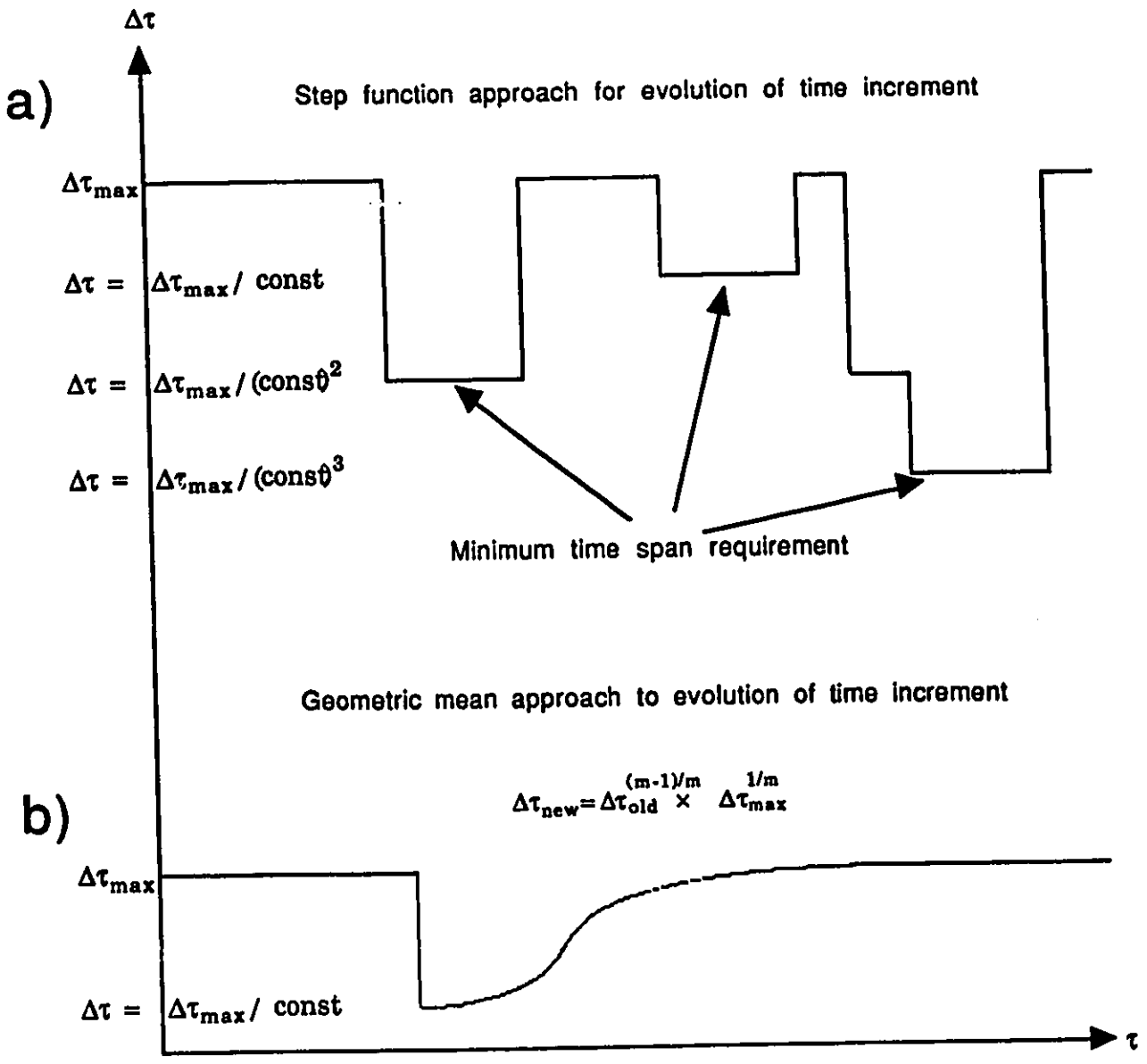

Fig. 3.6 - Two possible evolution schemes for the time increment $\Delta\tau$. The first, a), is a step function approach while the second, b), is our geometric mean approach.

distribution of integrated time with respect to the chosen Langevin (stochastic) forces to be identical with the (Gaussian) probability distribution function of Langevin forces). We also want the time increment to increase very slowly so that the residual stresses are sufficiently damped and yet, the time increment gets optimized (i.e., increased whenever possible).

3.8.3 Effects damping factor on accuracy and CPU process time

The choice of damping parameter m has a marked effect on simulation accuracy and CPU time. A series of simulations were chosen to determine the relationship between the choice of damping parameter and simulation accuracy as well as process CPU time (see Table 3.1). Several different damping factors (m=1, 3, 10, 32, 100, 316, 1000, 3162, 10000, 31623, 100000, 316228, and 1000000) were chosen for the case of a five bead chain with a maximum time increment of $\Delta\tau_{max}$=0.01. The chains were simulated in absence of fields, obstacles or constraints with an ensemble size of 10000 chains for each simulation run (i.e., for each chosen value of m).

We examined the effect of the choice of damping parameter m on the accuracy for cases with known results. The results are plotted in Fig. 3.7. For a M=5 bead chain, the corresponding ratio of the dispersion of the centre-of-mass to time is expected to be precisely $4\times d_{cm}=0.4$ (in scaled units) according to the definition of the diffusion constant D_{cm} (Eq. 44). As we can see, there is a marked discrepancy between the expected value (solid line) and the experimental values (points) of the diffusion constant as m decreases below the value $m_{crit}=1000$. We note the value of $4\times d_{cm}$ for $m=1$ is much too low (i.e., by about 20% for M=5) and indicates quite strongly that there is a bias in the system. We can thus conclude that, by sufficiently damping the evolution of the time increment $\Delta\tau_{new}$, we can effectively eliminate any stochastic cooling.

damping parameter m	$\text{Log}_{10}(m)$	$<4\times d_{cm}>$ (exact=0.4)	CPU time /10^4 sec IBM RISC/6000 model 320
1	0	0.3202	1.67
3	0.477	0.3271	1.71
10	1	0.3516	1.88
32	1.505	0.3719	2.31
100	2	0.3846	2.79
316	2.500	0.3951	3.49
1000	3	0.3937	4.03
3162	3.500	0.3997	4.53
10000	4	0.4026	4.97
31623	4.500	0.4034	5.40
100000	5	0.4055	5.84
316228	5.500	0.4036	6.63
1000000	6	0.4051	7.68

Table 3.1 - The effect of m on simulation accuracy and CPU time. All runs were conducted with $\Delta\tau_{max}$=0.01 and τ_{sim}=0.5 (the simulation time in scaled units) for M=5 bead chains.

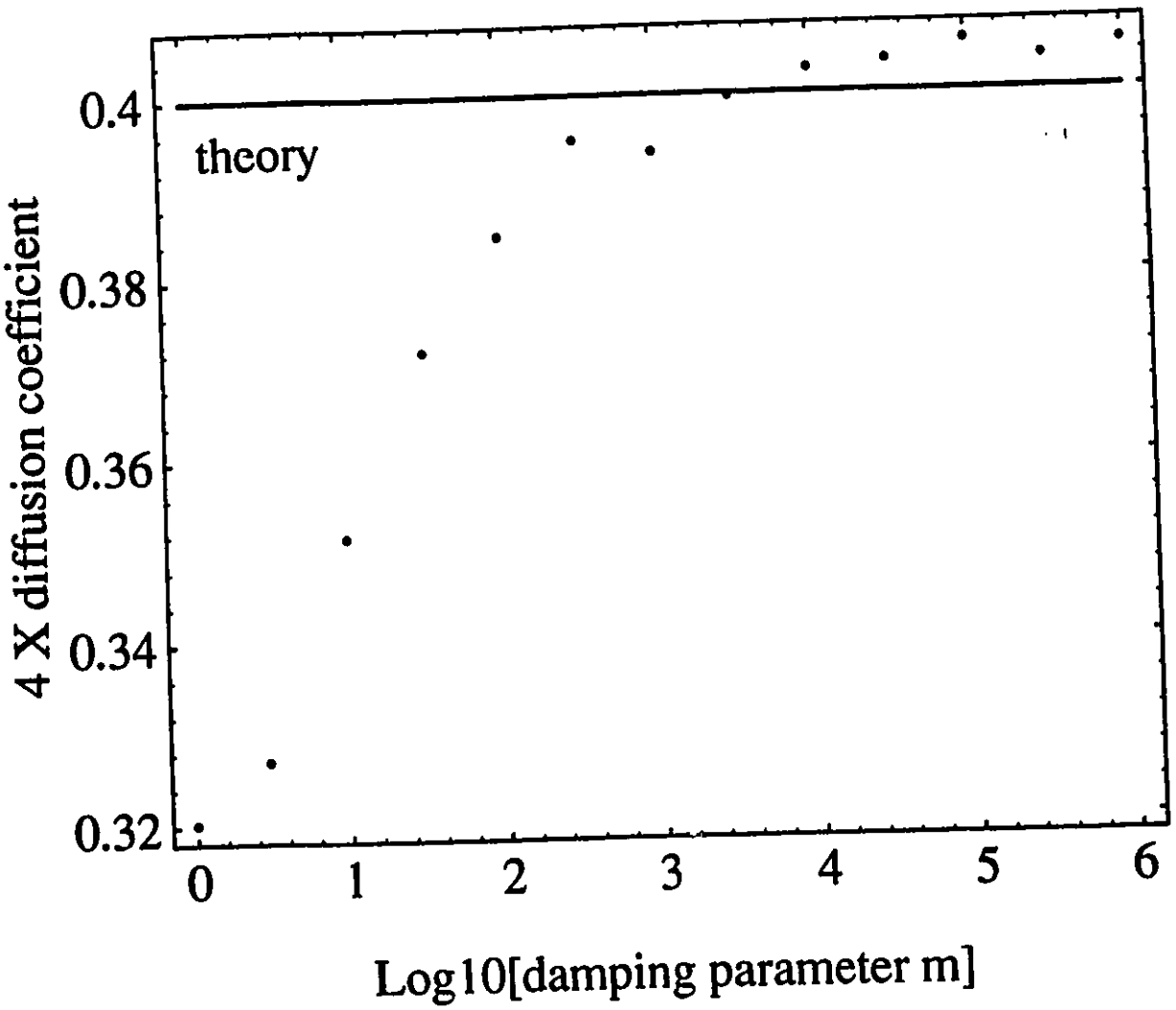

Fig. 3.7 - The effect of the damping parameter (*m*) on the diffusion constant (d_{cm}) for a M=5 bead chain. Plotted is $\langle(\Delta r_{cm})^2\rangle=4\times d_{cm}$ vs. Log[m]. The ensemble size was 10000 chains per run.

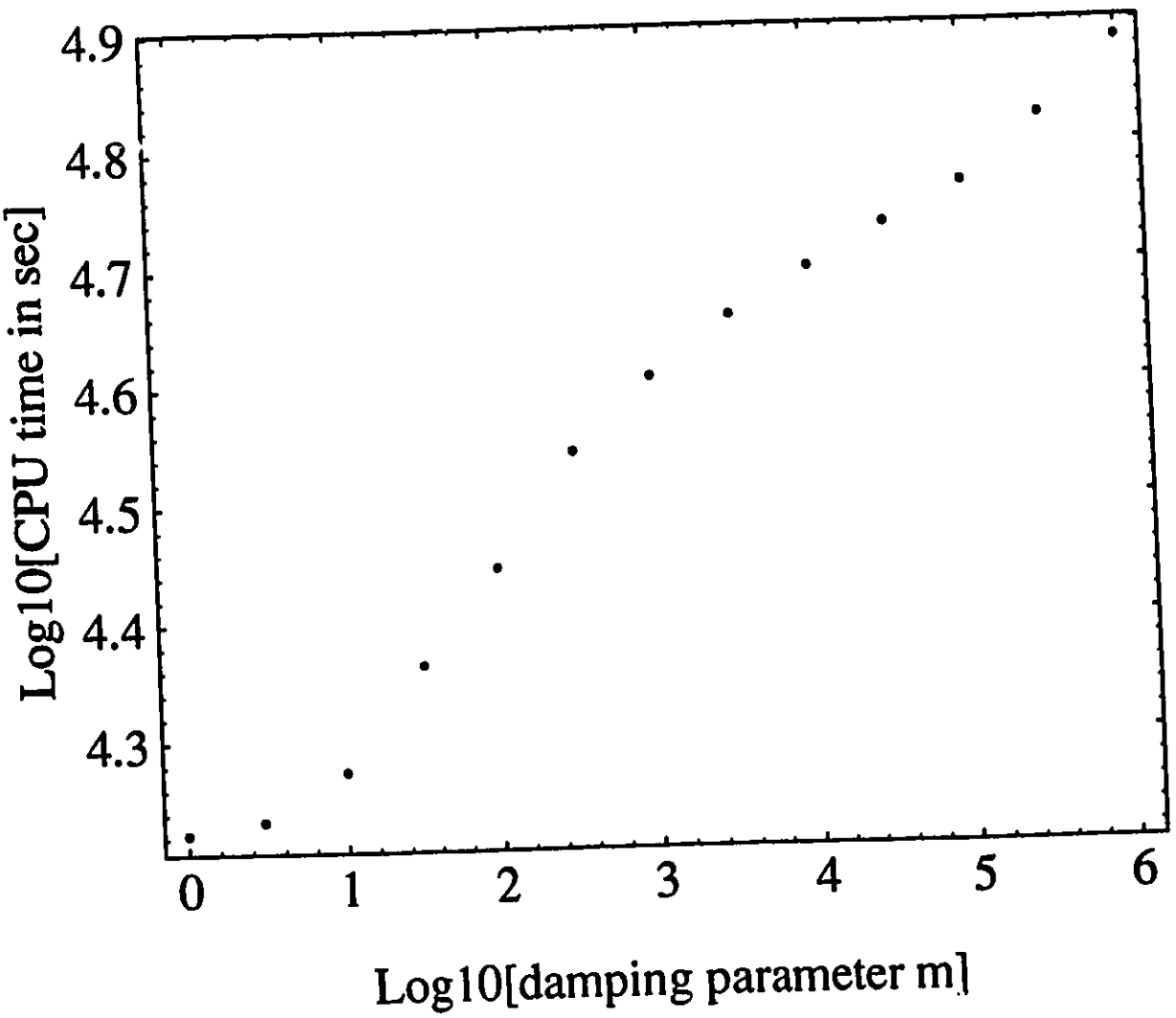

Fig. 3.8 - The effect of the damping parameter *m* on CPU time.

As for the effect of m on CPU process time, the results are plotted in Fig. 3.8. As can be seen, the CPU process time is a monotonic but slowly increasing function of the damping parameter m.

It is most fortunate, then, that one can improve simulation accuracy (i.e., by increasing m) significantly with little penalty with regards to the CPU time.

3.8.4 Effect of choice of $\Delta\tau_{max}$ on simulation accuracy.

When it comes to the choice of the maximum time increment $\Delta\tau_{max}$ with respect to simulation accuracy, there appears to be a slight overall effect: the larger the time increment, the larger the mean-square spring extension and the larger the error (see Table 3.2). The inclusion of a large damping constant tends to screen the net effect of increasing the maximum time increment. We note, however, that keeping the time increment relatively large possesses great advantages in the way of simulation time. For the purposes of verifying the effect on accuracy, we removed the maximum jump size (λ) constraint, removed all obstacles and fields, and carried-out the simulations for a molecule of 10 beads for a simulation time span of τ_{sim}=5 (in scaled units). The ensemble size for each run was 10000 chains and the simulation was performed on a Sun Sparcstation™ model 10 platform. We note that increasing the maximum time increment beyond a certain threshold value (within the range $\Delta\tau_{max}$≈0.1 to 1.0 for a 10 bead chain) actually slows down the simulation since the need to cut the time increment increases in frequency (the springs tends to overstretch more often). The trial results appear in the following table:

max time incr. $\Delta\tau_{max}$	$Log_{10}(\Delta\tau_{max})$	Mean-square spring extension $\langle(\Delta r)_{cc}^2\rangle$	Diffusion coefficient $\langle 2\times d_{cm}\rangle$	Rouse time τ_R	CPU time / 10^4 s Sparcstation 10
0.0001	-4	x: 0.07986 y: 0.08014	x: 0.1015 y: 0.09791	x: 1.41 y: 1.41	76.38
0.001	-3	x: 0.08019 y: 0.08035	x: 0.09960 y: 0.09772	x: 1.43 y: 1.51	8.66
0.01	-2	x: 0.08135 y: 0.08102	x: 0.09927 y: 0.09882	x: 1.39 y: 1.39	2.42
0.1	-1	x: 0.08200 y: 0.08214	x: 0.09928 y: 0.09826	x: 1.46 y: 1.42	1.64
1	0	x: 0.08267 y: 0.08248	x: 0.09981 y: 0.1007	x: 1.42 y: 1.40	1.83

Table 3.2 - The effect of the maximum time increment $\Delta\tau_{max}$ on the simulation accuracy. All runs were conducted with M=10, t_{sim}=5.0, m=1000, and an ensemble size of 10000 chains.

The effects of increasing the maximum time increment $\Delta\tau_{max}$ on the mean-square spring extension ($\langle(\Delta r)^2\rangle = \langle(\Delta r_x)^2\rangle + \langle(\Delta r_y)^2\rangle$ vs. $\Delta\tau_{max}$) is plotted in Fig. 3.9 and differs by no more than about 3% over a range of $\Delta\tau_{max}$ spanning four orders of magnitude! The effect of $\Delta\tau_{max}$ on the Rouse time is not significant (as can be seen from Table 3.2). In most cases of interest, however, we will generally try to use as large a time increment as possible for the desired size of the data set which is usually several hundred events; by an "event" in simulation time, we mean the state of the desired output statistics (e.g., the autocorrelation function of the end-to-end distance, the mean-square spring extension, etc.).

3.8.5 Conclusion

One must ensure that the damping factor m is reasonably high. As one can see, the threshold for the case of the free chain lies approximately at $m=1000$. Thus, for cases involving fields, it might prove prudent to increase the damping factor m by a factor of ten ($m=10000$). However, $\Delta\tau_{max}$ can be chosen large (e.g., $\Delta\tau_{max}$=0.5) for increased efficiency.

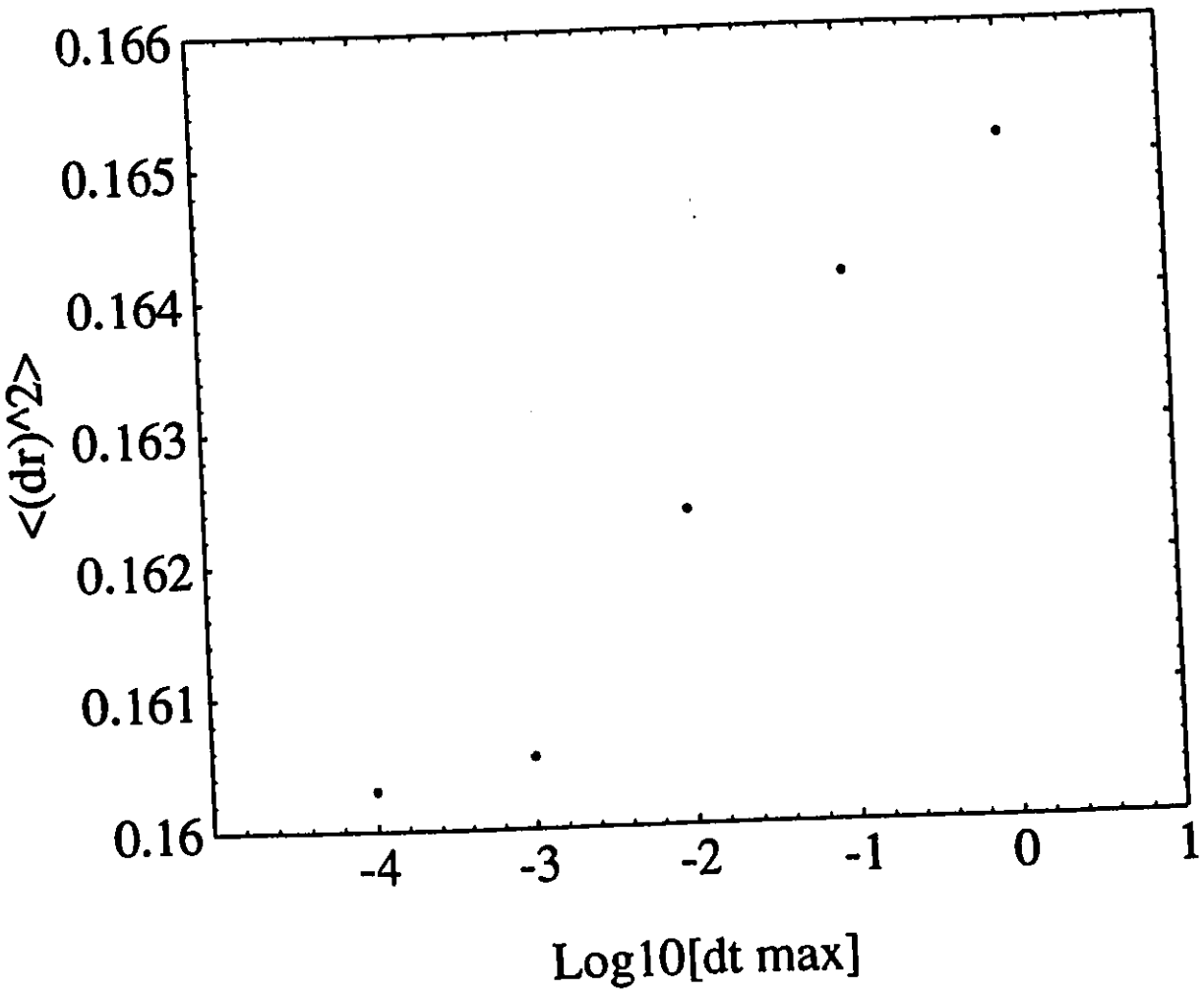

Fig. 3.9 - Plotted is the effect of the maximum time increment $\Delta\tau_{max}$ on the mean-square spring extension $\langle(\Delta r)^2\rangle$ for M=10 bead chains when the damping parameter is set at m=1000. We note that there is very slight over stretching of $\langle(\Delta r)^2\rangle$ above the expected value $\langle(\Delta r)^2\rangle_{Eq.(53)}$=0.161 with increasing $\Delta\tau_{max}$.

Chapter 4.

Case studies

4.1 Study of free chains in the absence of an electric field

Before embarking on a study of new problems it is prudent to first verify the algorithm for well known cases. In this section, we have carried out computer simulations of the statics and dynamics of polymer chains in a free-solution solvent in the absence of self-excluded volume or hydrodynamic interactions. Since the general aspects of the theory of Brownian motion of polymers have already been incorporated into the Rouse model, it provides us with a useful benchmark against which to test our integration scheme. From the Rouse model, we can predict analytically the large-scale dynamical behaviour of a bead-spring-like chain with harmonic springs. The nature of the spring force, as far as dynamics are concerned, only affects relaxation times (e.g., the Rouse time) but does not (and should not) affect the migration of the centre-of-mass of the system and, consequently, does not alter the diffusion coefficient or the mean velocity. As for the static properties, we expect the same scaling laws; the numerical coefficients will, of course, show marked discrepancies due to the use of nonlinear (anharmonic) entropic "spring" forces which have different mean properties (e.g., extension). We will examine here some static and dynamic properties obtained by numerically simulating the dynamical evolution of such chains.

4.1.1 Theoretical analysis

The consequences of the Rouse model are easily described when harmonic springs are used (see Section 2.3). It is then found that the Rouse time of a M-bead chain (for dimensionality d=2) is given by (the subscript zero denotes the use of harmonic springs)

$$t_{R_0} = \frac{\zeta M^2 \langle (\Delta R)^2 \rangle_0}{2\pi^2 k_B T} = \left(\frac{M}{\pi}\right)^2 \frac{\langle (\Delta R)^2 \rangle_0}{L^2} \tau_L \qquad (66)$$

where we have used Eq. (10), i.e., $\tau_L = \zeta L^2/2k_BT$. Therefore, using Eq. (28) for the mean-square spring extension for harmonic springs, i.e. $\langle (\Delta r)^2 \rangle_0 = \langle \Delta R^2 \rangle_0 / L^2 = 1/N$, (with N=5 segments per spring), we may write the Rouse time in scaled units

$$\tau_{R_0} = \frac{t_{R_0}}{\tau_L} = \left(\frac{M}{\pi}\right)^2 \langle (\Delta r)^2 \rangle_0 = \frac{(M/\pi)^2}{5} \qquad (67)$$

The diffusion coefficient of the centre-of-mass is given, in scaled units, by Eq. (45):

$$d_{cm} = \frac{1}{2M} \qquad (68)$$

The second moment of the end-to-end vector **p** is given by

$$\langle p^2_{x \text{ or } y} \rangle = (M-1) \langle (\Delta r_{x \text{ or } y})^2 \rangle \qquad (69)$$

and the radius of gyration, by

$$\langle r^2_{g_{x \text{ or } y}} \rangle = \frac{M+1}{6M} \langle p^2_{x \text{ or } y} \rangle = \frac{M^2-1}{6M} \langle (\Delta r_{x \text{ or } y})^2 \rangle \qquad (70)$$

For harmonic springs, the time-dependence of the autocorrelation function for **p** is given by

$$\langle \vec{p}(\tau)*\vec{p}(0)\rangle_0 = \langle p^2\rangle_0 \sum_{k=1,3,\ldots} \left[\frac{8}{k^2\pi^2}\exp\left(\frac{-\tau k^2}{\tau_{R_0}}\right)\right] \qquad (71)$$

where $\langle p^2\rangle_0=\langle p^2_x\rangle_0+\langle p^2_y\rangle_0$, and $\tau=t/\tau_1$, is the time in dimensionless units. Using our scaled units then, we may write

$$\ln\left[\frac{\langle \vec{p}(\tau)*\vec{p}(0)\rangle_0}{\langle p^2(0)\rangle_0}\right] \approx -\frac{\tau}{\tau_{R_0}} + const, \qquad \tau>\tau_{R_0} \qquad (72)$$

We see that the Rouse time τ_{R0}, defined by the longest relaxation time of the autocorrelation function, can be extracted by plotting the logarithm of the correlation function of the end-to-end vector **p** versus time.

4.1.2 Simulation Results

The results for various chain sizes M are presented in the Table 4.1 and in the accompanying graphs.

Static Properties

First, the static properties are to be verified against the known scaling laws. We take note, however, that the average spring extension will differ (i.e., be smaller) since our spring force includes the unharmonic terms and consequently, the spring force is greater. We find, once we average over all chains in Table 4.1, that the average spring extension is $\langle(\Delta r)^2\rangle_{springs} = \langle(\Delta r_x)^2\rangle + \langle(\Delta r_y)^2\rangle = 0.1624$, in excellent agreement with the theoretically predicted value (see Eq. (53)) of $\langle(\Delta r)^2\rangle_{theory} = 0.1610$.

#beads	5	10	15	20	40	80
τ_{warm}	1	5	10	16	60	260
τ_{sim}	5	10	20	30	120	520
$\langle(\Delta r_x)^2\rangle$ $\langle(\Delta r_y)^2\rangle$	0.08146 0.08158	0.08159 0.08142	0.08137 0.08128	0.08120 0.08120	0.08090 0.08092	0.08064 0.08058
$\langle p_x^2\rangle$ $\langle p_y^2\rangle$	0.3163 0.3171	0.7142 0.7063	1.097 1.094	1.487 1.484	3.049 3.054	6.309 6.052
Eq.(36)	0.32	0.72	1.12	1.52	3.12	6.32
$\langle r_{g_x}^2\rangle$ $\langle r_{g_y}^2\rangle$	0.06387 0.06398	0.1314 0.1304	0.1960 0.1954	0.2612 0.2611	0.5223 0.5236	1.067 1.033
Eq.(62)	0.064	0.132	0.1991	0.266	0.533	1.0665
$2\ d_{cmx}$ $2\ d_{cmy}$	0.2007 0.2030	0.1006 0.1004	0.0668 0.0668	0.0495 0.0489	0.0248 0.0250	0.0119 0.0126
Eq.(47)	0.2	0.1	0.0666	0.05	0.025	0.0125
τ_R in x	0.393	1.58	3.38	6.12	24.8	97.3
τ_R in y	0.394	1.55	3.34	5.99	23.4	94.1

Table 4.1 - Results for various chain sizes M in absence of electric field (ε=0). Here, τ_{warm} is the warmup period for the chain to relax from its initial conformation, and τ_{sim} is the simulation time. The maximum time increment for the numerical integration of the equations of motion was chosen to be $\Delta\tau_{max}$=0.05. The equations cited refer to the theoretically predicted values. The values of $\langle(\Delta r_x)^2\rangle$...$\langle r_{gy}^2\rangle$ are the mean values during the whole simulation time τ_{sim}. Both d_{cmx} and d_{cmy} were computed from fitting the mean squared displacement of r_{cmx} and r_{cmy}, respectively, versus time. The Rouse time τ_R was calculated using a nonlinear fitting function (using Mathematica™) and Eq. (72). The damping parameter was m=1000 for all runs while the ensemble size was 10000 chains except for the 80 bead run which used an ensemble size of 3001 chains.

Now, as is customary, we can demonstrate the scaling behaviour of polymers by plotting the mean-square end-to-end vector (see Fig. 4.1) with the following scaling form in mind:

$$\langle p^2 \rangle = (M-1)^{\alpha} \langle (\Delta r)^2 \rangle_p \tag{73}$$

which was fitted with a log-log graph yielding α=0.9958 and $\langle (\Delta r)^2 \rangle_p$=0.1589 (or 0.1570 when we force the fit with α=1). This fit conforms well with the predictions of the Eqs. (36), (53) and (69). The mean-square radius of gyration is plotted in Fig. 4.2 as a function of M and was fitted with Eq. (40) in mind. We find that the best fit is

$$\langle r_g^2 \rangle = \frac{M^2-1}{6M} \langle (\Delta r)^2 \rangle_{r_g} = \frac{M^2-1}{6M} (0.1579) \tag{74}$$

which is the correct scaling if we take into account the statistical error inherent to this fitting scheme. We note that all computed averages for the mean-squared spring extension ($\langle (\Delta r)^2 \rangle_{springs}$=0.1624, $\langle (\Delta r)^2 \rangle_{r_g}$=0.1579 and $\langle (\Delta r)^2 \rangle_p$=0.1570) are in reasonable agreement with $\langle (\Delta r)^2 \rangle_{theory}$=0.1610. Note that the value of $\langle (\Delta r)^2 \rangle_{springs}$ is computed with a larger ensemble and, consequently, is the more accurate average. Also note that $\langle (\Delta r)^2 \rangle_{springs}$ more closely approximates $\langle (\Delta r)^2 \rangle_{theory}$=0.1610 as $M \to \infty$ (see Table 4.1); this is due the fact that the algorithm then diminishes the mean time increment $\langle \Delta\tau \rangle$ since the probability of requiring a cut of the time increment increases with the number of beads in the chain. Thus, the integration of the equations of motion (Eq. (12)) is smoother and more accurate.

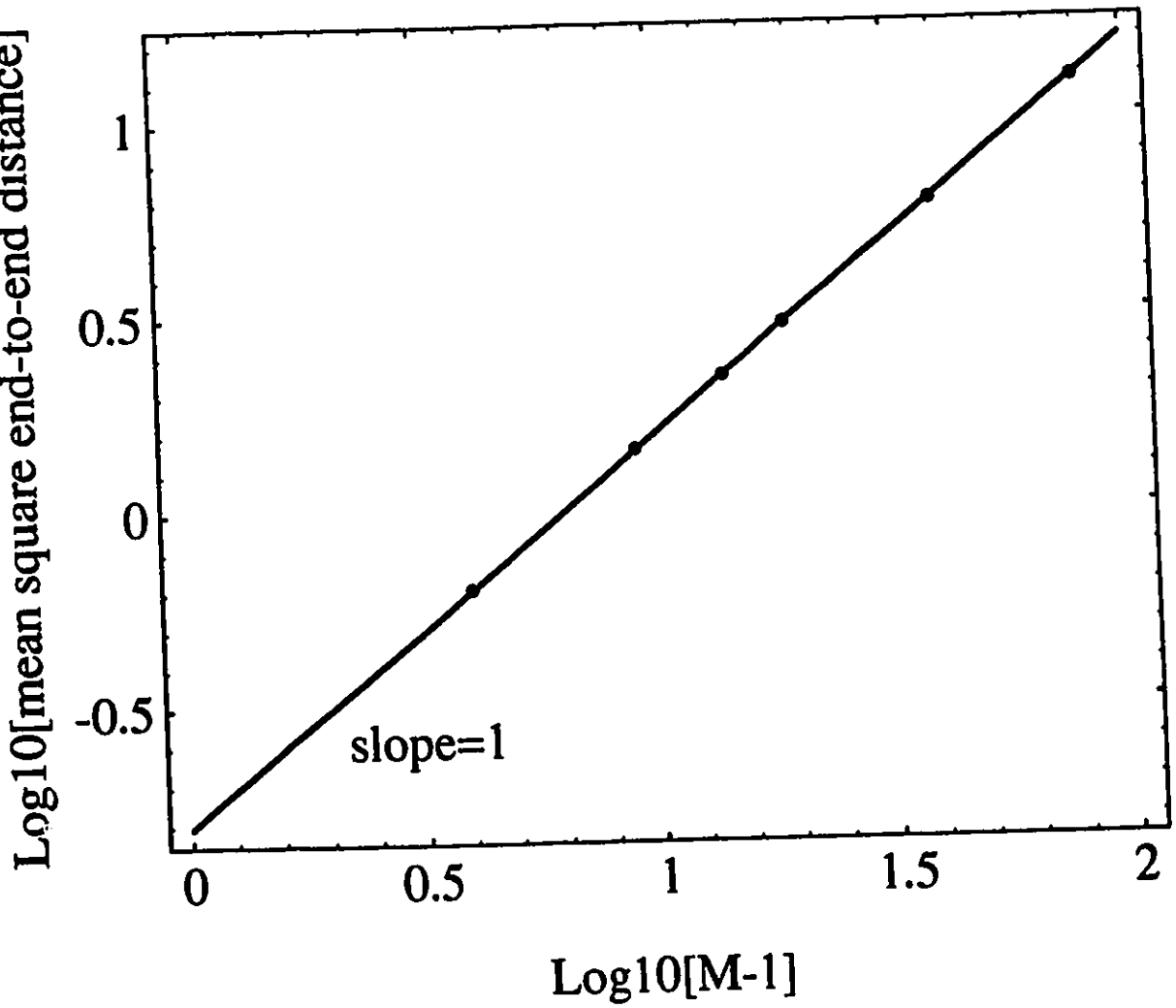

Fig. 4.1 - Log-Log plot of the mean-square end-to-end distance $\langle p^2 \rangle$ vs. the number of springs (M-1).

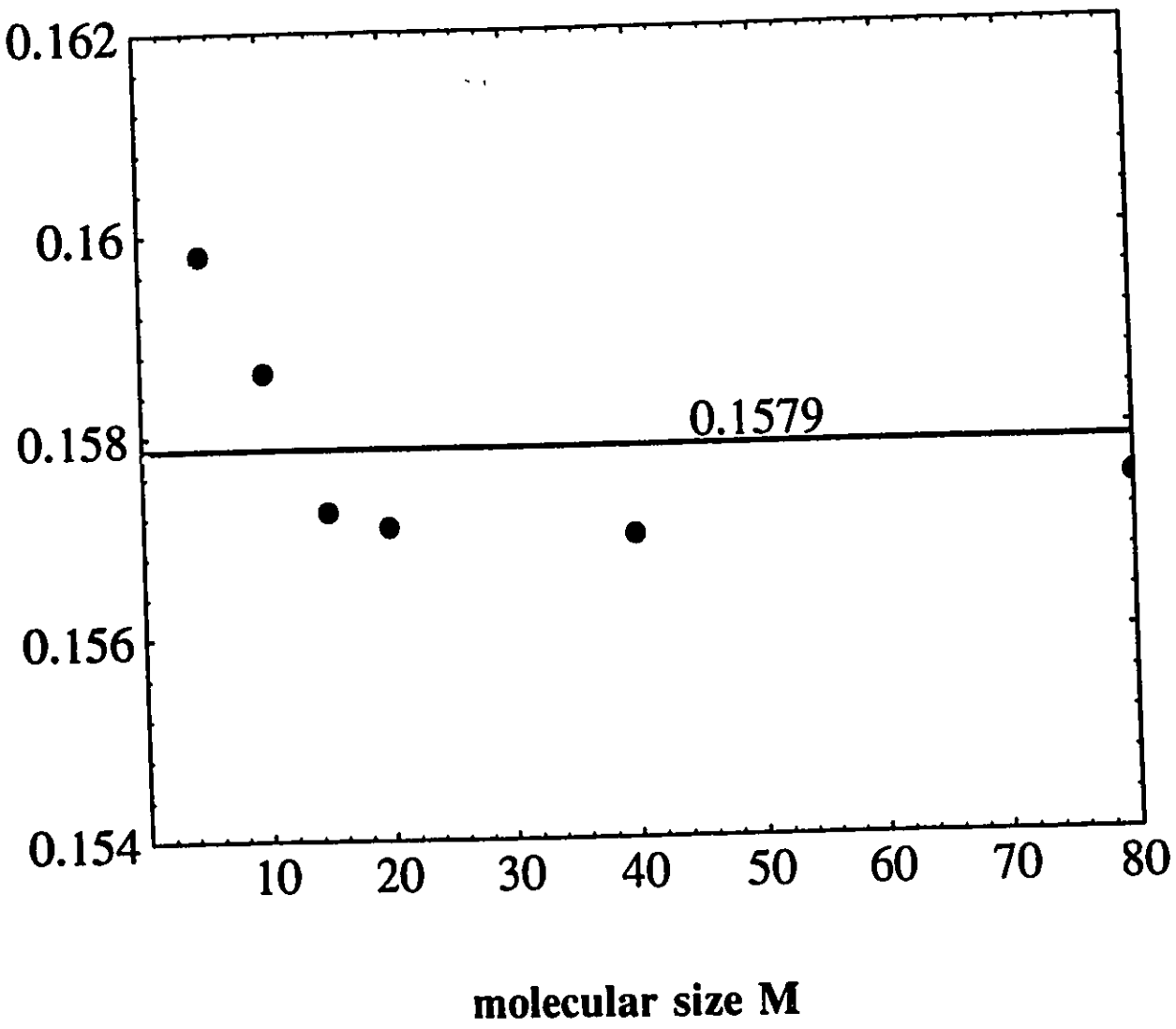

Fig. 4.2 - The Log-Log plot of 6 M $\langle r_g^2 \rangle$ / (M^2-1) vs. molecular size M.

Dynamic Properties

In this section, we present two dynamical properties of the single polymer chain, namely the diffusion coefficient of the centre-of-mass and the relaxation time of the autocorrelation function of the end-to-end vector **p**. These properties have a scaling behaviour which is demonstrated in graphs which follow this discussion. First, the diffusion coefficient, as obtained from the slope of $\langle(\Delta r_{cm})^2\rangle$ vs. τ (see, e.g., Fig. 4.3), was found to obey the relationship

$$d_{cm} = \frac{\alpha}{2} M^{\beta} = \frac{0.9729}{2} M^{-1.011} \tag{75}$$

When re-fitted, forcing $\beta=-1$, we yield the result (see Fig. 4.4)

$$d_{cm} = \frac{1.004}{2} \frac{1}{M} \tag{76}$$

which is accordance with Eq. (68).

From Eq. (67), we expect the terminal relaxation time of the autocorrelation function of the end-to-end vector **p**, in the linear region of the $\ln[\langle \mathbf{p}(\tau)\cdot\mathbf{p}(0)\rangle]$ vs. τ plot (where $-1/\tau_R$ is given by the slope, as seen from Fig. 4.5), to obey a scaling relation of the form

$$\tau_R = \frac{1}{C}\left(\frac{M}{\pi}\right)^{\beta} \tag{77}$$

We find that $\beta=1.981$ and $C=6.423$. Confident that τ_R does indeed scale as M^2, just as in the harmonic case, we re-fit, forcing $\beta=2$, and now find that $C=6.646$ (see Fig. 4.6), that is,

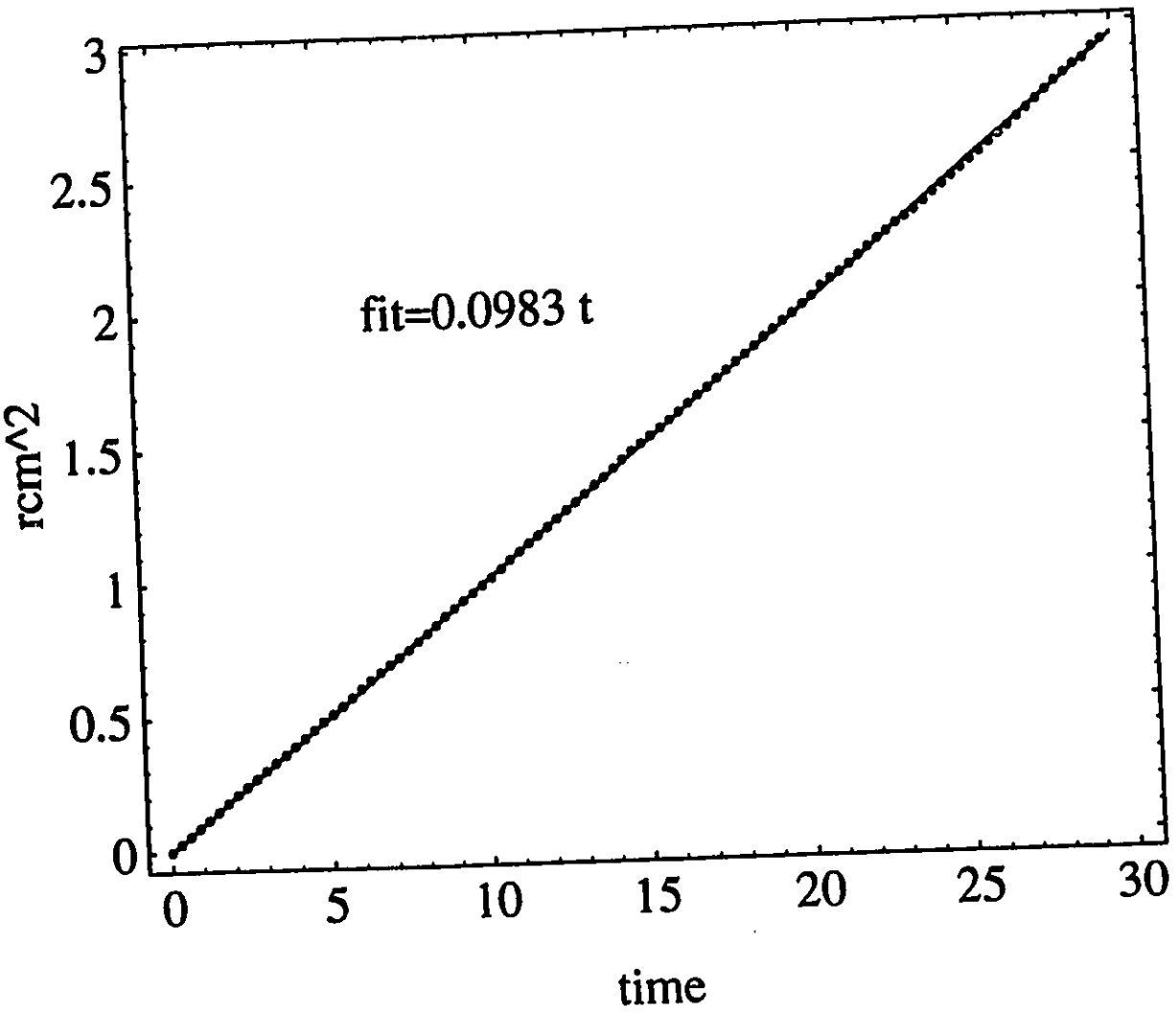

Fig 4.3 - Plot of the mean position of the centre-of-mass $\langle r_{cm}^2 \rangle$ versus time τ for a M=20 bead chain. The slope equals $4 \times d_{cm}$ and thus determines the diffusion coefficient d_{cm}. The warmup time was τ=20, the damping parameter was m=1000, and the ensemble size was 10000 chains.

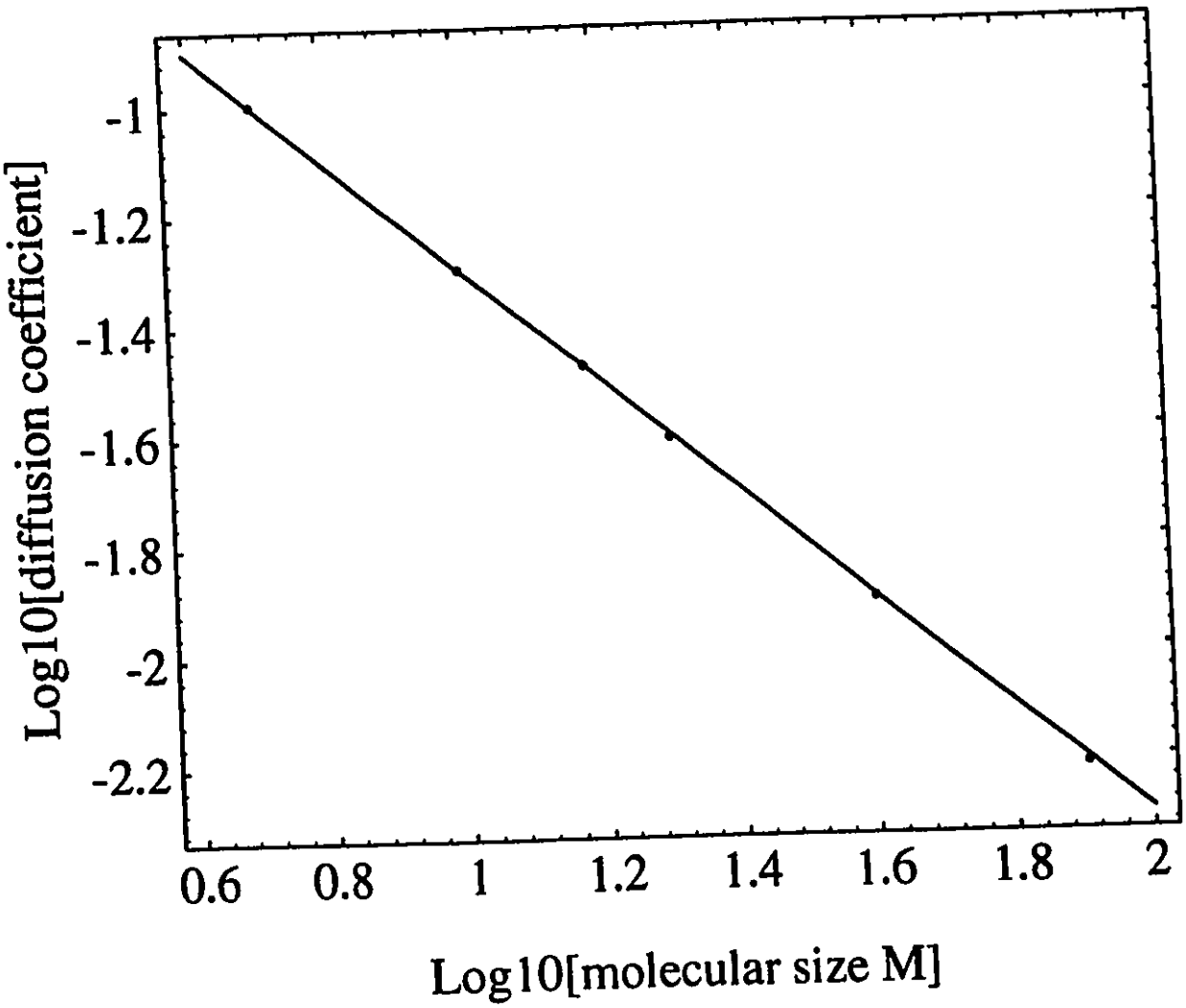

Fig 4.4 - Plot of the diffusion coefficient d_{cm} versus the number of beads M (molecular size).

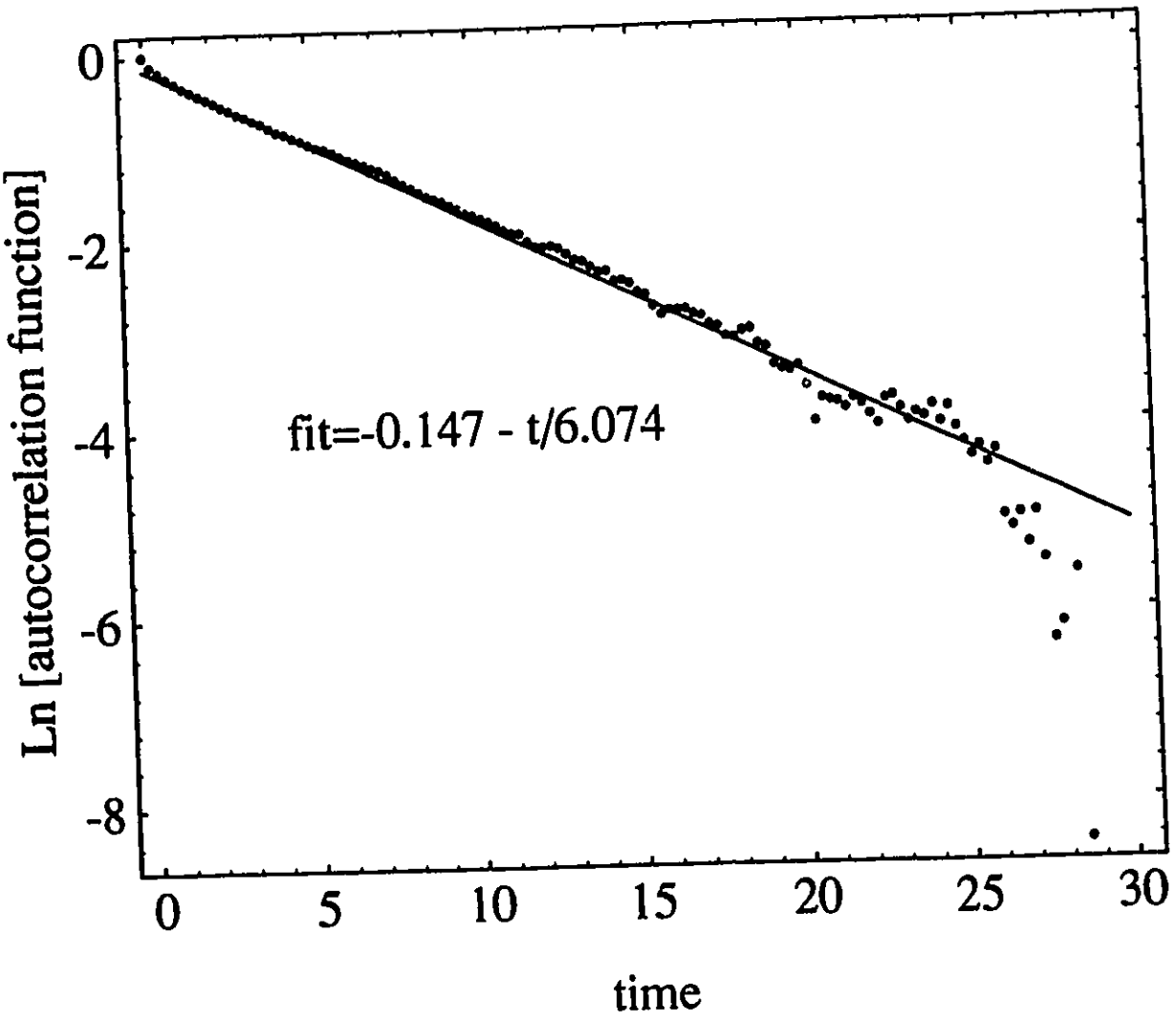

Fig. 4.5 - Plot of the natural logarithm of the two-dimensional autocorrelation function (not the one-dimensional components x or y) of the end-to-end vector versus time τ for a M=20 bead chain; the slope of the linear part equals $-1/\tau_R$ and thus determines the Rouse time τ_R. Consult the legend of Fig. 4.3 for further details.

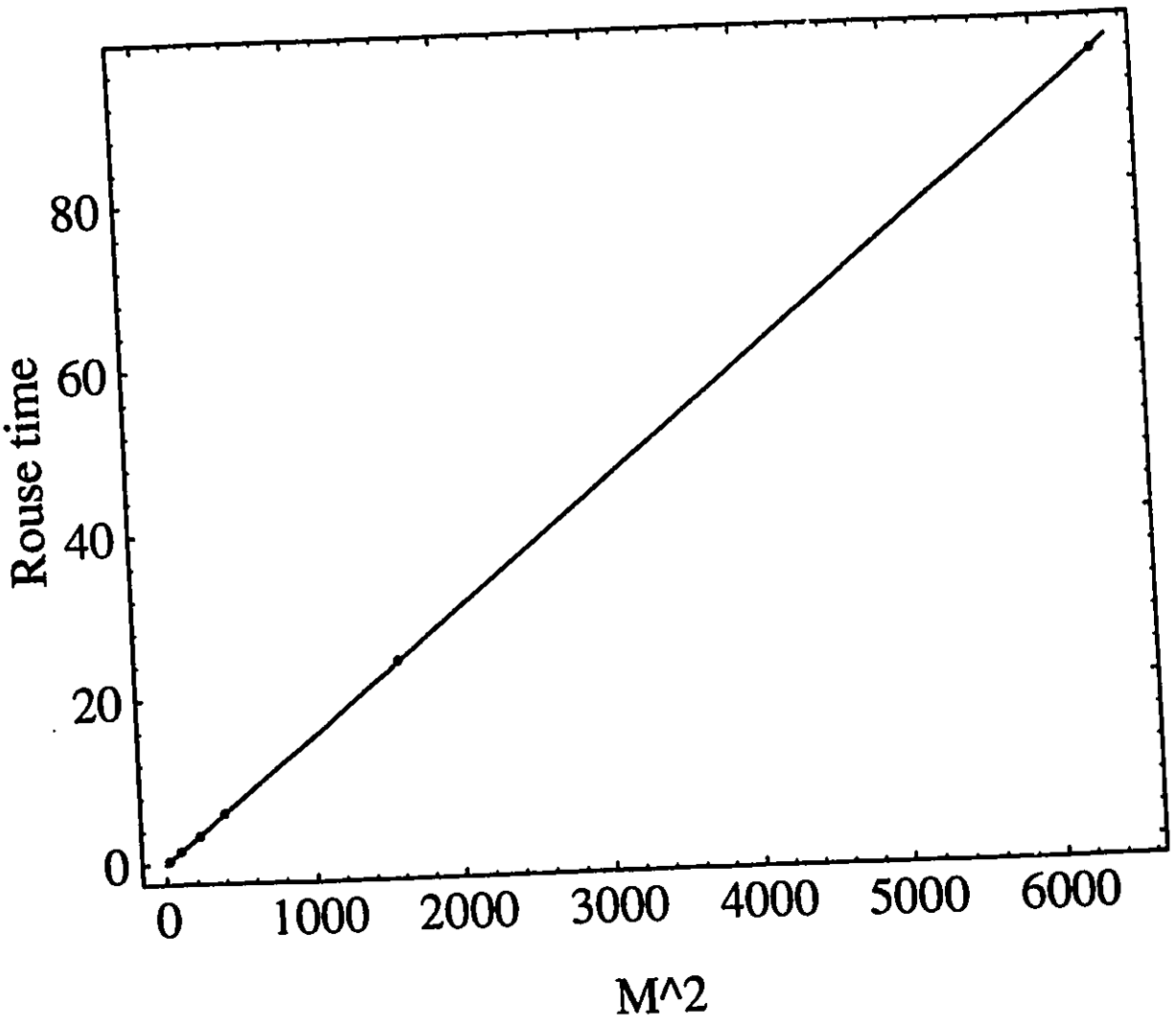

Fig. 4.6 - The Rouse time is shown to follow the power law $\tau \sim M^2$.

$$\tau_R = \frac{1}{6.646}\left(\frac{M}{\pi}\right)^2 \qquad (78)$$

The fitted value for the constant C contrasts with the harmonic result $C_{harm}=N=5$ (see Eq. (67)) and indicates that anharmonic springs cause the chain to relax faster than harmonic springs.

How do we explain Eq. (78)? We can replace the (M-1) springs joining the chain ends with one equivalent spring along the axis of the end-to-end vector **p** with mean-square length $\langle p^2\rangle=(M-1)\,\langle(\Delta r)^2\rangle$. This is valid regardless of the nature of the springs if M≫1. We then use a simple force balance equation[29] for **p** valid for small extensions (harmonic limit): $\zeta_M \partial \mathbf{p}/\partial\tau + k_{(M-1)}\mathbf{p} = 0$ where ζ_M is the global friction term (for M beads) and $k_{(M-1)}$ is the effective spring constant for (M-1) springs (taken as monomers). This equation yields $\tau_R=\xi_M/k_{(M-1)}$ and, using the harmonic result (for d=2 dimensions) $k_{(M-1)} = 2k_BT/\langle p^2\rangle = 2k_BT/(M-1)\langle(\Delta r)^2\rangle$, we have directly the relation $\tau_R \sim \langle(\Delta r)^2\rangle$ and hence, $\tau_R/\tau_{R0} = \langle(\Delta r)^2\rangle/\langle(\Delta r)^2\rangle_0$, independent of M. Therefore, the mean-square spring extension, from our fitted value of $\tau_R(M)$, is given by

$$\langle(\Delta r)^2\rangle_{\tau_R} \approx \frac{\tau_R(M)}{\tau_{R_0}(M)}\,\langle(\Delta r)^2\rangle_0 = \left(\frac{5}{6.646}\right)\frac{1}{5} = 0.1505\,, \quad M \gg 1 \qquad (79)$$

independent of M, and is in fair agreement with our previous results. We note, therefore, that anharmonic springs reduce the Rouse time τ_R by making the springs (hence the chain) more compact, *not* because having stiffer springs changes the overall behaviour of the relaxation process of the end-to-end vector **p**. It follows that stiffer springs will change the small-lengthscale relaxation times $\tau_p=\tau_R/p^2$ as well, but this was not pursued further.

---

[29]Here, we follow the method of Kuhn and Péterlin using the dumbbell model. See de Gennes (1990), pp. 4-5.

4.2 A polymer chain in a narrow tube

The dynamics of a polymer chain confined into straight tubes is a variation of the isotropic case described above. Scaling considerations will be re-examined with particular emphasis on the coordinate perpendicular to the tube axis. Brownian dynamics simulations of chains of M=15 and M=200 beads in tubes with diameters (in our scaled units) $d_T \in [0.25,16]$ and $d_T \in [2.5,4]$, respectively, are presented and analyzed in terms of scaling models. While the scaling predictions for measurements along the tube axis are the same as that of the free chain, the simulations reveal interesting features in the direction perpendicular to the tube axis: (i) The mean-square radius of gyration $\langle \mathbf{r}_g^2 \rangle$ in the direction of the tube diameter is a simple function of the tube diameter in the limit where the springs are not compressed, and the number of beads, M, is large enough. This behaviour is discussed in terms of the analogy with a one-dimensional polymer chain composed of blobs. (ii) The relaxation time of the end-to-end vector $\mathbf{p}$ of the M=200 bead chain along the direction parallel to the tube diameter is a simple function of the tube diameter d_T; this is explained in terms of the relaxation of the individual blobs.

4.2.1 Theoretical analysis of chains confined into tubes

As we begin to confine a polymer within a tube, the polymer beads are being subjected to a confinement potential yielding a force that acts only in a direction perpendicular ($\perp$) to the tube axis. The static and dynamic properties of the polymer in the direction parallel ($\parallel$) to the tube axis are not expected to differ from the free-chain expectation values since we are employing RW polymers. As for the direction $\perp$ to the tube axis, we expect, for large enough

polymer chains (such as the M=200 bead chains we employed), that the static and dynamical properties can be analyzed according to the following blob model.

We examine the case of a large chain squeezed in a narrow[30] tube with $\langle(\Delta r)^2\rangle \ll d_T^2 \ll \langle r_g^2\rangle$, where d_T is the tube diameter, $\langle(\Delta r)^2\rangle$ is the mean-square spring extension in the absence of a tube, and $\langle r_g^2\rangle$ is the mean-square radius gyration in the absence of the tube. We employ a method exploited by de Gennes[31] where we introduce the notion of a blob, which is defined as the largest section of the chain that is small enough to be left unperturbed by the constraints. Since the tube has a diameter d_T, the blob size $\langle r_{g\perp}^2\rangle^{1/2}$ is expected to follow a relation of the form (see Eq. (70))

$$\left\langle r_g^2 \right\rangle = \frac{M_{blob}^2 - 1}{6M_{blob}} \left\langle (\Delta r_\perp)^2 \right\rangle \approx \frac{M_{blob}}{6} \left\langle (\Delta r_\perp)^2 \right\rangle \sim \left(\frac{d_T}{2}\right)^2 \tag{80}$$

where M_{blob} is the number of beads per blob (assumed large). From this last relation, we can isolate for the number of beads per blob

$$M_{blob} = \frac{6\left\langle r_{g_\perp}^2 \right\rangle}{\left\langle (\Delta r_\perp)^2 \right\rangle} \sim \frac{d_T^2}{\left\langle (\Delta r_\perp)^2 \right\rangle} \tag{81}$$

and predict that the relaxation time (see Eq. (67)) in the direction perpendicular to the tube axis will follow the following scaling form

---

[30] i.e., the tube diameter must be much smaller than the free radius of gyration of the chain such as to permit the creation of several blobs but not so narrow as to compress the springs themselves (some lateral wiggling must be permitted).

[31] See de Gennes (1979), pp. 34-35, 49-51, 91.

$$\tau_{R\perp} = \tau_{blob} = \left(\frac{M_{blob}}{\pi}\right)^2 \langle(\Delta r_\perp)^2\rangle \sim \frac{d_T^4}{\langle(\Delta r_\perp)^2\rangle} \qquad (82)$$

Therefore, we expect the transverse Rouse relaxation time to scale as d_T^4.

4.2.2 Numerical results

The results for M=15 bead chains within tubes of diameters d_T=0.25 to d_T=16 are presented in Table 4.2. The statistics generated for the ∥ direction compare directly with the results for the free chain (cf. Table 4.1). This demonstrates that, in spite of severe constraints, namely confining the chain within a narrow tube, our simulation algorithm produces the correct averaging statistics just as we would expect for a RW chain in the ∥ direction.

In the direction ⊥ to the tube axis, we are confronted with two limiting effects. Firstly, in the case of the M=15 bead chain, the number of beads is small and therefore the free radius of gyration $\langle r_g^2\rangle_{free}^{1/2}=[(M^2-1)/(6M)\langle(\Delta r)^2\rangle_{free}]^{1/2}=(0.3982)^{1/2}=0.6310$ is small compared with the largest tube radius $d_{T\,max}/2=8$. However, the smallest tube radius $d_{T\,min}/2=0.125$ is much smaller than the free radius of gyration but not small enough to create several blobs in the chain. Secondly, the smallest tube diameter is smaller than the free spring extension in the ⊥ direction $\langle(\Delta r_\perp)^2\rangle_{free}^{1/2}=(0.081)^{1/2}=0.28$. Therefore the interpretation of the M=15 bead results for the ⊥ direction is not readily portable to any set method such as the blob model. Moreover, under such circumstances, the results are non physical since the springs are compressed by the wall potential (something that should be avoided with this model). In circumstances where the lengthscales in the ⊥ direction are of interest, the appropriate measure is to rescale the dimensions of the polymer so that the springs are of a scale below dimensions of relevance; the bead-spring model

d_T	16	8	4	2	1	0.5	0.25
#chains	6501	6500	10000	10000	10000	1815	249
$\langle(\Delta r_\perp)^2\rangle$ $\langle(\Delta r_\parallel)^2\rangle$	0.07966 0.08001	0.07913 0.08012	0.07739 0.08064	0.07054 0.08049	0.05326 0.08160	0.02522 0.08211	0.007884 0.08454
$\langle p_\perp^2\rangle$ $\langle p_\parallel^2\rangle$	1.063 1.116	1.024 1.107	0.8041 1.114	0.3994 1.113	0.1168 1.138	0.0275 0.9040	0.008322 1.205
$\langle r_{g\perp}^2\rangle$ $\langle r_{g\parallel}^2\rangle$	0.1929 0.1987	0.1872 0.1976	0.1588 0.1991	0.1010 0.1993	0.04195 0.2028	0.01387 0.1912	0.003831 0.2139
$2\ d_{cm\parallel}$	0.06537	0.06597	0.06647	0.06554	0.06597	0.04849	0.06896
$\tau_{R\perp}$	3.50	3.32	2.83	1.42	0.157	0.015	0.01029
$\tau_{R\parallel}$	3.63	3.40	3.51	3.56	3.82	4.44	4.25

Table 4.2 - Results for M=15 bead chains in tubes with no electric field (ε=0). The warmup period for the chain to relax from its initial state (conformation) was chosen to be τ_{warm} =5 (>$\tau_{R\parallel}$=3.431). The simulation time was also set to τ_{sim} =5, the maximum time increment was $\Delta\tau_{max}$=0.01 in scaled units, and the damping parameter was set to m=1000. The values of $\langle(\Delta r)_{\perp\ or\ \parallel}^2\rangle$...$\langle r_{g\perp\ or\ \parallel}^2\rangle$ are the mean values during the whole simulation time τ_{sim}. The diffusion constant parallel to the tube axis, $d_{cm\parallel}$, was computed from fitting the mean squared displacement of y_{cm} versus time (e.g., see Fig. 4.3). The relaxation times $\tau_{R\parallel or\perp}$ were obtained from fitting the linear portion of the graph $Ln\langle p(\tau)*p(0)\rangle_{\parallel or\perp}$ vs. time τ which yields a slope of $-1/\tau_{R\parallel or\perp}$ (e.g., see Fig. 4.5).

is not meant for studies of lengthscales of the order of the spring size. The main motivation for carrying out the simulations in the case of the M=15 beads was to demonstrate the ability of the integration scheme to handle such extreme confinement scenarios as well as handle the great forces inherent to such constraining situations. Furthermore, we wished to demonstrate that the direction ∥ to the tube axis remains unaffected and this was shown to be the case. This does not imply, however, that the polymer, under simulation conditions, does not have any confinement situations that would occur over these ranges. For this reason, and to demonstrate the coping ability of the algorithm w.r.t. the resulting stresses, we ran several simulations under various confinement conditions. One should note the advantages, namely, the savings in way of memory and CPU time, when a chain with fewer beads can be substituted for one with more beads, especially when the statistics sought do not require many beads

If we are to have any of the predictive power that the blob model affords, we need to ensure that the springs are not compressed (i.e., that d_T is large compared with $\langle(\Delta r_\perp)^2\rangle_{free}^{1/2} \approx ((0.08)^{1/2} \approx 0.28)$ so that some lateral wiggling is afforded. We must also ensure that the free radius of gyration is large compared with $d_T/2$ (the tube radius); this allows for the creation of a large number of blobs. In Table 4.3, we have data for a 200 bead chain confined within a tube of various diameters $d_T \in [2.5, 4]$, which will be analyzed in terms of the blob picture. We note, from the table, that the spring extension, in the direction ⊥ to the tube axis, is relatively constant[32] for the range of diameters studied, and nearly equal with the free spring extension (last column of Table 4.3).

---

[32]There were practical considerations to be made in the way of CPU time. Obviously, using a chain with many more springs and larger diameters could be used if we wish better conformity with the blob picture.

d_T	2 1/2	3	3 1/3	3 1/2	3 2/3	4	∞
#chains	1206	1907	1397	896	1247	592	theory
$\langle(\Delta r_\perp)^2\rangle$	0.07329	0.07512	0.07595	0.07628	0.07658	0.07708	0.0810
$\langle p_\perp^2\rangle$	0.6416	0.8891	1.080	1.214	1.291	1.526	16.12
$\langle r_{g\perp}^2\rangle$	0.2198	0.2955	0.3530	0.3825	0.4151	0.4773	2.700
$\tau_{R\perp}$	2.74	4.82	5.88	7.45	8.63	11.4	609.8

Table 4.3 - Collected data for the case of M=200 bead polymers confined within a tube of various diameters d_T. Here, the blob picture will be applied and we present only the information of interest, namely in the direction $\perp$ to the tube axis. The last column represents results for a free chain (see Sect. 4.1). The damping parameter was chosen to be m=1000 and the warmup time was chosen to be τ_{warm}= 5 to 10, the simulation time τ_{sim}= 5 to 10 (i.e., longer times were used for larger tube diameters), and the maximum time increment was chosen to be $\Delta\tau_{max}$=0.025. The electric field strength was ε=0.0.

4.2.3 Analysis of the results for M=200 in the direction ⊥ to the tube axis

4.2.3.1 Static properties

We find that the transverse radius of gyration (see Fig. 4.7) is consistent with Eq. (80):

$$\left\langle r_{g_\perp}^{\,2} \right\rangle = const.\ d_T^{\alpha} = 0.04811\ d_T^{1.6557} \tag{83}$$

which is in fair agreement with the expected power law, namely $\alpha=2$. With $\alpha=2$, we obtain:

$$\left\langle r_{g_\perp}^{\,2} \right\rangle = 0.03114\ d_T^{2} \tag{84}$$

We estimate from Table 4.3 and Eq. (80) (using the tabulated mean-square spring extensions in the ⊥ direction) that the number of beads per blob varies from $M_{blob}=18$ to $M_{blob}=37$ with increasing d_T. Consequently, we have of the order of 5 to 11 blobs in the M=200 bead chain for the respective tube diameters $d_T=4$ and $d_T=2.5$. We can therefore, at best, expect semi-quantitative agreement with the predicted scaling forms since the number of blobs is not very large (thus incurring finite size effects). Moreover, the springs are slightly compressed.

4.2.3.2 Dynamic Properties

The transverse Rouse relaxation time $\tau_{R\perp}$ of the autocorrelation function of the end-to-end distance $\mathbf{p}_\perp$ was verified against the scaling predictions of Eq. (82). The best straight-line fit yields (Fig. 4.8):

$$\left\langle \tau_{R\perp} \right\rangle \times \left\langle \Delta r_\perp^2 \right\rangle = 0.003623\ d_T^4 \tag{85}$$

The results are excellent even though the number of springs per blob was fairly small and the springs somewhat compressed.

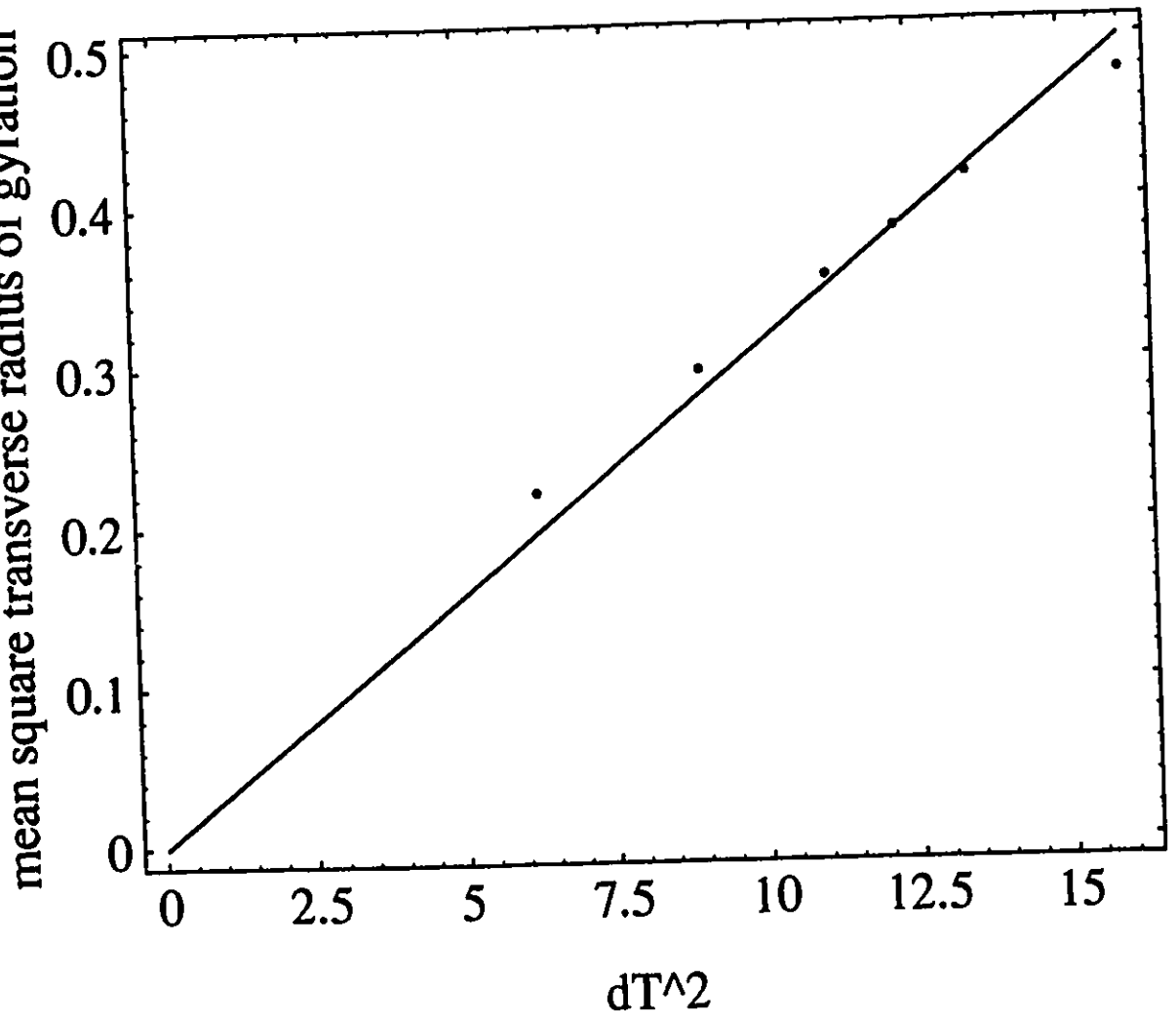

Fig. 4.7 - Transverse radius of gyration as a function of tube diameter for a large M=200 bead chain (consult legend of Table 4.3 for details).

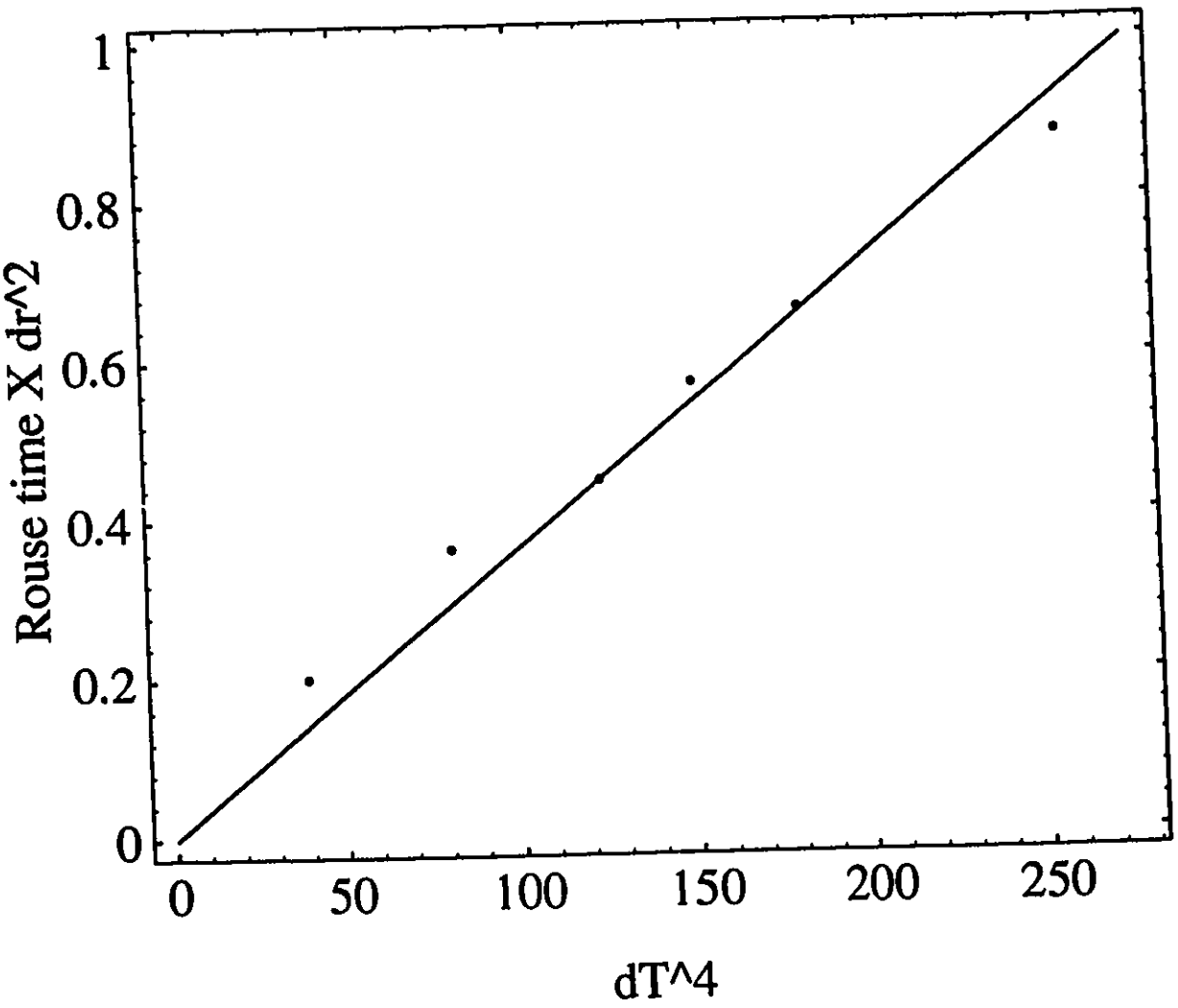

Fig. 4.8 - Relaxation time of the chain in the transverse direction times the mean-square spring extension as a function of tube diameter (consult legend of Table 4.3 for details).

4.3 Simple electrophoretic collisions

We now consider the electrophoretic collision between an obstacle (e.g., a gel fibre) and a large diffusing polyelectrolyte[33]. Collisions may be considered to be the basic elementary sieving phenomenon behind all electrophoretic separation methods. This fact is beautifully demonstrated in the case of electrophoretic pinning and this situation has been shown to occur in experiments using even moderate field intensities[34] (also see Fig. 3.1). Here we will analyze the underlying mechanisms of a collision/pinning/escape/relaxation process between a linear polyelectrolyte, such as DNA, with a single isolated obstacle centred in a narrow channel (or capillary) as depicted in the series of movie slides of Fig. 4.9. We assume, implicitly, that the charge per bead q=Q/M is positive (unlike DNA) in order to omit negative signs in the analysis.

4.3.1 Theoretical analysis

Let us make some simplifying assumptions, namely: (i) the chain stretches fully before slipping and (ii), the springs relax much slower than the unravelling time τ_{esc} of the chain; the mean spring extension, consequently, may be considered as constant during the process. Both of these assumptions amount to requiring large electric fields ε. We may then describe the pinning process, giving rise to U-shaped conformations, as a random process equivalent to a 1-d random walk with the number of springs (steps) in each arm (branch) being n_1 and $n_{2,}$, respectively, and the total number of steps being $n=n_1+n_2$ (see Fig. 4.10). The total number of

---

[33]See Nixon and Slater (1994).

[34]See, for example, Gurrieri et al. (1990); Schwartz and Koval (1989); and Volkmuth and Austin (1992).

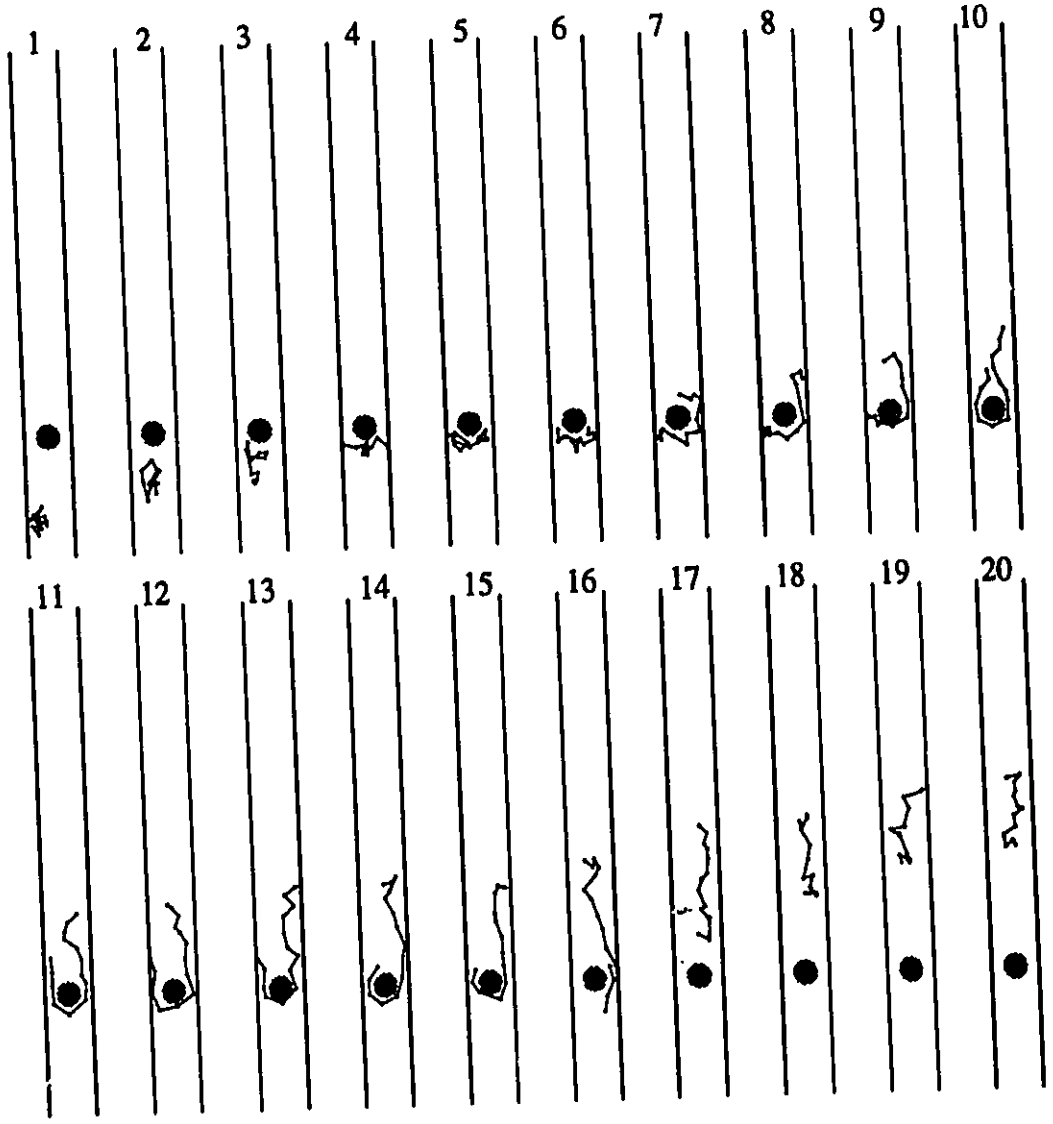

Fig. 4.9 - A M=15 bead polyelectrolyte, subjected to an electric field ε=1.0 (directed vertically upward) is incident on an obstacle of diameter $2\rho_{obst}$=1.0 within a tube of diameter d_T=2.0. The time span between frames is $\Delta\tau_{frame}$=13/12. Initially (frames 1-2), the chain is in free drift with a free-drift velocity $v_0=\varepsilon$ (independent of M). In frames 3-10, a U-shape or pulley conformation is formed where the springs become very stretched. In frames 11-16, the chain unravels (escapes) from the pulley scenario before continuing once again in free drift in frames 17-20. Note that, in the final free-drift stage, the chain relaxes back to a random-walk conformation (just as before the onset of collision).

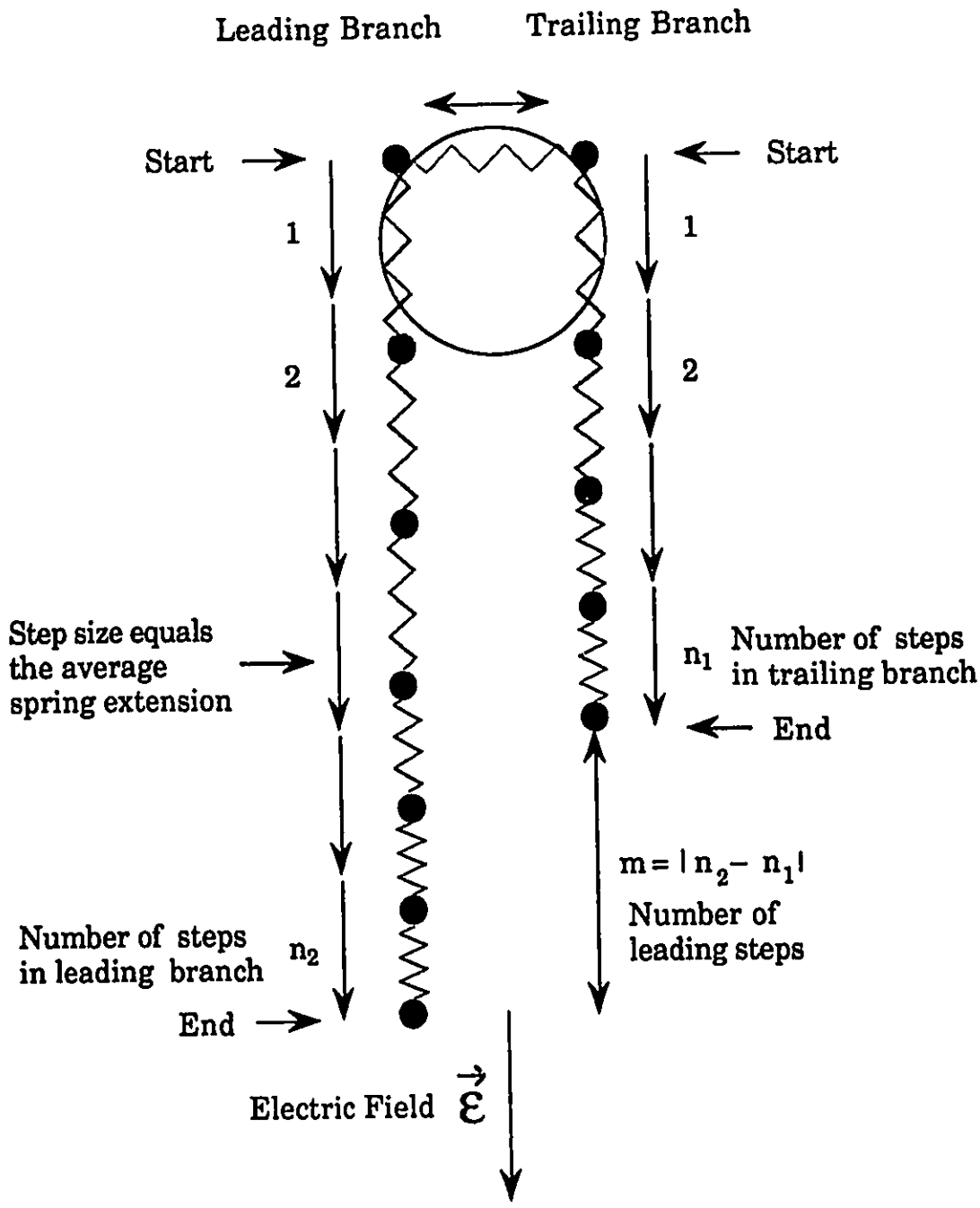

Fig. 4.10 - Simplified schematic portraying the geometry of a simple pinning process. The mean spring extension $\langle \Delta r \rangle$ acts as a fundamental unit step length. The total number of steps is $n=M-1=n_1+n_2$ where n_1 and n_2 are the number of steps in the respective arms (branches).

springs (steps) is n = M − 1 where M is the number of beads. If we define the difference in the number of springs between the two branches (the "impact parameter") as

$$m = |n_2 - n_1| > 0 \tag{86}$$

then the probability of having such a conformation is simply given by the binomial distribution

$$P_n(m) = \frac{n!}{[(n+m)/2]!\ [(n-m)/2]!} \left(\frac{1}{2}\right)^n \tag{87}$$

from which we can derive the ubiquitous Gaussian distribution function approximation

$$p(h) = \left(\frac{2}{\pi n \langle \Delta r \rangle^2}\right)^{1/2} \exp\left[-\frac{h^2}{2n\langle \Delta r \rangle^2}\right] \tag{88}$$

where p(h) dh is the probability of having an end-to-end distance h within a range dh centred about h. Here we have implicitly defined the net (positive) distance between the end beads, in the direction of ε, as

$$h = m \langle \Delta r \rangle' \tag{89}$$

This, therefore, is the defining relation between h and m. Our chosen unit step distance $\langle \Delta r \rangle'$ being approximately equal to the average spring extension $\langle \Delta r \rangle$ for large M and ε. Now, the equation of motion of the end bead of the leading branch, once the chain has assumed an (inextensible) U-shaped conformation (such as the one shown in Fig. 4.10) can be expressed as

$$\zeta_M \frac{\partial Y}{\partial t} - mqE = 0 \tag{90}$$

where $\zeta_M = M\,\zeta$ is the global friction constant (i.e., that of the chain) and Y is the distance (in the direction of E) of the leading branch's end bead from the obstacle (which is centred at the

origin) that is pinning the polymer. Since the impact parameter m is the difference in the number of springs between the two branches (or the number of extra beads in the leading branch subjected to the electric field E), it is, consequently, the parameter controlling the driving force of the dynamics of depinning. Thus, the polymer as a whole experiences a net force mqE in the direction of E. We can scale this equation of motion using Eqns. (9, 10, 11, and 13) to yield the dimensionless form

$$\frac{d}{d\tau} y - \frac{h}{s'} \epsilon = 0 \tag{91}$$

where

$$s' \equiv M \langle \Delta r \rangle' \tag{92}$$

is roughly equal to the contour length. Integrating w.r.t. τ and solving for (scaled) time, we have, using $h = 2y - s$,

$$\tau(y) = \ln\left[\frac{2y - s}{h(0)}\right] \tau_\epsilon \tag{93}$$

and the escape time

$$\tau_{esc} \equiv \tau(s) = \ln\left[\frac{s}{h(0)}\right] \tau_\epsilon. \tag{94}$$

i.e., the time required for the leading bead to attain a distance from the obstacle equal to the contour length

$$s = (M-1)\,\langle \Delta r \rangle \tag{95}$$

In Eq. (94), we have implicitly defined a scaled time unit[35], the mean pulley time (for M→∞), given by

$$\tau_e = \frac{M\langle \Delta r \rangle'}{2\epsilon} = \frac{s'}{2\epsilon} \tag{96}$$

We can make use of the distribution function p(h) to compute the expectation values for the moments of τ_{esc} to yield

$$\langle \tau_{esc} \rangle = [\ln(2n) + \gamma]\,\frac{\tau_e}{2} \tag{97}$$

and

$$\langle \tau_{esc}^2 \rangle = \left([\ln(2n) + \gamma]^2 + \frac{\pi^2}{2} \right) \left(\frac{\tau_e}{2} \right)^2 = \langle \tau_{esc} \rangle^2 + \frac{\pi^2}{8}\,\tau_e^2 \tag{98}$$

where $\gamma = 0.577\,215\,...$ is Euler's constant. From these two moments, we yield the dispersion for the escape time

$$\begin{aligned} \langle (\Delta \tau_{esc})^2 \rangle &= \langle \tau_{esc}^2 \rangle - \langle \tau_{esc} \rangle^2 \\ &= \frac{\pi^2}{8}\,\tau_e^2 \end{aligned} \tag{99}$$

and, from Eqs. (97) and (99), we yield the relative mean-square uncertainty

---

[35]It turns out (setting $\langle \Delta r \rangle' = \langle \Delta r \rangle$) that $\tau_e = \langle \tau_{pulley} \rangle_{M\to\infty}$ where $\langle \tau_{pulley} \rangle_{M\to\infty}$ is the mean pulley time for large molecular sizes M. We may therefore view τ_e as the mean time required for the polyelectrolyte coil to "assume" a pulley-like conformation once its centre-of-mass is at the position of the obstacle. This will be discussed in Section 4.3.2.

$$\sigma_{\tau_{esc}} = \frac{\langle \Delta\tau_{esc}^2 \rangle^{1/2}}{\langle \tau_{esc} \rangle} = \frac{\pi/\sqrt{2}}{\ln[2(M-1)] + \gamma} \tag{100}$$

which is independent of applied electric field ε. Moreover, (Eq. 100) is non-vanishing for all realistic molecular sizes (e.g., $\sigma_{\tau_{esc}} < 0.1$ implies $M > 10^9$). Of course, in order for this expression to apply to a real system, it is required that the n = M - 1 (n ≫ 1) springs be near maximal extension (⟨(Δr)⟩ ≈ 1) which, in turn, requires that the electric force M×ε→∞. In general, ⟨Δr⟩ will depend both on ε and M; we will now determine this dependence.

We know, using Eq. (19), that the extension of j^{th} end spring in an arm (see Fig. 4.10) can be expressed (in d=2 dimensions) as

$$\Delta r_j = \frac{I_1(jf_\epsilon)}{I_0(jf_\epsilon)} = \frac{\partial}{\partial(jf_\epsilon)} \ln[I_0(jf_\epsilon)] \tag{101}$$

where we have made use of Eq. (20), and

$$f_\epsilon = \frac{2\epsilon}{N} \tag{102}$$

in analogy with Eq. (21). Assuming that the total number of springs, z, is large enough, we can compute the average spring extension viz.

$$\langle \Delta r \rangle \approx \frac{1}{z} \int_{j=0}^{z} \Delta r_j \, dj = \frac{1}{zf_\epsilon} \int_0^{zf_\epsilon} \frac{\partial}{\partial(jf_\epsilon)} \ln[I_0(jf_\epsilon)] \, d(jf_\epsilon) \tag{103}$$

$$= (zf_\epsilon)^{-1} \ln[I_0(zf_\epsilon)] = (2z\epsilon/N)^{-1} \ln[I_0(2z\epsilon/N)]$$

Since the number of springs in each branch is of the order[36] z=M/2. we then have

$$\langle \Delta r \rangle \approx (M\epsilon/N)^{-1} \ln[I_0(M\epsilon/N)] \tag{104}$$

or, for large argument[37] $M\epsilon/N \gg 1$, we may write[38]

$$\langle \Delta r \rangle \approx (M\epsilon/N)^{-1} \ln\left[\frac{e^{M\epsilon/N}}{\sqrt{2\pi M\epsilon/N}}\left(1 + \frac{1}{8M\epsilon/N} + \ldots\right)\right] \tag{105}$$

$$\approx 1 - \frac{\ln(2\pi M\epsilon/N)}{2M\epsilon/N}$$

where we keep only the first term of the expansion. Hence, as a first-order approximation, we expect from Eqs. (96), (97), (99) and (105) (with $M\epsilon/N \gg 1$ and $\langle \Delta r \rangle' \approx \langle \Delta r \rangle$) that

$$\langle \tau_{esc} \rangle \approx \frac{M}{4\epsilon}\left[\ln[2(M-1)] + \gamma\right]\left[1 - \frac{\ln(2\pi M\epsilon/N)}{2M\epsilon/N}\right] \tag{106}$$

and

$$\left\langle (\Delta \tau_{esc})^2 \right\rangle \approx \frac{\pi^2}{32\,\epsilon^2} M^2 \left[1 - \frac{\ln(2\pi M\epsilon/N)}{2M\epsilon/N}\right]^2 \tag{107}$$

which means that the dispersion of the escape time is, in fact, a rapidly varying function of both molecular size M and electric field ϵ.

---

[36]In this analysis, we are assuming $M \to \infty$ and are implicitly neglecting the subtraction of a term roughly of the order $\langle m \rangle = \langle h \rangle / \langle \Delta r \rangle = |2(M-1)/\pi|^{1/2}$.

[37]In the low field limit, we have $\langle \Delta r \rangle = M\epsilon/(4N)$ as expected for the relevant harmonic approximation.

[38]See Abramowitz and Stegun (1964), Eq. (9.7.1).

#beads M	5	10	15	20	30	40
#chains	1091	3198	837	152	207	30
$\langle\tau_{coll}\rangle$	9.07	10.3	19.3	44.6	53.2	50.5
$\langle\tau_{pulley}\rangle$	1.02	1.39	5.84	17.4	18.8	14.8
$\langle\tau_{esc}\rangle$	2.49	2.84	6.80	17.4	18.9	14.8
$\langle\tau_{retard}\rangle$	1.69	2.20	3.22	5.54	9.83	11.5

Table 4.4 - The relevant statistics for a simple electrophoretic collision for polyelectrolytes of various molecular sizes (M=5 to M=40 beads) are tabulated along with particulars of the collision process. The definitions of the various parameters will be given in our example of an electrophoretic collision of a M=15 bead polyelectrolyte (see Table 4.5); this table thus serves as a comparison table for different molecular sizes M. The simulation settings were $\Delta\tau_{max}$=0.1, m=1000, d_T=2.0. The estimated times for $\langle\tau_{coll}\rangle$, $\langle\tau_{pulley}\rangle$, and $\langle\tau_{esc}\rangle$ were obtained from the dispersion curves for the centre-of-mass as indicated therein. The retardation times were obtained by extrapolation of the displacement of the centre-of-mass to the time axis (see, e.g., Fig. 4.14).

4.3.2 Example of an electrophoretic collision between a M=15 bead polyelectrolyte and a circular obstacle with an electric field of ε=1.

We now examine the statistics in the direction $\parallel$ to tube axis (i.e., the y-direction). For a M=15 bead chain, we have a polyelectrolyte of moderate length but one for which the previous analysis of depinning, as it applies to a chain with M>1, should still be applicable. Moreover, M=15 strikes a practical compromise between averaging statistics and CPU time.

Initially, the M=15 bead polyelectrolyte is in equilibrium and in free drift (see Fig. 4.9 a-c) where the drift velocity is given by $v_{drift}=\varepsilon$ in our scaled units. Consequently, the time required for the polymer's centre-of-mass r_{cm} (initially at y=0) to attain the position y is given roughly by (using Eq. (12))

$$\tau(y) = \frac{y}{\varepsilon}, \quad \textit{(free drift)} \tag{108}$$

where we expect the stochastic terms to average-out to zero. The migration distance before the onset of the collision should be roughly $y_{coll}\approx y_{obst}-\rho_{obst}-\langle r_{g\parallel}^2\rangle^{1/2}$ where y_{obst} is the position of the obstacle's centre-of-mass, ρ_{obst} is the obstacle's radius, and $\langle r_{g\parallel}^2\rangle^{1/2}$ is the root-mean-square (r.m.s.) radius of gyration of the chain. Since, from Table 4.1 (the y-direction is the $\parallel$-direction), $\langle r_{g\parallel}^2\rangle_{equil}^{1/2}\approx(0.1958)^{1/2}\approx0.4425$ and the obstacle radius is ρ_{obst}=0.5, we find, by substituting y_{coll} into Eq. (108), that the expectation value for the elapsed time before collision should be τ_{obst} $_{Eq(108)}=\tau(y_{coll})\approx14.05$. Our simulations indicate that the mean square spring extension in the $\parallel$-direction $\langle(\Delta r_\parallel)^2\rangle$ (see Fig. 4.11), as well as the mean square end-to-end distance $\langle p_\parallel^2\rangle$, (Fig. 4.12), and mean square radius of gyration $\langle r_{g\parallel}^2\rangle$ (Fig. 4.13) all undergo a transition from their equilibrium values (see Table 4.1) $\langle(\Delta r_\parallel)^2\rangle_{equil}\approx0.081$, $\langle p_\parallel^2\rangle_{equil}\approx1.1$ and $\langle r_{g\parallel}^2\rangle_{equil}\approx0.20$, respectively,

M=15	$\langle(\Delta r_x)^2\rangle$	$\langle(\Delta r_y)^2\rangle$	$\langle p_x^2\rangle$	$\langle p_y^2\rangle$	$\langle r_{gyr\ x}^2\rangle$	$\langle r_{gyr\ y}^2\rangle$
$\langle\tau_{obst}\rangle$	12.5	12.0	12.6	11.7	11.7	12
$\langle\tau_{min}\rangle$ minima	16.6 0.06061	14.45 0.07037	Not Avail.	14.2 0.7592	Not Avail.	14.25 0.14025
$\langle\tau_{max}\rangle$ maxima	21.35 0.07437	20.85 0.1114	16.2 0.6578	21.65 3.391	16.15 0.1470	21.55 0.6046

Table 4.5 - Single-obstacle collision for the case of a 15-bead chain subjected to an electric field of strength e=1.0. The ensemble size was 837 and the obstacle radius was ρ_{obst}=0.5 (centred at y_{obst}=15.0) such that the obstacle's diameter is larger than the extension of the springs (thus the chain cannot pass through the obstacle). The time $\langle\tau_{obst}\rangle$ represents estimates of the time at which the polymer begins to "feel" the obstacle according to the respective tabulated mean-square lengths (i.e., the onset of collision); $\langle\tau_{min}\rangle$ represents the time at which the tabulated mean square lengths reach their minimum values; and, conversely, $\langle\tau_{max}\rangle$ is the time at which one attains maximal values. We note that some fields are left blank due to lack of resolution.

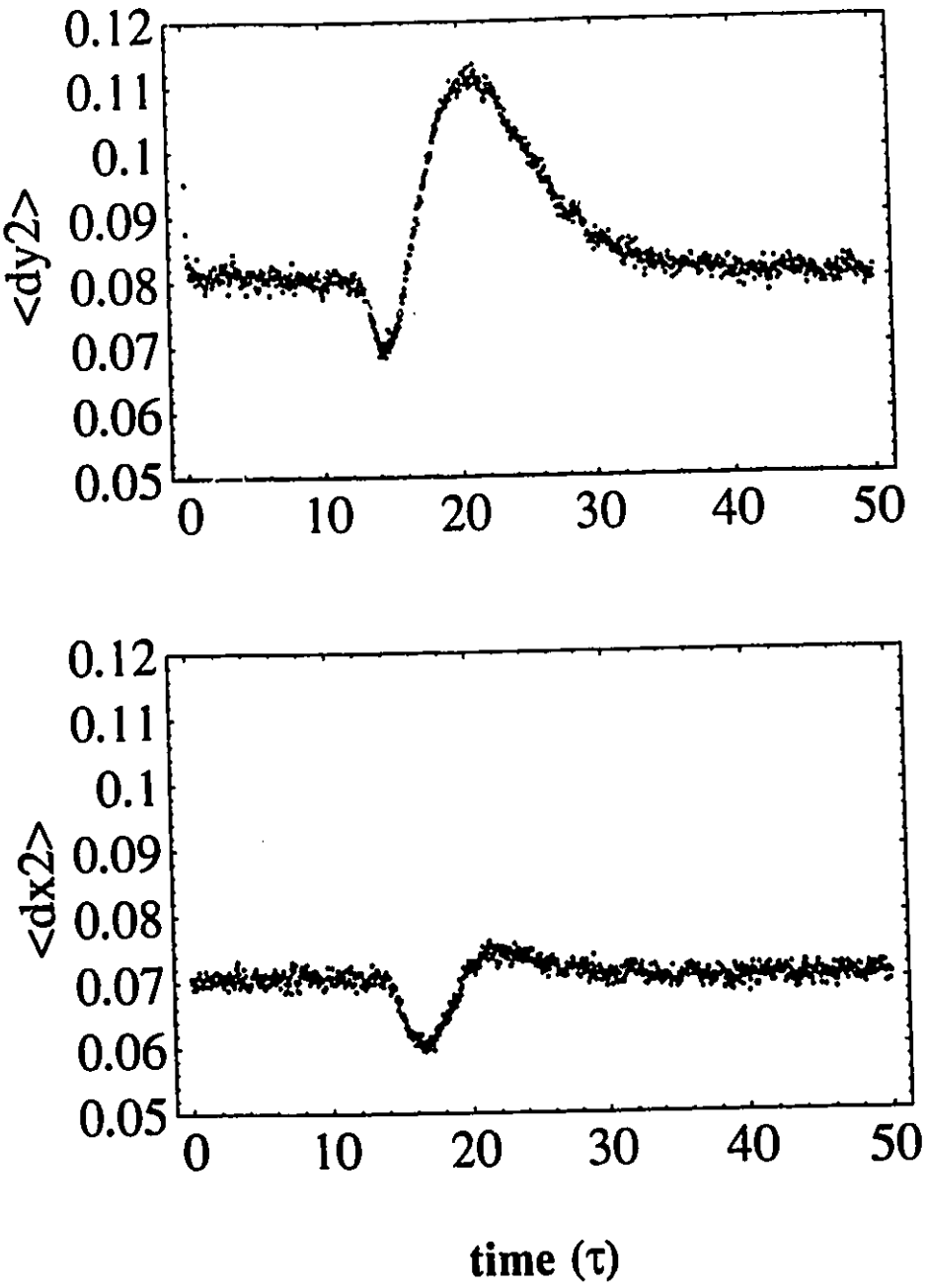

Fig. 4.11 - The mean square spring extension for our M=15 bead chains is plotted as a function of time for both the x and y components.

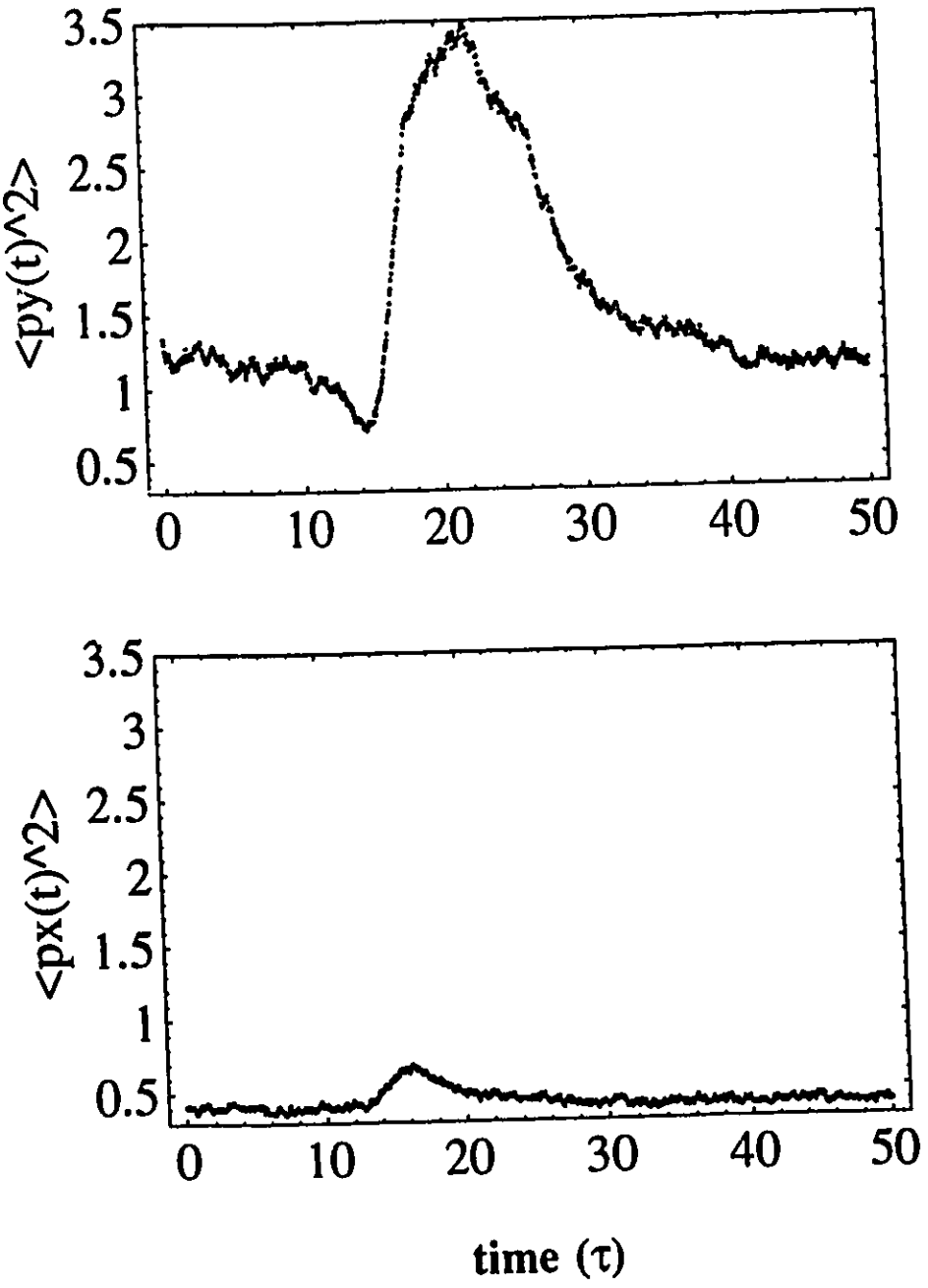

Fig. 4.12 - The mean square end-to-end distance for our M=15 bead chains is plotted as a function of time for both the x and y components.

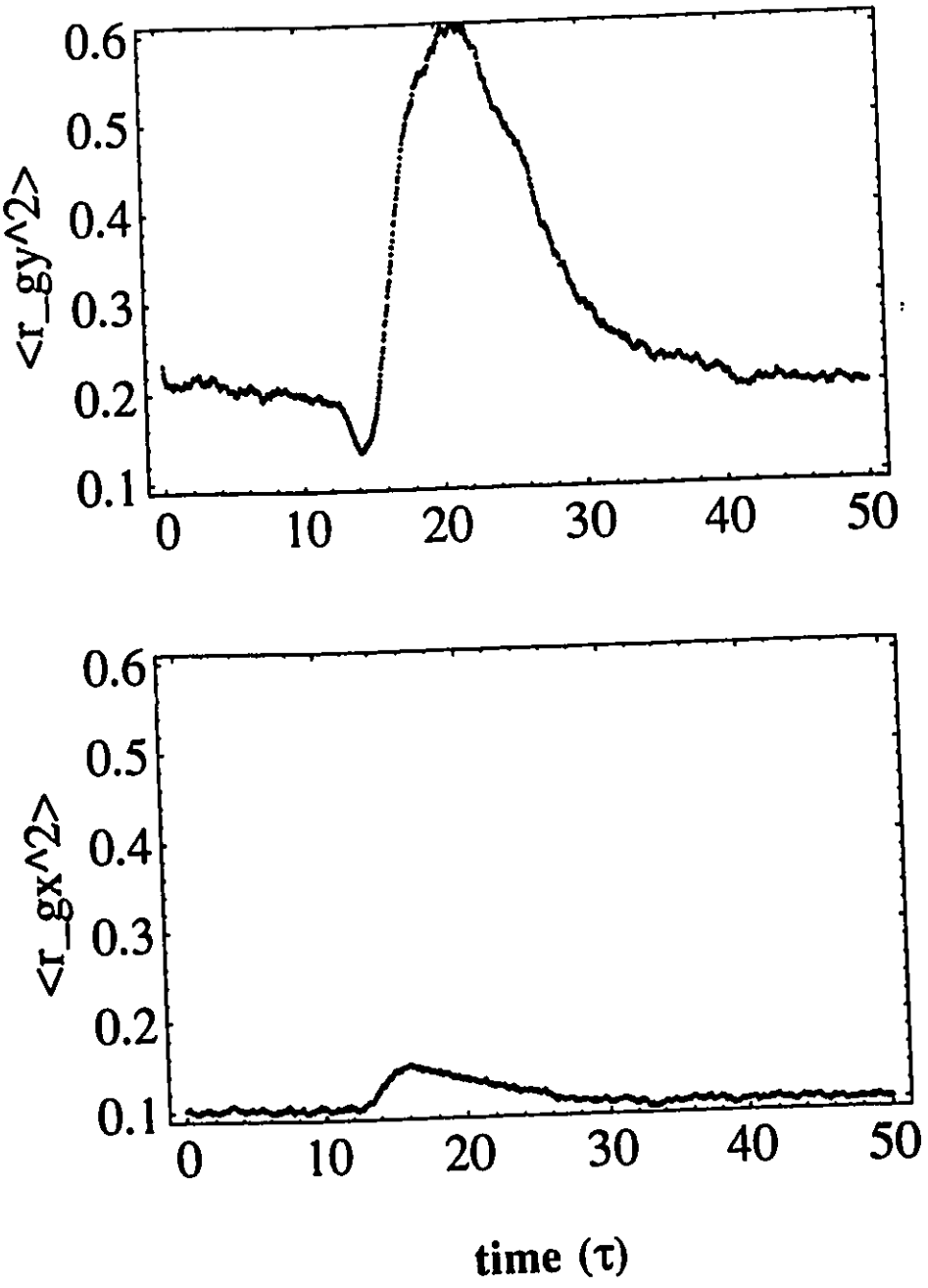

Fig. 4.13 - The mean square radius of gyration for M=15 beads is plotted as a function of time for both the x and y components.

as the polyelectrolyte attains the obstacle at time $\langle\tau_{obst}\rangle$=12.0. This time, corresponding to frame #3 in Fig. 4.9, is shorter than our theoretical value of 14.05. The discrepancy lies simply in the fact that we implicitly assumed the conformation of the polyelectrolyte to be a sphere with a radius equal to the r.m.s. radius of gyration. In fact, it is not a sphere but an irregular ellipsoid-like shape whose breadth is, typically, larger than the radius of gyration[w].

At the beginning of a gel-electrophoresis experiment, the electrolytes are driven against the gel before they finally permeate the surface. This phenomenon is known as stacking and this effect is most desirable in that the stronger the stacking effect, the narrower the molecular bands at the beginning of the run and the smaller the inherent systematic error. Indeed, we observe this stacking phenomenon as a small dip in the dispersion curve of the centre-of-mass in Fig. 4.17.

Let us call that time required for the polyelectrolyte to impale itself fully on the obstacle (see Fig. 4.9 frames 5-10) from the time its centre-of-mass has already reached the obstacle's position, forming a U-shape or pulley-like conformation, the pulley time τ_{pulley}. This should be given approximately by the time required for the end beads to reach their respective positions within the pulley-like conformation by way of free drift (since the latter will not feel the effects of the other springs of their respective branches until after such time). With approximately M/2 beads per branch on the average, we expect (with $M\to\infty$ and $\langle\Delta r\rangle' \approx \langle\Delta r\rangle$)

$$\langle\tau_{pulley}\rangle \approx \frac{M\,\langle\Delta r\rangle}{2\epsilon} \approx \tau_\epsilon \qquad (109)$$

where $\langle\Delta r\rangle$ is the equilibrium mean spring extension within the pulley-like conformation, that is, just before slipping occurs (see Fig. 4.9 frame 10), and τ_ϵ is the time unit we defined previously

---

[w]Rudnick and Gaspari (1987).

in Eq. (96). Thus, τ_ϵ can be viewed as the mean pulley time for large molecular sizes M. From Eq. (109), we thus expect a pulley time of about 4.8 for our simulations. This corresponds well with what we'd expect as viewed from the time span ($5\times\Delta\tau_{frame}\approx5.4$) between frames 5 and 10 in Fig. 4.9. The experimental value (as seen from Table 4.4 and Fig. 4.17 where the relevant time span appears to be approximately $\langle\tau_{pulley}\rangle\approx24.75-18.91=5.84$) is in fair agreement.

We are now in a position to estimate the mean collision time $\langle\tau_{coll}\rangle$ which we define as the total interaction time between the polyelectrolyte and the obstacle. First, we note that the expectation value for $\langle\Delta r\rangle$ is $\langle\Delta r\rangle_{Eq.(105)}\approx0.51$ which compares very well with the experimental value $\langle\Delta r\rangle\approx[\langle p_l^2\rangle_{max}/(M-1)]^{1/2}\approx0.49$. Now, if we seek the total collision time, we must add the pulley time to the escape time viz. $\tau_{coll}\approx\tau_{esc}+\tau_{pulley}$. With Eqs. (106) and (109), we obtain

$$\langle\tau_{coll}\rangle \approx \frac{M}{4\epsilon}\times[\gamma+2+\ln(2M)]\times\left[1-\frac{\ln[2\pi M\epsilon/N]}{2M\epsilon/N}\right],\quad M>1 \qquad (110)$$

The expected collision time is therefore about $\langle\tau_{coll}\rangle_{Eq.(110)}\approx11.4$ which is in fair agreement with the value obtained from Fig. 4.17 where we have $\langle\tau_{coll}\rangle\approx31.54-12.25\approx19.3$. Now, the retardation time due to the collision is the extra time over the course of the collision that the polyelectrolyte spent as compared with the same scenario in absence of the obstacle (where the free drift velocity is $v_0=\epsilon$). We thus add the excess time during pulley formation (the chain centre-of-mass drifts over a distance $(M/4)\langle\Delta r\rangle$ during the pulley formation time) to the excess time during the escape process (where the polyelectrolyte's centre-of-mass drifts from $y_{cm}(\tau=0)=(M/4)\langle\Delta r\rangle$ to position $y_{cm}(\tau=\tau_{esc})=(M/2)\langle\Delta r\rangle$), i.e.,

$$\begin{aligned}\langle \tau_{retard} \rangle &\approx \left[\langle \tau_{pulley} \rangle - \frac{(M/4)\,\langle \Delta r \rangle}{\epsilon} \right] + \left[\langle \tau_{esc} \rangle - \frac{(M/4)\,\langle \Delta r \rangle}{\epsilon} \right] \\ &\approx \langle \tau_{coll} \rangle - \langle \tau_{pulley} \rangle \\ &\approx \langle \tau_{esc} \rangle \end{aligned} \qquad (111)$$

Note that we are implicitly neglecting the finite size effects due to the obstacle's radius and due to the small size of the polyelectrolyte in this simple scaling argument which is valid strictly in the large molecular size limit. From Eq. (106), we expect that $\langle \tau_{retard} \rangle_{Eq.(111)} \approx 7.5$. Our simulation results (see Table 4.5 and Fig. 4.14) indicate that the retardation time caused by the collision is actually smaller (i.e., $\langle \tau_{retard} \rangle \approx 3.2$) while the escape time (see Fig. 4.17) was found to be about $\langle \tau_{esc} \rangle = 31.54\text{-}24.75 = 6.8$. Note also that this idealized treatment does not take into account the possibility where pulley formation does not take place (e.g., the polyelectrolyte coil may lodge itself between the obstacle and the wall and simply squeeze through) the net effect of which would be to reduce the mean retardation time.

Equation (111) actually predicts that the retardation due to a collision increases roughly as M×Ln[M] for large molecular sizes M. We have plotted the retardation times (as defined by Fig. 4.14; see Table 4.4) as a function of M×Ln[M] for M=10, 15, 20, 30 and 40 in Fig. 4.15. We see that there is reasonably good agreement between the retardation time and the scaling predictions of Eq. (111). The reason that we exclude the M=5 bead results for the analysis is, as can be seen in Fig. 4.16, that the dynamics are markedly different from those of M≥10 (cf. Figs. 4.12 and 4.16). This follows from the fact that, for M=5 beads, the polyelectrolyte's radius of gyration w.r.t. the obstacle radius ρ_{obst}=0.5 is small and the chain simply slides over the obstacle.

If the time at which we have fullest extension of the springs in the ‖ direction is taken as the onset of the escape process (Fig. 4.9, frame 10), we may compare the approximate expression for the escape time (Eq. (106)) of $\langle \tau_{esc} \rangle_{Eq(106)} \approx 7.5$ to the experimental escape time (see Table 4.4 for M=15) of $\langle \tau_{esc} \rangle \approx 6.8$ which is in reasonable agreement. In Fig. 4.9, this process corresponds to frames 10-16 where we have $\tau_{esc}=6.5$, again in close accord with the theoretical value of 7.5.

The escape time was shown to have a wide variance $\langle (\Delta\tau_{esc})^2 \rangle_{Eq.\ (99)} = (\pi^2/8)\tau_c^2$. This temporal variance results in a corresponding variance in the spatial distribution of molecules viz.

$$\left\langle (\Delta y_{cm})^2 \right\rangle_{coll} \approx \frac{v_{drift}^2}{2} \left\langle (\Delta \tau_{esc})^2 \right\rangle = \frac{\pi^4 \epsilon^2}{128} \tau_{pulley}^2 = \frac{\pi^4 \langle \Delta r \rangle^2 M^2}{512} \qquad (112)$$

Our experimental results (see Fig. 4.17) indicate a value of $\langle (\Delta y_{cm})^2 \rangle_{coll} \approx 9$ which is in good agreement with the theoretical value of $\langle (\Delta y_{cm})^2 \rangle_{coll\ Eq(112)} \approx 11$. This result is, of course, far more than what we found for the free diffusion case in the absence of collisions (see Section 4.1). We note that the dispersion of the molecular band, characterized by M, goes approximately as the square of the molecular size and is a weak function of the electric field ε through $\langle \Delta r \rangle_{Eq(105)}$ (since $M\epsilon/N \gg 1 \rightarrow \langle \Delta r \rangle \approx 1$). In absence of collisions, the dispersion of the centre-of-mass has the form $\langle (\Delta y_{cm})^2 \rangle = 2d_{cm}\tau = \tau/M$. Hence, during the course of the escape process, the dispersion of the centre-of-mass increases by a factor (with $M \gg 1$, $M\epsilon/N \gg 1$)

$$\frac{\left\langle (\Delta y_{cm})^2 \right\rangle_{coll}}{\left\langle (\Delta y_{cm})^2 \right\rangle_{free}} \approx \frac{\pi^4 \epsilon^2 M}{128} \frac{\tau_{pulley}^2}{\langle \tau_{esc} \rangle} \approx \frac{\pi^4 \langle \Delta r \rangle}{128} \frac{M^2 \epsilon}{\ln M} \qquad (113)$$

We therefore have, for $M \rightarrow \infty$, a massive increase in the rate of dispersion over the course of the escape time which goes linearly with the electric field and goes as $M^2/\ln M$ for the molecular size.

Since there is a retardation time, we know that the drift of the molecular bands slows down while the width of the bands increase their rate of spreading. The retardation of the bands, being a strong function of M, is not enough to offset this rapid spread of the molecular bands. In fact, the whole process is catastrophic since the resolution factor $R=|\partial y_{retard}/\partial M|/|\Delta y_{coll}| \sim \ln M / M$ vanishes for large molecular species M. There is, consequently, no hope of using a series of these isolated collisions for the purposes of improving the resolution of electrophoresed molecular bands.

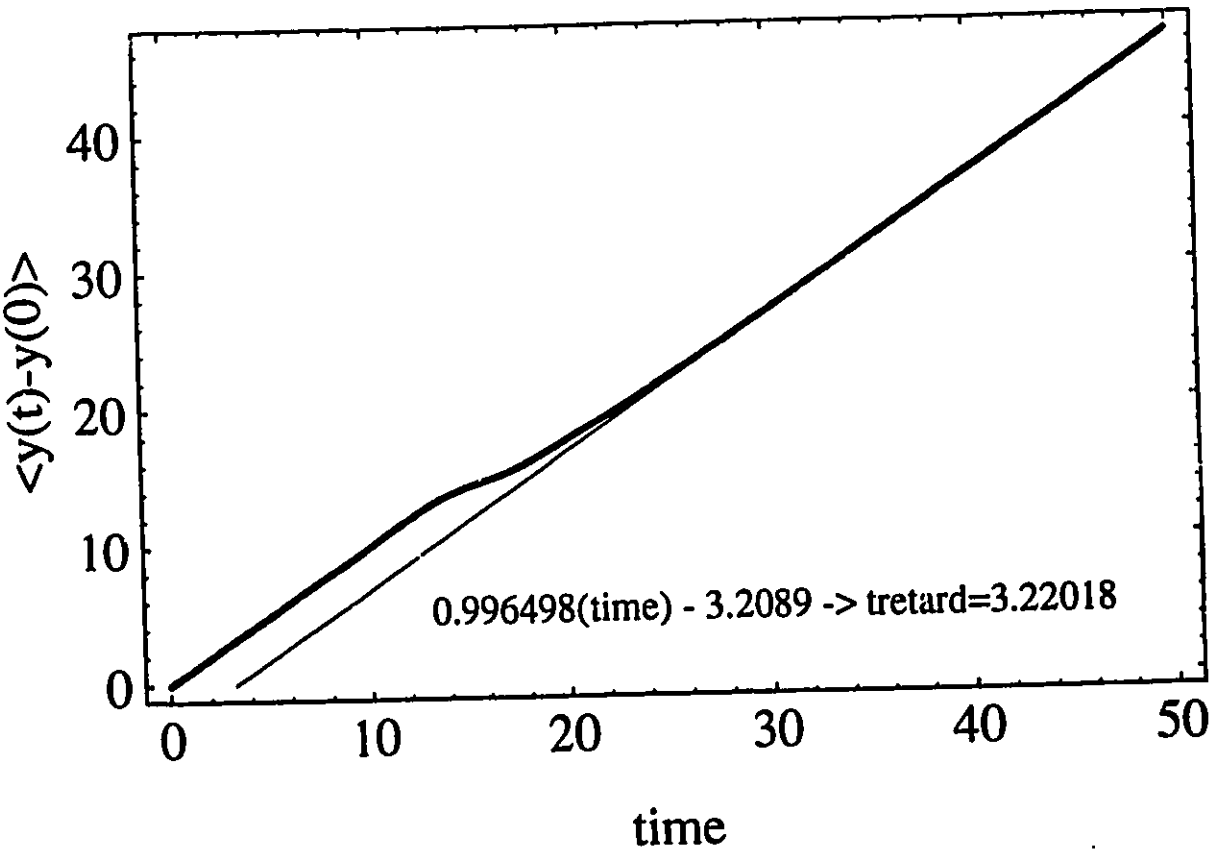

Fig. 4.14 - The position of the centre-of-mass for the y component is plotted versus time. We note that the retardation time is given by the extrapolated ordinate value of τ_{retard}=3.22. The free-drift velocity is v_0=ε=1.0.

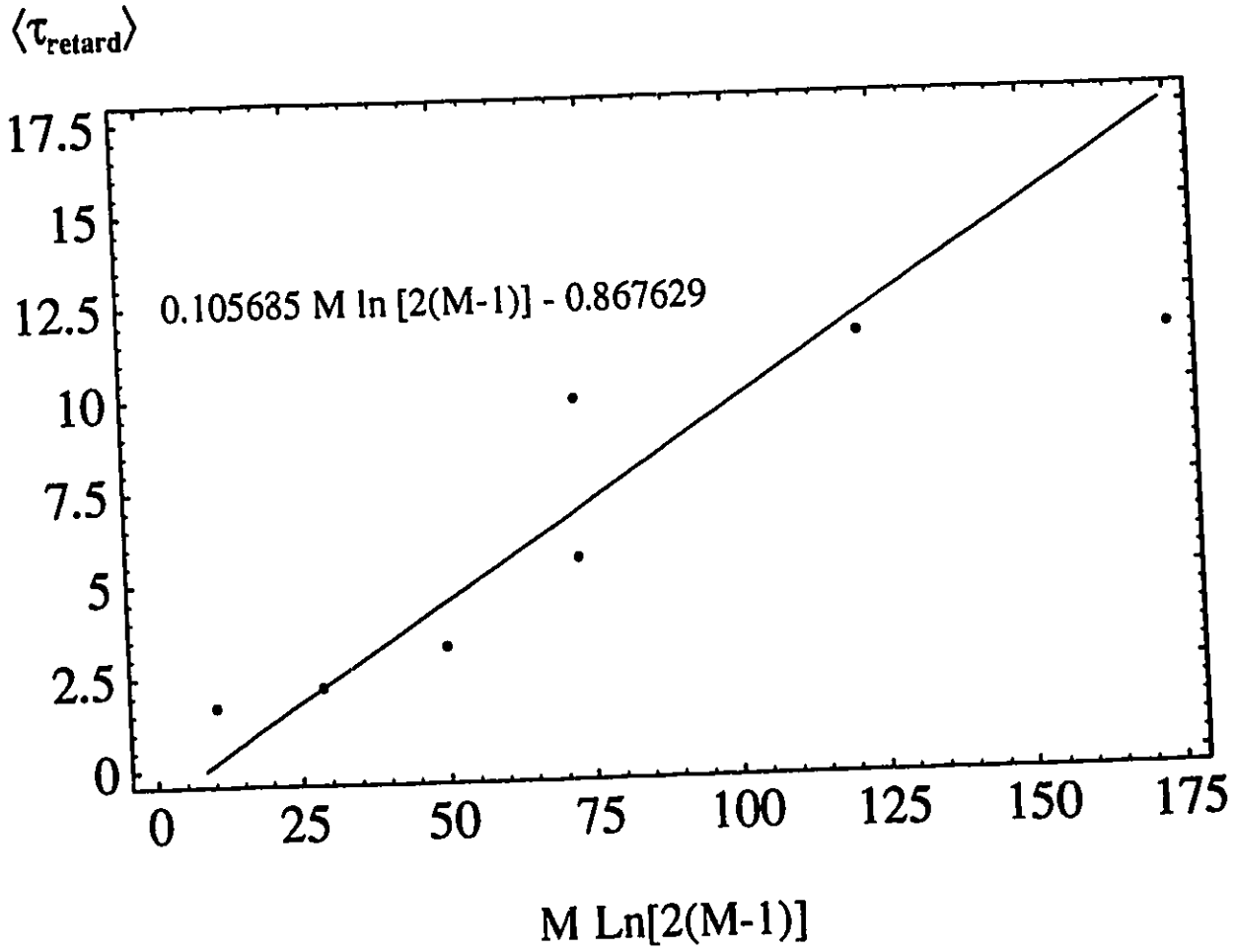

Fig. 4.15 - The mean retardation time $\langle \tau_{retard} \rangle$ is plotted as a function of M ln[2(M-1)] for molecular sizes M=10 to M=40. We see that the scaling form is in good agreement with Eq. (111).

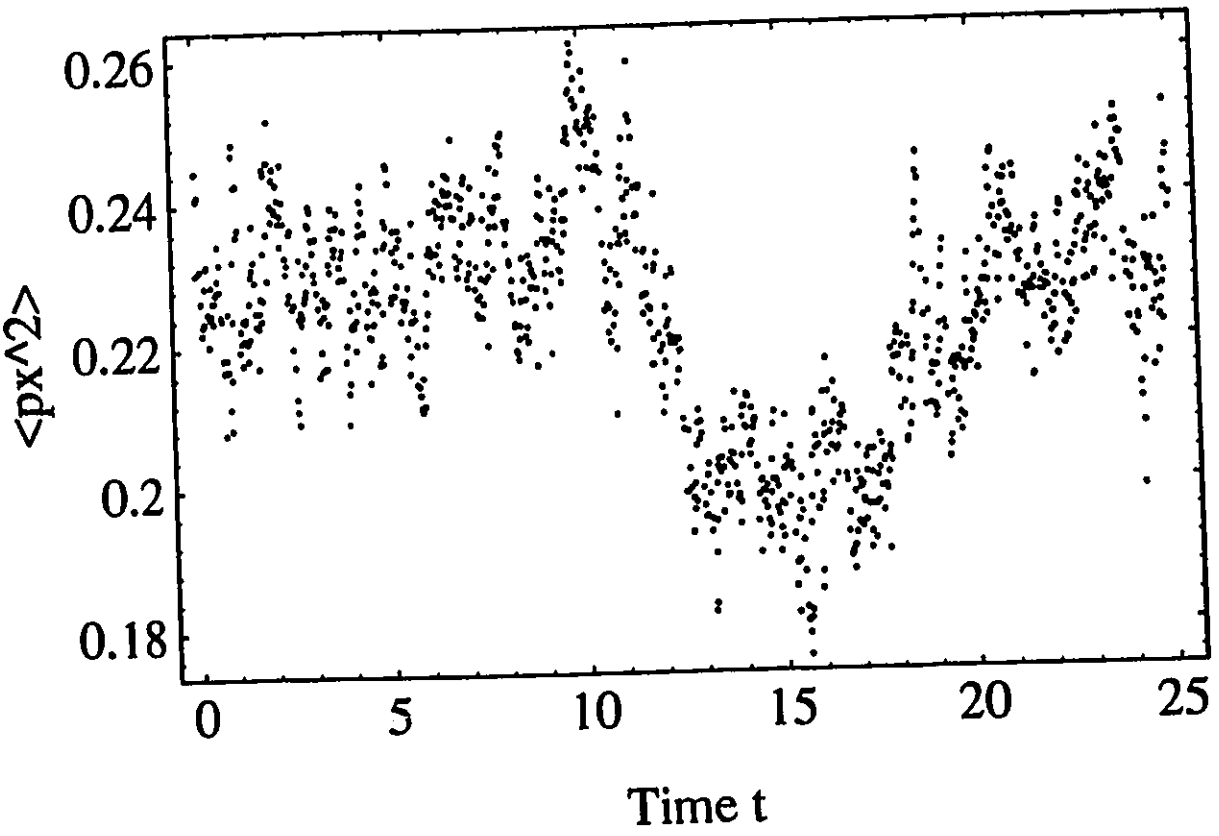

Fig. 4.16 - The x-component of the mean-square end-to-end distance for a M=5 bead chain. We note that there is actually a minimum where we would expect to see a maximum (e.g., see Fig. 4.12). This occurs because relatively few of these small chains actually form pulley conformations; the majority simply slide over the obstacle and sieve through the gap between the obstacle and the tube wall.

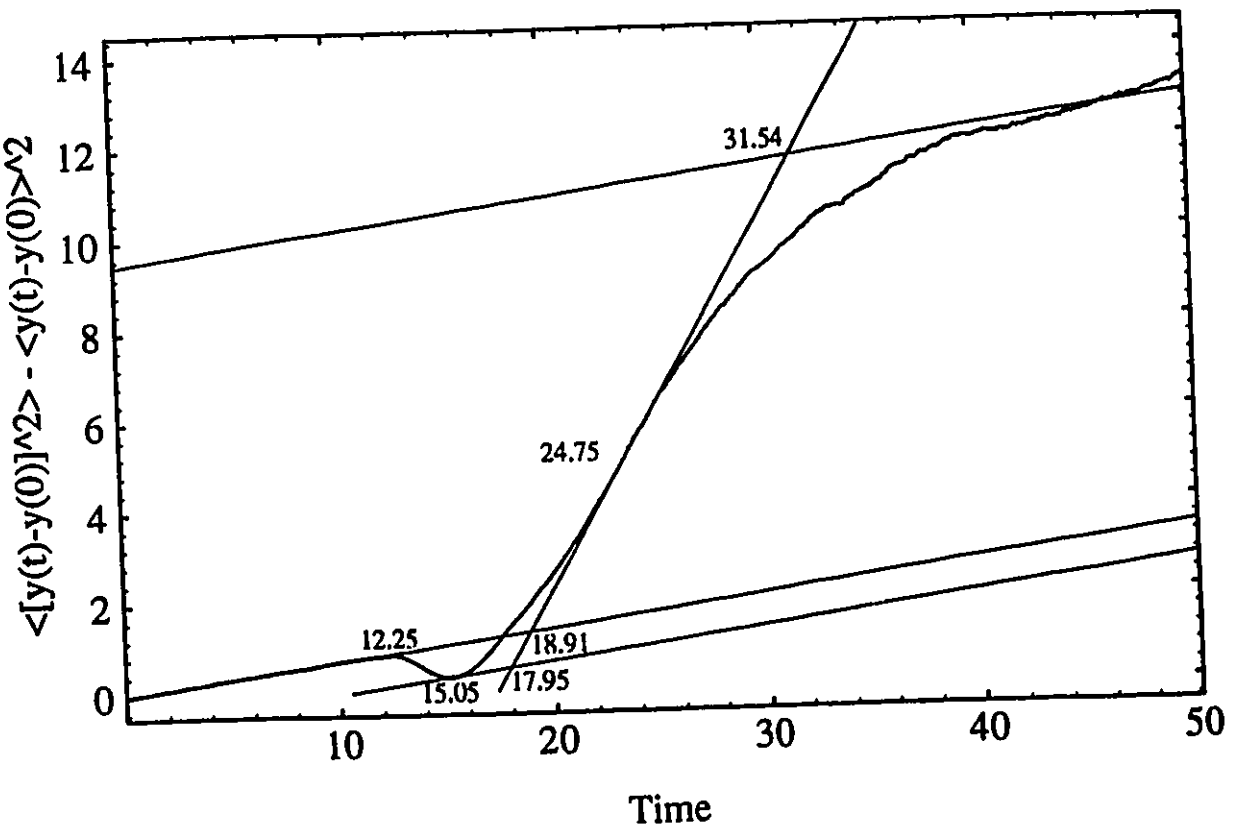

Fig. 4.17 - The dispersion of the position of the centre-of-mass is plotted vs. time for the y component of a M=15 bead chain. Note that the y component experiences maximum stacking at time τ=15.05. This stacking, however, is followed by a steep increase beyond which the dispersion again assumes the characteristics of Rouse-like diffusion only now, it is as if it was offset in time by an amount τ=139 as given by the extrapolated time. The collision starts at τ=12.25 and ends at τ=31.54 thus $\langle\tau_{coll}\rangle$=31.54-12.25=19.29; stacking begins at τ=12.25 and ends roughly at τ=18.91 thus $\langle\tau_{stack}\rangle$=18.91-12.25=6.66; the pulley formation time starts at τ=18.91 and ends at τ=24.75 thus $\langle\tau_{pulley}\rangle$=24.75-18.91=5.84; and, finally, unravelling starts at τ=24.75 and ends approximately at τ=31.54 thus $\langle\tau_{unc}\rangle$=31.54-24.75=6.79.

4.4 Dynamics in Rough tubes - Entropic Barriers

The dynamic properties of a RW polymer in an infinite linear periodic array of cavities separated by narrow bottlenecks (strictures) were investigated using our Brownian dynamics algorithm and analyzed by scaling arguments. When in the vicinity of a bottleneck, entropic forces are set up due to the reduction of the number of possible chain conformations in the narrow passage. Consequently, the chain diffusion coefficient d_{cm} is smaller than that of a free chain. Recent[40] scaling analysis by Muthukumar and Baumgartner (1989) suggests an exponential relationship between the diffusion coefficient and the chain length M. Furthermore, we investigated the effect of electric fields on the migration of the polyelectrolytes through a series of channels and voids. Our investigations of these *f*ield-*a*ssisted *e*ntropic *m*igrations (FAEM) do not suggest any obvious features to be exploited by separation scientists due to large diffusion effects (more work remains to be done). We demonstrate that chain diffusion under the effects of entropic traps, especially in the presence of electric fields, is actually counter-productive w.r.t. the resolution of the migrating electrophoretic bands; this is in agreement with experimental evidence[41].

4.4.1 Theoretical considerations

The transport of polymer chains from regions of relatively large volume (or area in our 2-d model) to regions of relatively smaller volume, and consequently lower entropy, is an issue

---

[40]Muthukumar and Baumgartner (1989).

[41] Pascal Mayer (unpublished results).

of broad relevance. It underlies many phenomena including membrane separation, protein partitioning, etc. Because there are usually many factors present in these systems, it proves useful to reduce the problem to cases where the geometry is simple, and the model not too complex. Such is the approach we have adopted. We have a tube with semi-circular protrusions (or wall obstacles) on the inside edges of opposite sides and with a well defined periodicity (see Fig. 4.19). The geometry is such that it allows for analytical *scaling* calculations (based on a simplified one-dimensional anisotropic random walk of a point-like particle) as well as for simple interpretation of simulation results.

In a lattice model, the number of possible conformations Ω for a M-bead chain scales as

$$\Omega \sim z^{M-1} \tag{114}$$

where z is the coordination number of the lattice. The entropy is then given by

$$\frac{S}{k_B} = \ln\Omega \sim (M-1)\ln z \sim M \tag{115}$$

for a large M; therefore, the entropy is a linear function of molecular size. We also expect that the reduction in entropy due to confinement will scale as some function of the length ratio of the free radius of gyration to the diameter D_c of the narrow channels

$$\frac{\Delta S}{k_B} \approx f\left(\frac{R_{g_{free}}}{D_C}\right) \approx \left(\frac{R_{g_{free}}}{D_C}\right)^{\alpha} = \left(\frac{r_{g_{free}}}{d_C}\right)^{\alpha} \tag{116}$$

where $\alpha>0$ is some power to be established. We know from Eq. (41) that

$$R_{g_{free}} \sim r_{g_{free}} \sim M^{1/2} \tag{117}$$

and so it follows directly that $\alpha=2$, i.e.,

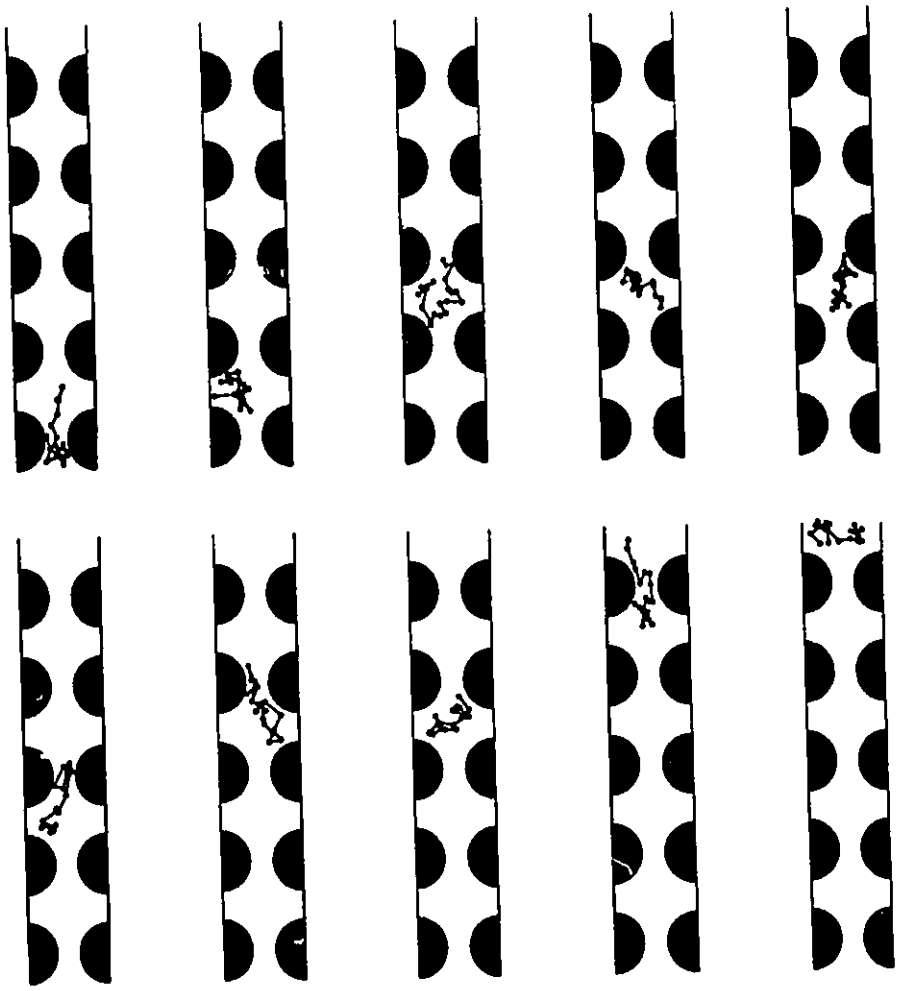

Fig. 4.19 - Movie slide (from upper left to bottom right) of a M=20 bead chain migrating in a rough tube under the effect of an electric field ε=1.0 directed upwards. The tube diameter is d_T=2.8, the semi-circular protrusions have unit radius and are separated along the tube at intervals of Δy=3. The free radius of gyration for the molecule is $\langle r_g^2 \rangle^{1/2} \approx 0.51$ (see Table 4.1) which is smaller than the width of the channel 2.8-2×1=0.8.

$$\frac{\Delta S}{k_B} \sim \left(\frac{R_{g_{free}}}{D_C}\right)^2 = \left(\frac{r_{g_{free}}}{d_C}\right)^2 \tag{118}$$

The corresponding change in the free energy is

$$\Delta F = T\,\Delta S \sim T\left(\frac{r_{g_{free}}}{d_C}\right)^2 \tag{119}$$

If we wish to find the probability of jumping from one pore to another (an activated process), then the relevant expression is given by the Boltzmann factor

$$p_{jump} \sim e^{-\gamma' (r_{g_{free}}/d_C)^2} \tag{120}$$

where γ' is a system-dependent (topological) factor. If an electric field **E** is present, the expression must be modified to take into account the change in scaled potential energy (with net charge Q=Mq)

$$\pm\frac{QE(\Delta Y/2)}{k_B T} = \pm M\epsilon\Delta y \tag{121}$$

where ΔY (or $\Delta y=\Delta Y/L$ in scaled form) is the distance between the pores ($\Delta y/2$ being approximately the distance between energy maxima and minima provided that the external field ϵ is not too great). We therefore have (using $\langle r_g^2\rangle=M\langle(\Delta r)^2\rangle/6$ from Eq. (41))

$$p_{jump\,\pm} \sim e^{M\left[\pm\epsilon\Delta y - \gamma\langle(\Delta r)^2\rangle/d_C^2\right]} \tag{122}$$

where "+" and "-" denote a jump in a direction parallel and anti-parallel, respectively, to the direction of the scaled electric field vector $\boldsymbol{\epsilon}$ and where $\gamma=\gamma'/6$.

The mean trapping time (mean time between transitions in the "+" or "-" directions) should thus be given by

$$\langle \tau_{trap\ \pm} \rangle \sim p_{jump\ \pm}^{-1} \tau_{\pm}^{*} \qquad (123)$$

where $\tau_{\pm}^{*}$ are the characteristic times between "attempted" jumps in the respective directions.

4.4.2 Effect of squeezing a M=10 bead chain in absence of field (ε=0)

We examine the effect of narrowing the width d_T of a "rough tube" (which will reduce the width d_c of the narrow channels (strictures) between pores since the wall obstacle radius ρ_{wobst}=1 is held constant) w.r.t. the static and dynamic properties. In particular, we investigate the onset of a "hopping" mechanism (activated process) for the free-migration of the chain as it migrates from pore to pore. The results are tabulated in Table 4.6 and Figs. 4.20 to 4.26.

Static properties

As per Table 4.6, the mean square spring extension is barely affected by the reduced tube width. However, both the parallel (∥ is the y-direction) end-to-end distance and radius of gyration decrease when the tube diameter is reduced: this is due to the increased localisation of the polymers in the small cavities between the bottlenecks (strictures). Of course, the transverse (perpendicular ⊥ or x-direction) radius of gyration is severely reduced, as expected.

Dynamic properties

Figure 4.19 shows snapshots of the motion of a single polymer chain inside a rough tube; clearly, the polymer spends most of its time between channels, i.e., in the large pores where it

assumes maximum entropy. The motion of the polymer thus follows a series of discrete jumps of length $\pm\Delta y$ as expected from an activated process. Figures 4.20 to 4.26 show the displacement of the molecules along the tube axis as a function of time for the different tube widths d_T. As the tube is reduced in diameter, the time spent in each pore increases, i.e., the chain becomes more localized and the "trapping" or "jumping" time increases substantially (there is no trapping as such for the largest tube diameters). Figure 4.27 shows how the net trapping time varies with channel width d_C. The net trapping time was defined as the time required to go from the centre of one pore to the next (i.e. the expected time of travel, in absence of the narrow channels, is given by $\langle\tau_{free\ drift}\rangle=\Delta y^2/2d_{cm}=\Delta y^2\times M=3^2\times 10=90$ for M=10 beads with $\varepsilon=0$). The fit shows that the exponential behaviour predicted by Eqs. (122) and (123) is indeed observed. This is similar to the behaviour found by Muthukumar and Baumgartner (1989) in a model system of boxes connected by narrow tubes. Of course, our error bars are very large since the number of trapping events is small.

4.4.3 The effect of different field intensities ε on M=10 bead chains

Here we analyze the effect of the electric field on the mobility $\mu=v_{cm}/\varepsilon$ of a M=10 bead chain confined within a tube a diameter $d_T=2.8$ where the width of the channels between pores is $d_C=0.8$. Equation (122) indicates that the behaviour should change dramatically for fields larger than the (topology-dependent) critical field intensity

$$\epsilon_{crit} \equiv \frac{\gamma}{\Delta y} \frac{\langle (\Delta r)^2 \rangle}{d_C^2} \qquad (124)$$

For fields below the critical field, $\epsilon < \epsilon_{crit}$, we expect the migration of the chain to be limited by the narrow channels (for entropic reasons, as described previously), whereas for fields above the critical field, $\epsilon > \epsilon_{crit}$, we expect the chains to be easily pulled through the channels by the strong electric forces. In the latter case, we should soon recover the molecular-size independent mobility which characterizes free-draining polymer coils. We note that the critical field is NOT predicted to be a function of the molecular size; both the loss of entropy due to the presence of the narrow channel and the electric force acting on the polyelectrolyte scale linearly with molecular size. However, we predict that the critical field is a strong function of the width d_C of the free channel.

The results for the M=10 bead chains are presented in Tables 4.7 and 4.8 as well as Figs. 4.28 to 4.32. It is clear that entropic trapping is completely killed (e.g., $\langle \tau_{trap} \rangle$ decreases substantially) by the electric forces when the field intensity exceeds 0.05; in other words, we have $\epsilon_{crit} \approx 0.03$.

In our treatment, the pores and the narrow passages were of similar lengthscale. If the relative distance between pores were greater, the frequency of attempted jumps in either direction would then differ substantially in non-zero field cases. This would correspond to a very dilute system of narrow passages and would lead to a number of different migration regimes. Another case would be a situation where the radius of gyration of the molecule is much larger than the channel length and the pore size; a chain would then be partitioned between many pores and therefore invalidating the treatment given (e.g., Eq. (120) would no longer be valid). Finally, at high field intensity ϵ, the field-driven time of migration between channels may become shorter

than the relaxation time (i.e., the Rouse time τ_R in Eq. (48)) and the polymer therefore remains in a "squeezed" conformation when it tries to get through the next channel; in this case, the loss of entropy in the channel is less and equilibrium arguments such as those given in Section 4.1 fail. This limiting field would be approximately $\varepsilon_{max} \approx \Delta y(\pi/M)^2/\langle(\Delta r)^2\rangle$ where we have simply equated the Rouse time with the free drift time between channels and solved for the field; situations for which the fields are around or above this limiting field strength do not apply to the simple model presented. We have not pursued such detailed models in this thesis. However, these scenarios are interesting as they may be relevant for some experimental conditions.

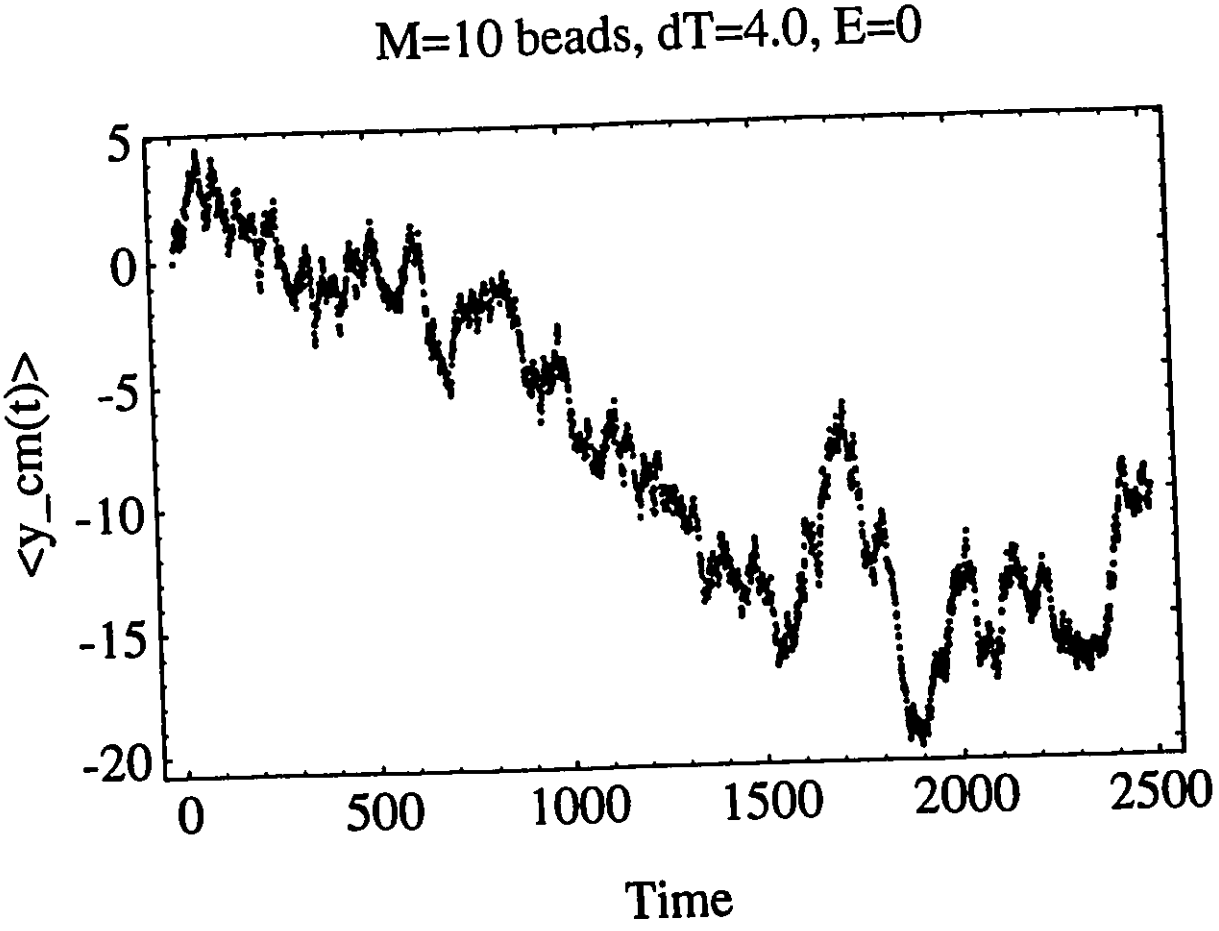

Fig. 4.20 - Displacement of the centre-of-mass y_{cm} with time for a single M=10 bead polymer chain within a tube of diameter d_t=4.0 in the absence of electric fields. The tube walls have semi-circular protrusions (wall obstacles) extending a radius ρ_{wobst}=1.0 from either wall face.

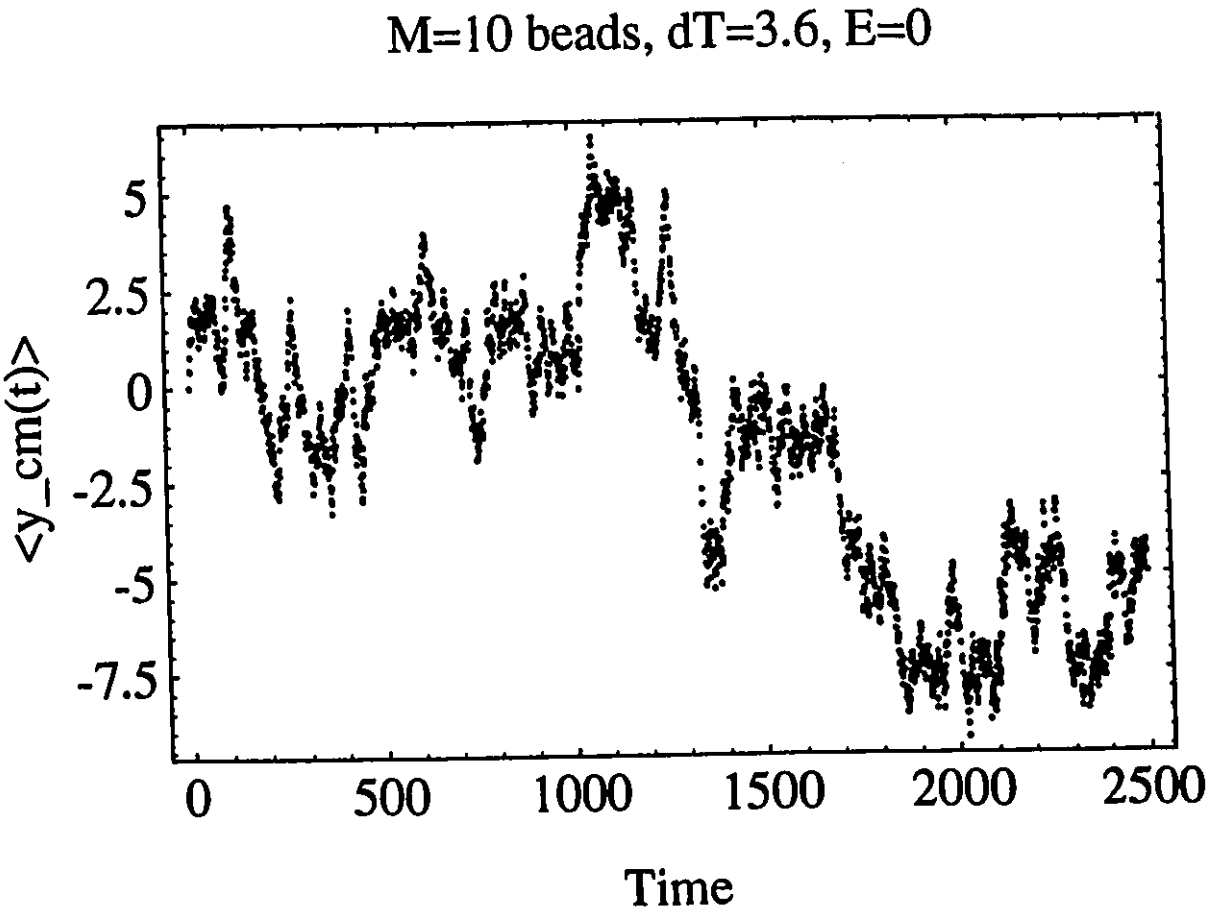

Fig. 4.21 - Displacement of the centre-of-mass y_{cm} with time for a single M=10 bead polymer chain within a tube of diameter d_T=3.6 in the absence of electric fields. The tube walls have semi-circular protrusions (wall obstacles) extending a radius ρ_{wobst}=1 from either wall face; the period of the wall obstacles is 3 units. Hence, the tube presents a series of pores and strictures (or channels) through which the polymer must migrate; here the channel width is d_C=1.6.

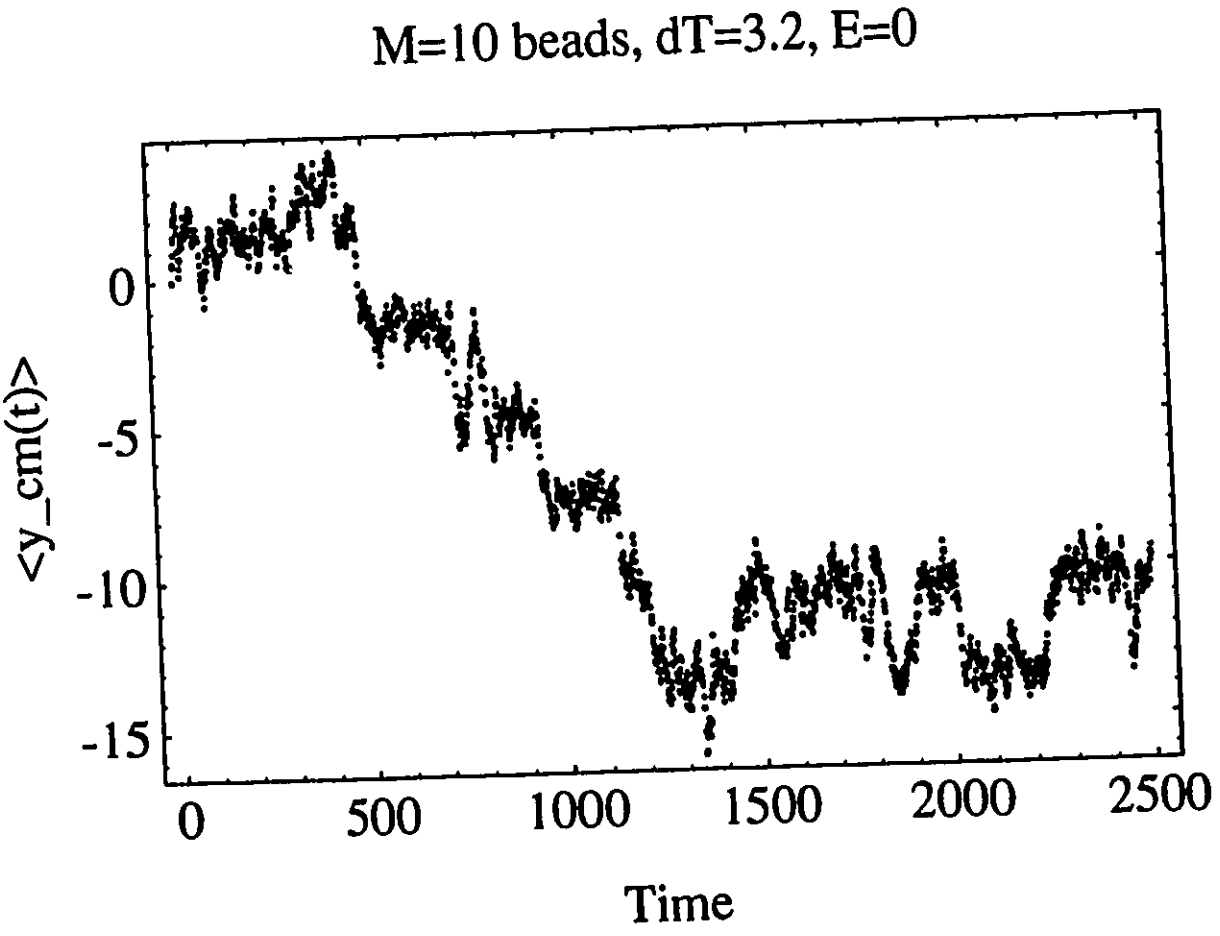

Fig. 4.22 - Displacement of the centre-of-mass y_{cm} with time for a single M=10 bead polymer chain within a tube of diameter d_T=3.2 in the absence of electric fields (ε=0). Here the channel width is d_C=1.2.

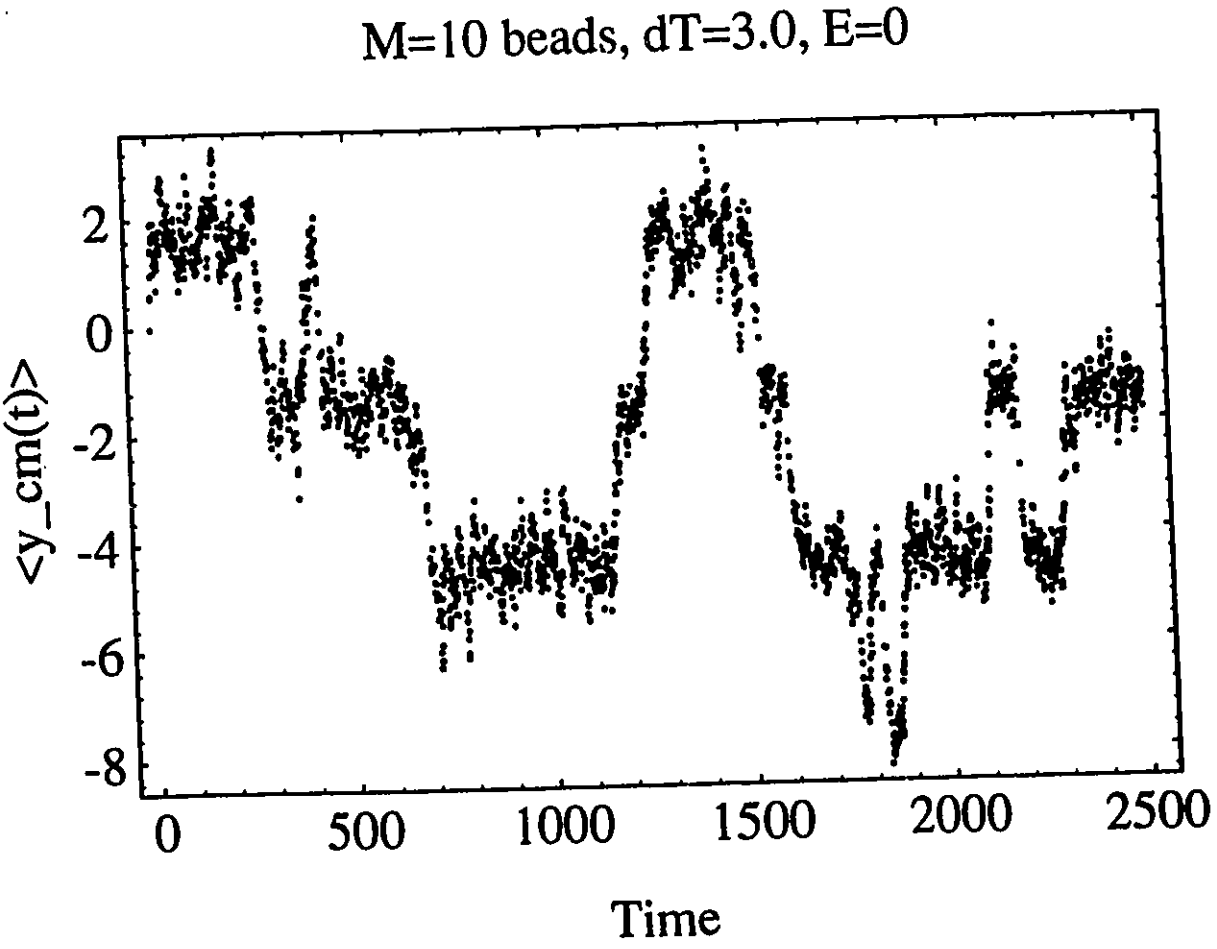

Fig. 4.23 - Displacement of the centre-of-mass y_{cm} with time for a single M=10 bead polymer chain within a tube of diameter d_T=3.0 in the absence of electric fields (ε=0). Here the channel width is d_C=1.0.

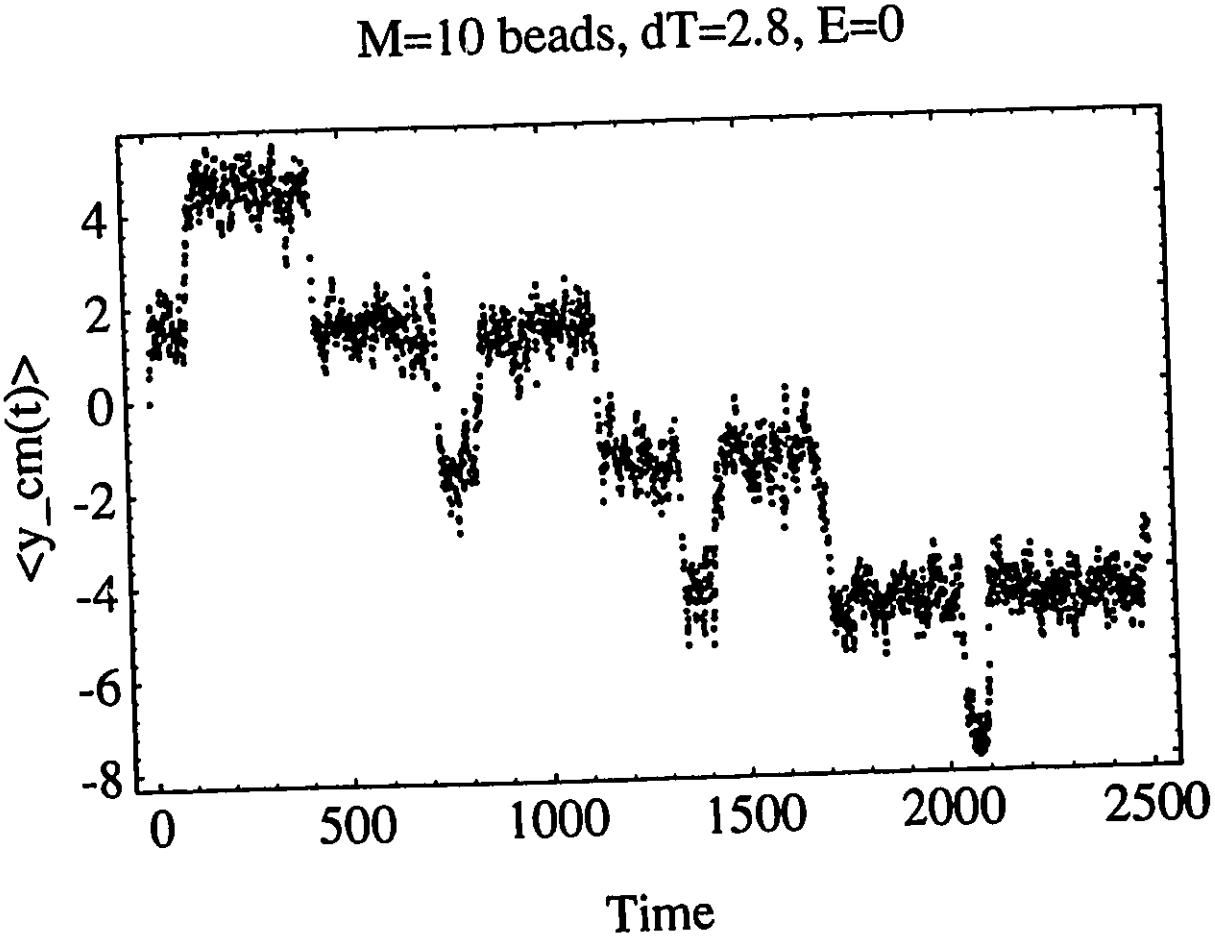

Fig. 4.24 - Displacement of the centre-of-mass y_{cm} with time for a single M=10 bead polymer chain within a tube of diameter d_T=2.8 in the absence of electric fields. The tube walls have semi-circular protrusions (wall obstacles) extending a radius ρ_{wobst}=1 from either wall face; the period of the wall obstacles is 3 units. Hence, the tube presents a series of pores and strictures through which the absence must migrate; here the channel width is d_C=0.8.

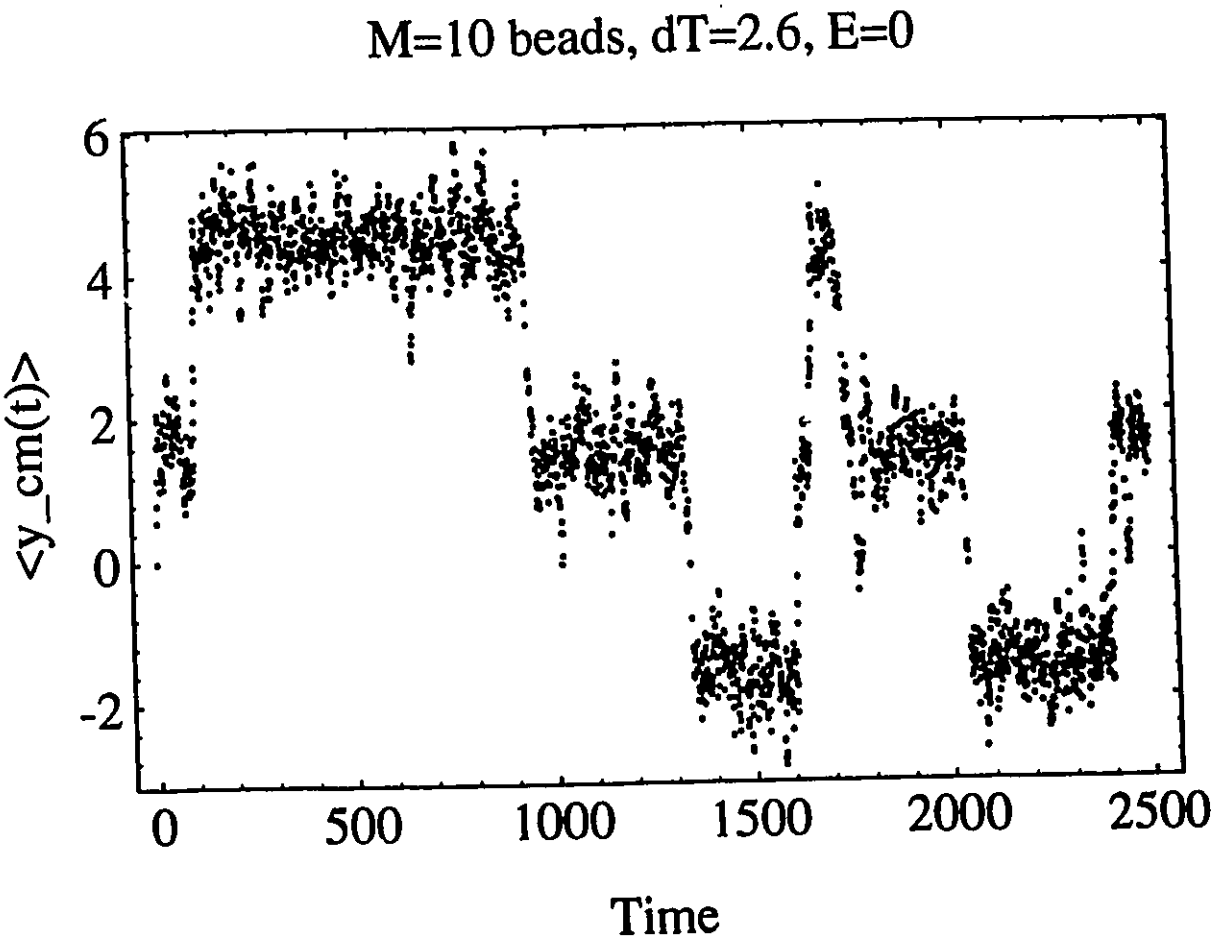

Fig. 4.25 - Displacement of the centre-of-mass y_{cm} with time for a single M=10 bead polymer chain within a tube of diameter d_T=2.6 in the absence of electric fields. The tube walls have semi-circular protrusions (wall obstacles) extending a radius ρ_{wobst}=1 from either wall face; the period of the wall obstacles is 3 units. Hence, the tube presents a series of pores and strictures through which the polymer must migrate; here the channel width is d_C=0.6.

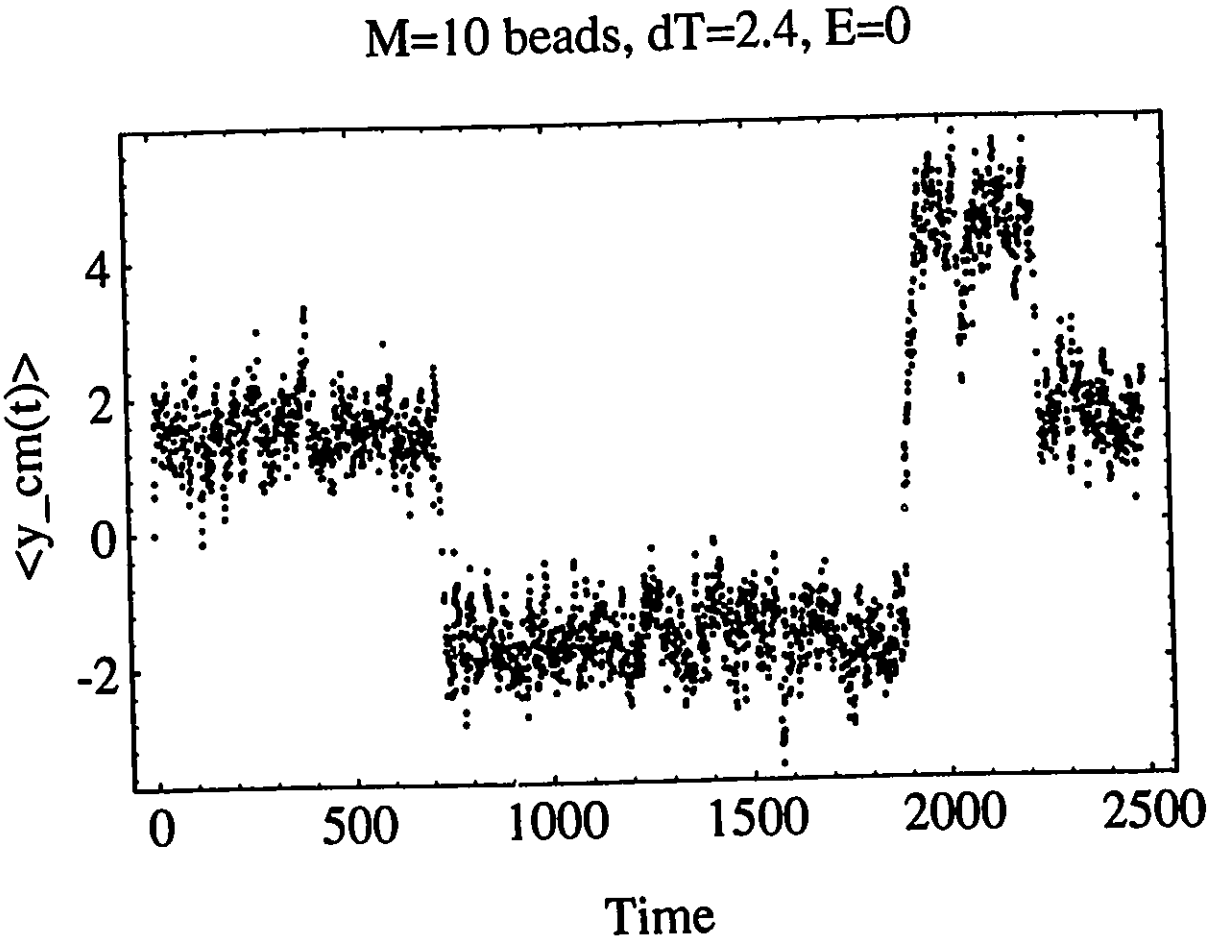

Fig. 4.26 - Displacement of the centre-of-mass y_{cm} with time for a single M=10 bead polymer chain within a tube of diameter d_T=2.4 in the absence of electric fields (ε=0). Here, the channel width is d_c=0.4.

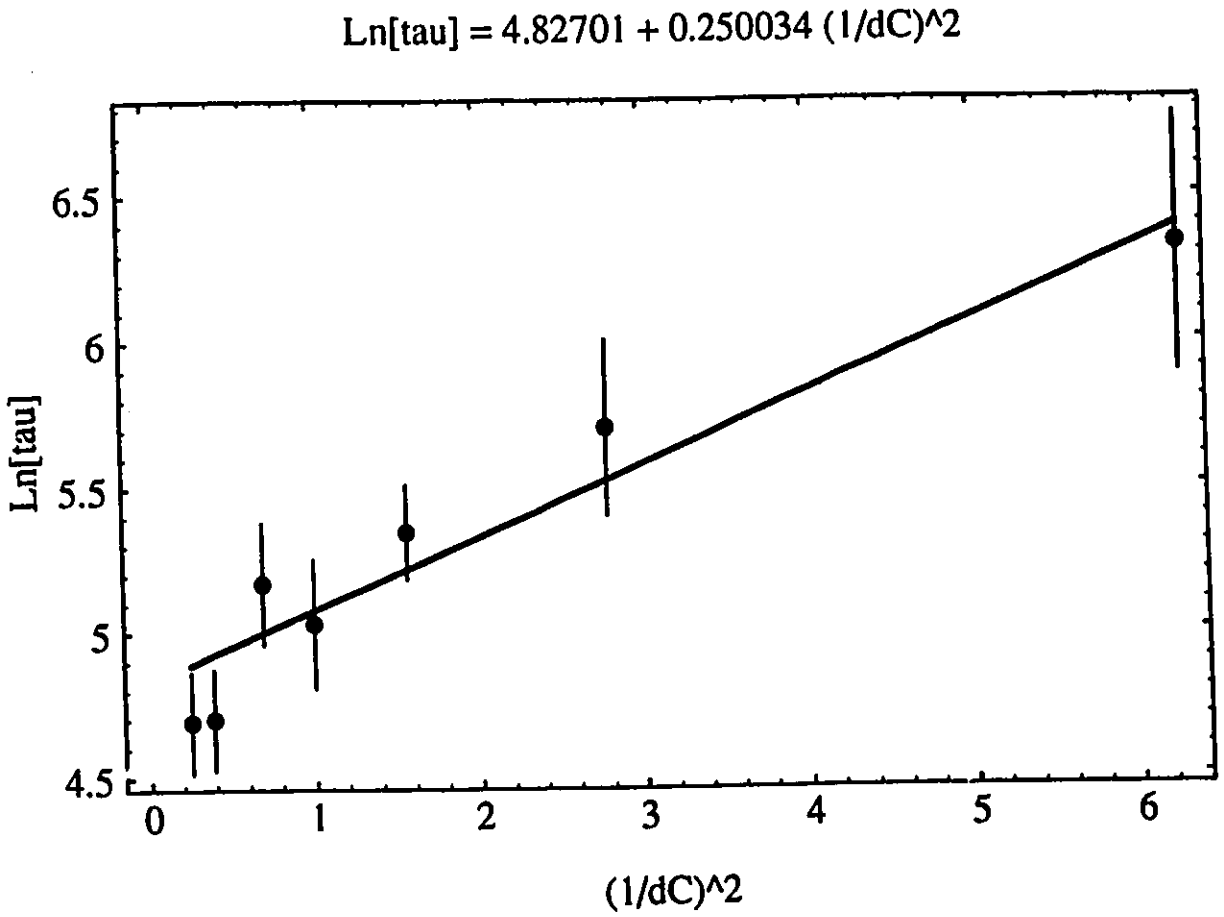

Fig. 4.27 - The mean trapping time $\langle \tau_{trap} \rangle$ is plotted versus the channel width d_C.

d_T	4	3.6	3.2	3	2.8	2.6	2.4
$\langle(\Delta r_x)^2\rangle$	0.07644	0.07496	0.07334	0.07303	0.07347	0.07281	0.07298
$\langle(\Delta r_y)^2\rangle$	0.08062	0.07901	0.08006	0.07780	0.07600	0.07667	0.07829
$\langle p_x^2\rangle$	0.4979	0.4637	0.4105	0.4109	0.4015	0.3882	0.3704
$\langle p_y^2\rangle$	0.6722	0.6114	0.6267	0.5590	0.5301	0.5411	0.5532
$\langle r_{gyr\_x}^2\rangle$	0.1039	0.09710	0.0913	0.0910	0.08983	0.0880	0.08682
$\langle r_{gyr\_y}^2\rangle$	0.1271	0.1204	0.1225	0.1114	0.1083	0.1083	0.1120
#trans	22	22	14	15	10	8	4
$\langle\tau_{trap}\rangle$	109(19)	110(19)	176(37)	153(34)	210(34)	300(91)	559(249)
$\#trans_+$	9	10	5	7	4	4	2
$\langle\tau_{trap}\rangle_+$	267(104)	241(57)	491(103)	329(34)	525(138)	600(347)	966(933)
$\#trans_-$	12	11	8	7	5	3	1
$\langle\tau_{trap}\rangle_-$	162(28)	196(49)	243(66)	271(104)	325(34)	366(36)	1505
$d_{cm\ y}$	0.0412(72)	0.0410(72)	0.0256(54)	0.0293(65)	0.0214(34)	0.0150(45)	0.0081(36)

Table 4.6 - The effect of squeezing on the static and dynamic properties of a M=10-bead chain with the exclusion of electric fields (ε=0) as seen from Figs. 4.20-4.27. All values were computed for a run of τ_{sim}=2500 and no warmup period (i.e., τ_{warm}=0). The direction perpendicular to the tube axis (the y-axis) is the x-axis. We distinguish the number of transitions in the direction of the positive y-axis, $\#trans_+$, from the number of transitions in the opposite direction, namely $\#trans_-$. Note that difference between the trapping time and the free-drift time $\langle\tau_{trap}\rangle$-$\langle\tau_{free\ drift}\rangle$ for the two largest tube diameters is nearly zero; the free drift time is simply $\langle\tau_{free\ drift}\rangle=\Delta y^2/2d_{cm}$=90 and twice this value for any particular direction $\langle\tau_{free\ drift}\rangle_\pm$=180. This implies that, for the larger d_C ($=d_T$-2×1) values, the chains barely exhibit any trapping.

field ε	0.01	0.025	0.05	0.2	0.4	0.5	0.75
#trans	63	26	57	439	1090	1433	2235
$\langle\tau_{trap}\rangle$	303(38)	348(44)	175(21)	22.77(71)	9.167(95)	6.972(44)	4.472(15)
$\#trans_+$	46	21	55	439	1090	1433	2235
$\langle\tau_{trap}\rangle_+$	415(61)	430(67)	181(25)	22.77(71)	9.167(95)	6.972(44)	4.472(15)
$\#trans_-$	16	4	1	0	0	0	0
$\langle\tau_{trap}\rangle_-$	978(199)	1949(190)	7114	N.A.	N.A.	N.A.	N.A.
v_{cm}	0.003590	0.004880	0.01693	0.1305	0.3260	0.4284	0.6688
mob. μ	0.3590	0.1952	0.3387	0.6524	0.8151	0.8567	0.8917

Table 4.7 - Tabulated results for the case of a M=10 bead chain confined in a tube of diameter d_T=2.8 with semi-circular protrusions (with period Δy=3) extending a distance ρ_{obst}=1 on the inside walls which yields a channel diameter of d_C=0.8. Note that the mobility is given by $\mu=v_{cm}/\varepsilon$ where the velocity of the centre-of-mass is $v_{cm}=\Delta y_{cm}/\Delta\tau$. All runs were conducted with a simulation time τ_{sim}=10000 except for the ε=0.01 case where τ_{sim}=19700.

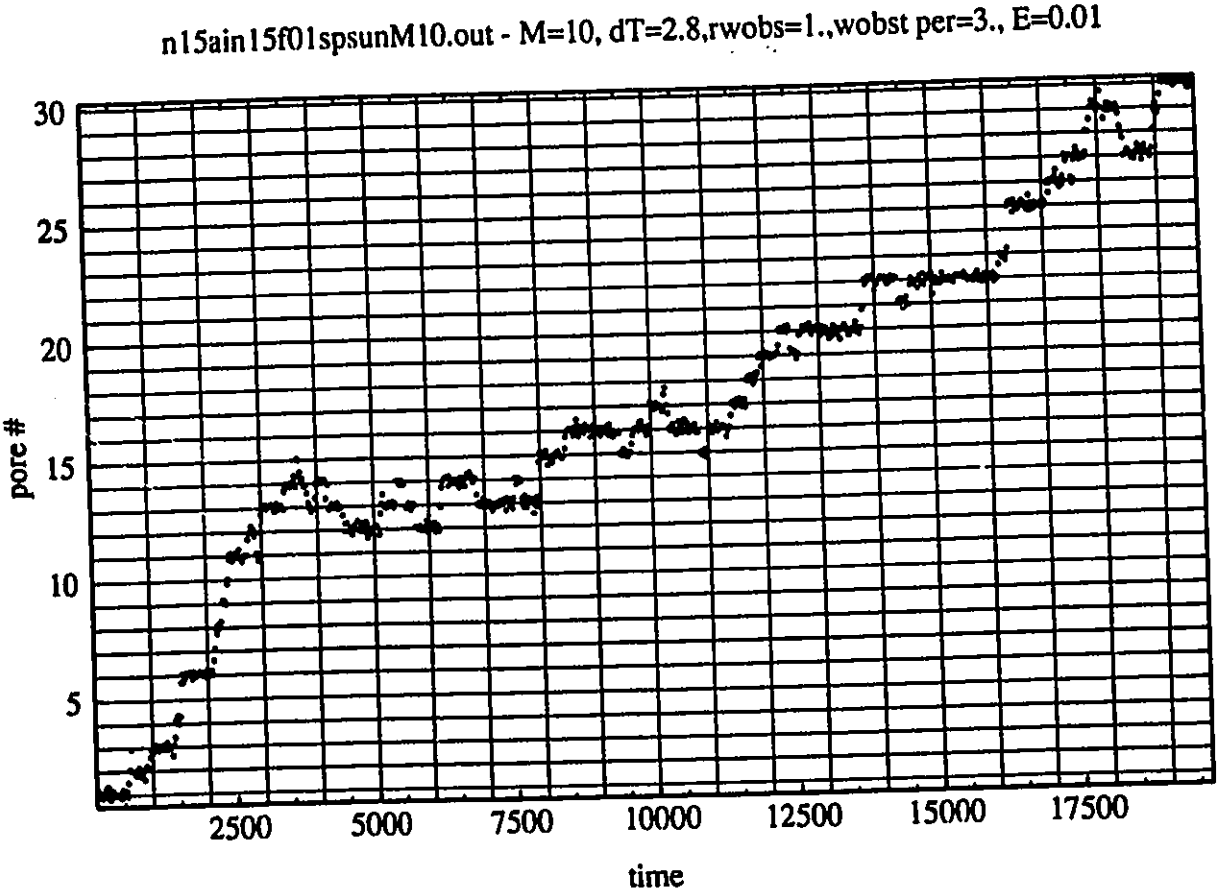

Fig. 4.28 - Position of centre-of-mass $y_{cm}(t)$ vs. time τ for a M=10 bead chain with a field intensity ε=0.01. The pore size is 3 units as given by the periodicity of the wall obstacles.

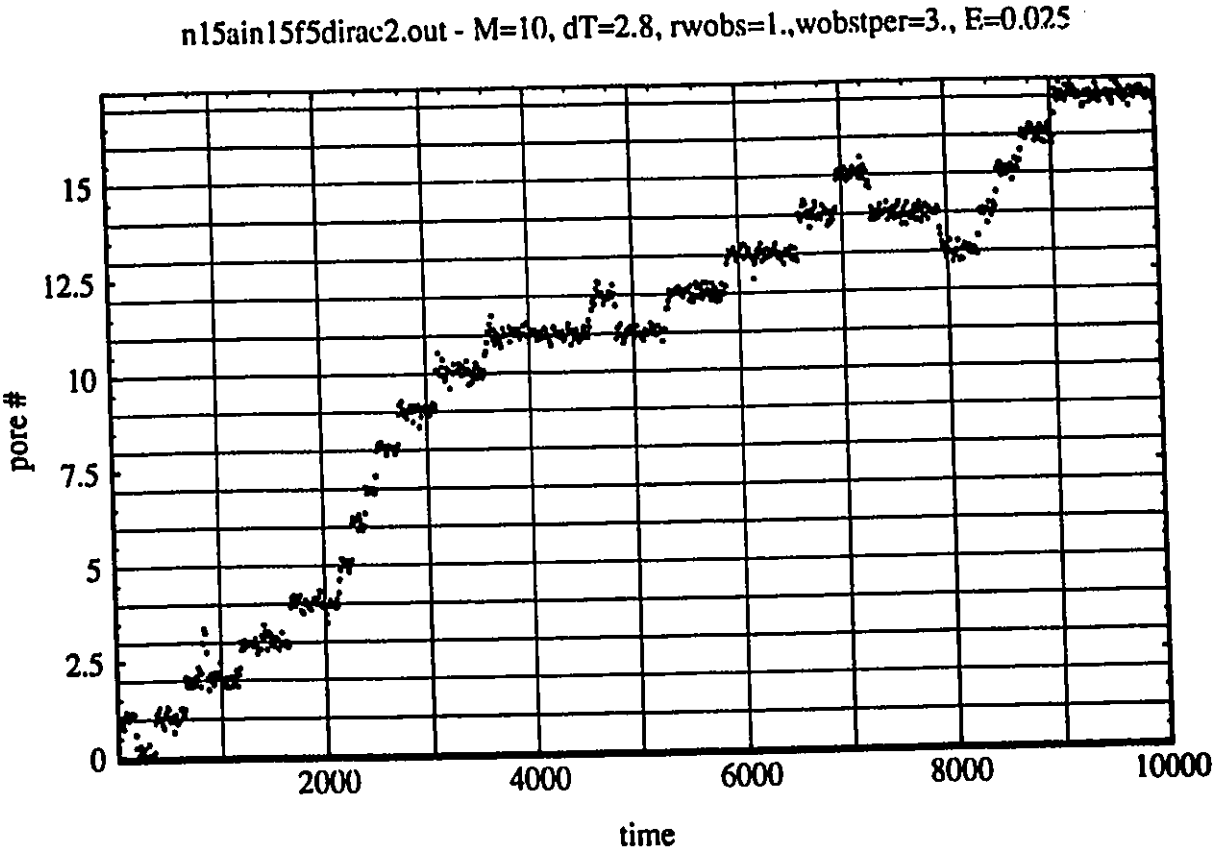

Fig. 4.29 - Position of centre-of-mass $y_{cm}(t)$ vs. time τ for a M=10 bead chain with a field intensity ε=0.025. The pore size is 3 units as given by the periodicity of the wall obstacles.

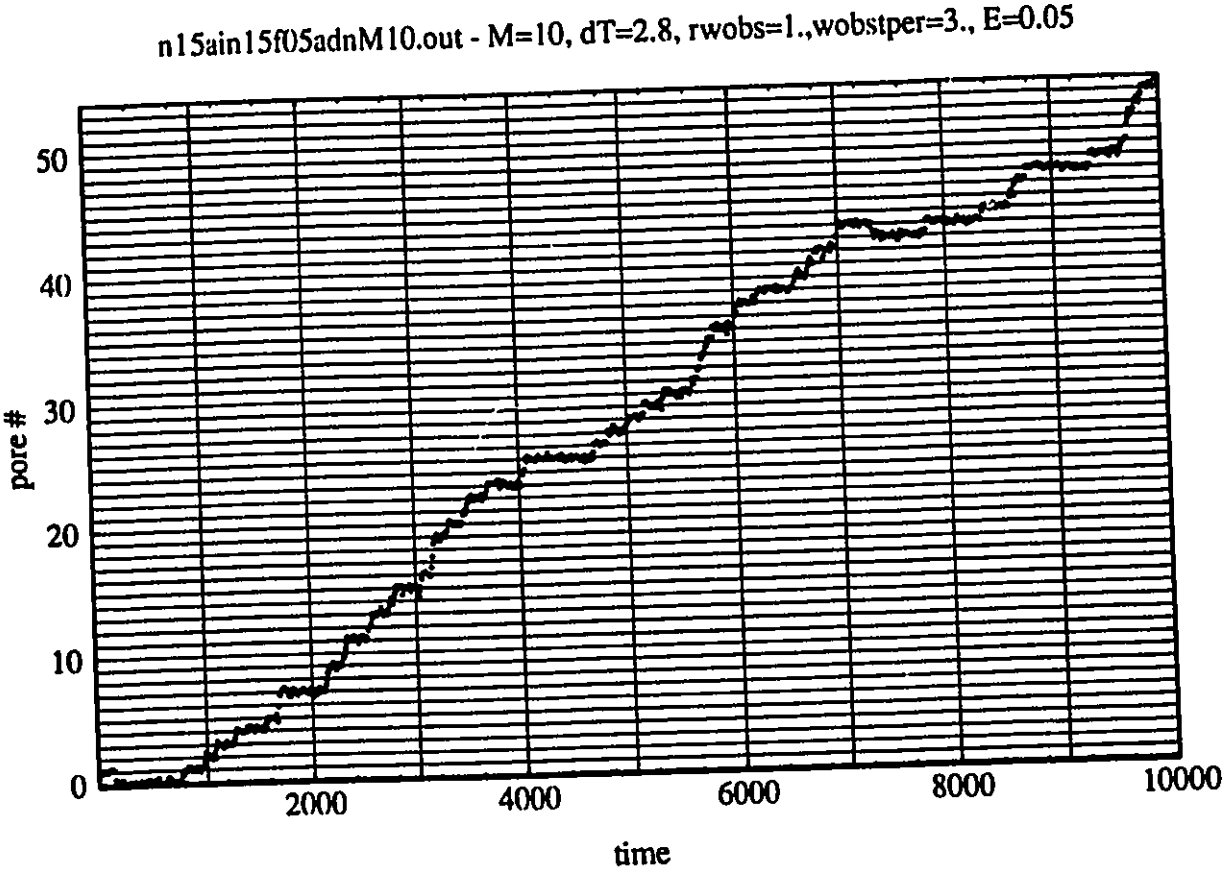

Fig. 4.30 - Position of centre-of-mass $y_{cm}(t)$ vs. time τ for a M=10 bead chain with a field intensity ε=0.05. The pore size is 3 units as given by the periodicity of the wall obstacles.

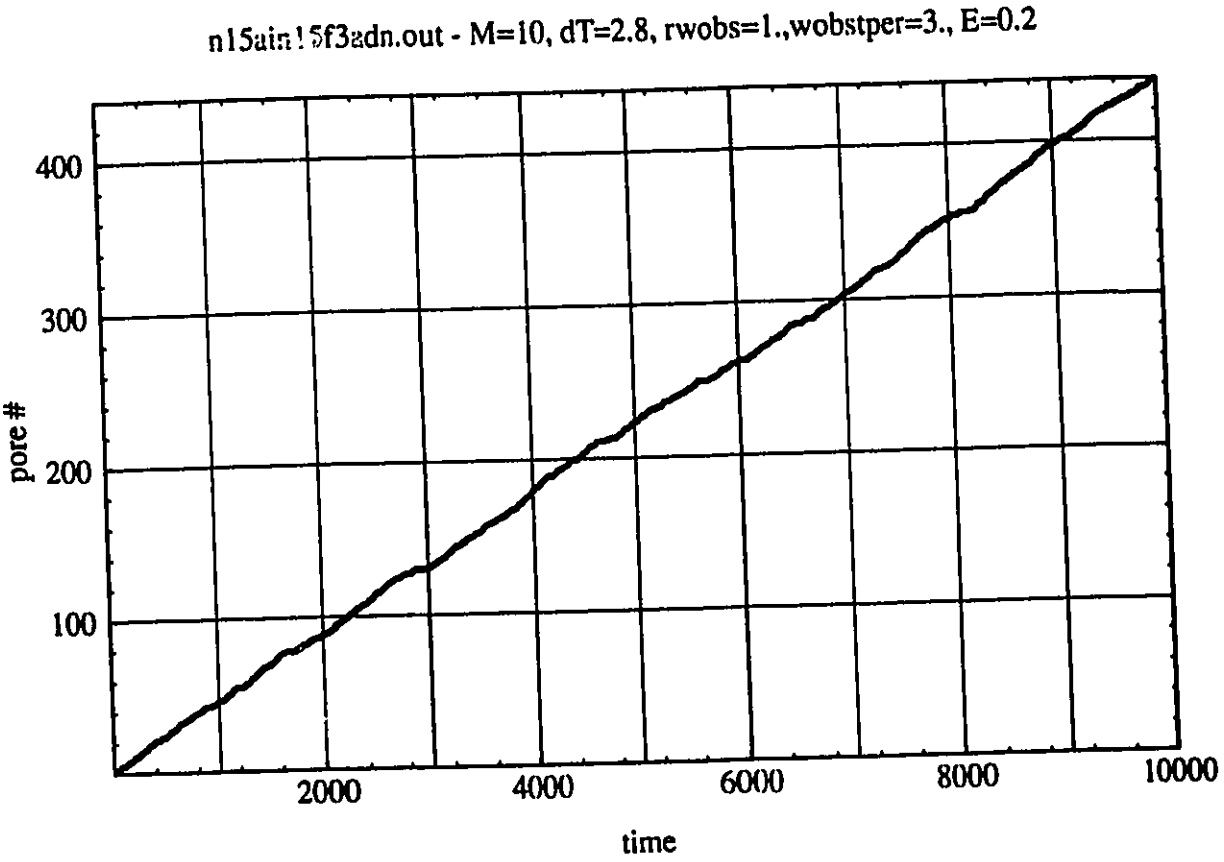

Fig. 4.31 - Position of centre-of-mass $y_{cm}(t)$ vs. time τ for a M=10 bead chain with a field intensity ε=0.2. The distance between pores is 3 units as given by the periodicity of the wall obstacles.

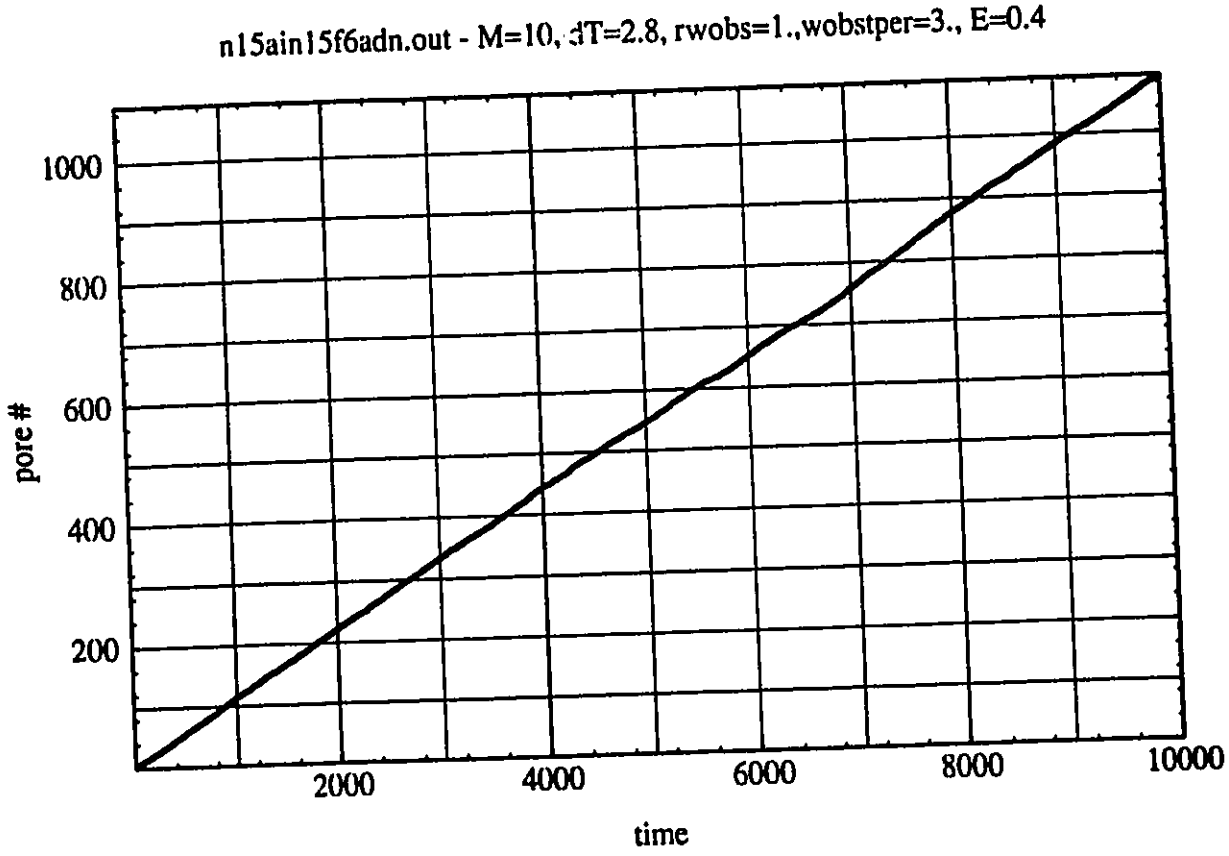

Fig. 4.32 - Position of the centre-of-mass $y_{cm}(t)$ vs. time τ for a M=10 bead chain with a field intensity ε=0.4. The pore size is 3 units as given by the periodicity of the wall obstacles.

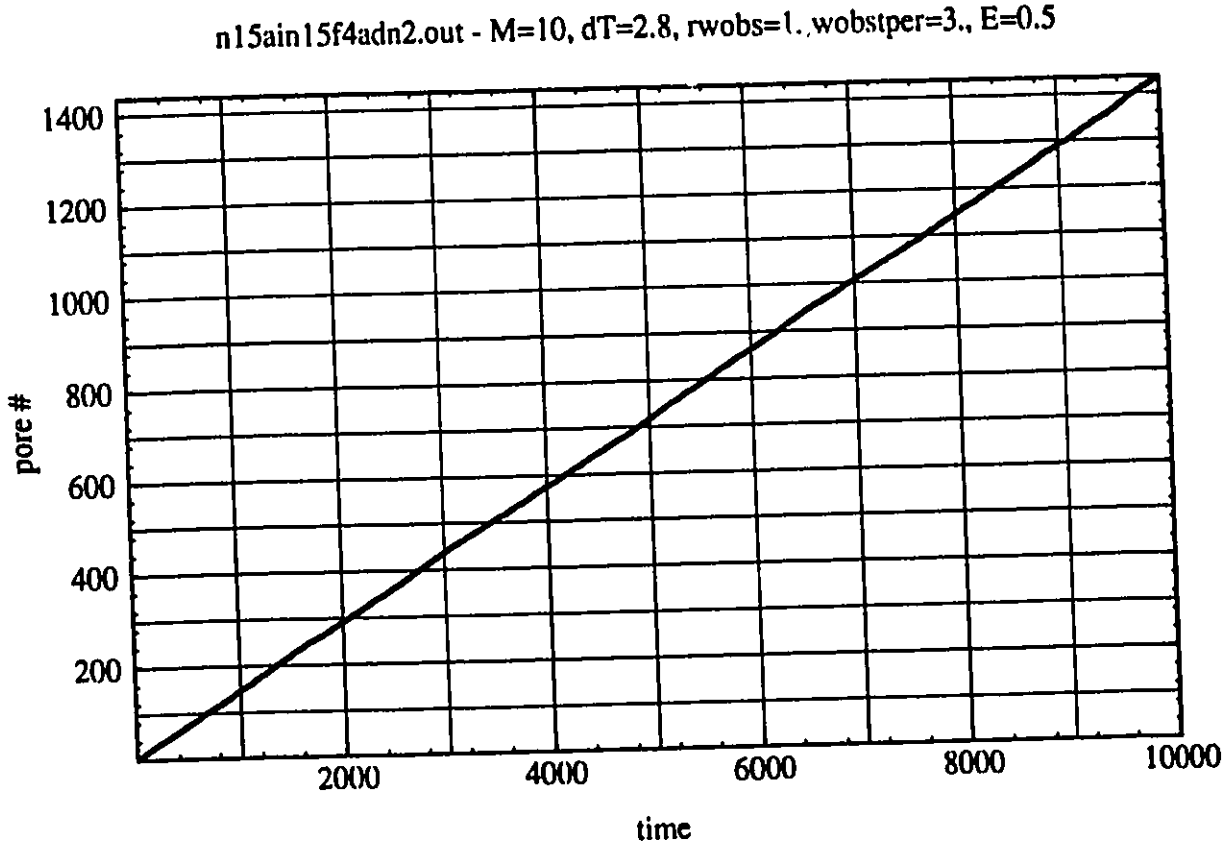

Fig. 4.33 - Position of centre-of-mass $y_{cm}(t)$ vs. time τ for a M=10 bead chain with a field intensity ε=0.5. The distance between pores is 3 units as given by the periodicity of the wall obstacles.

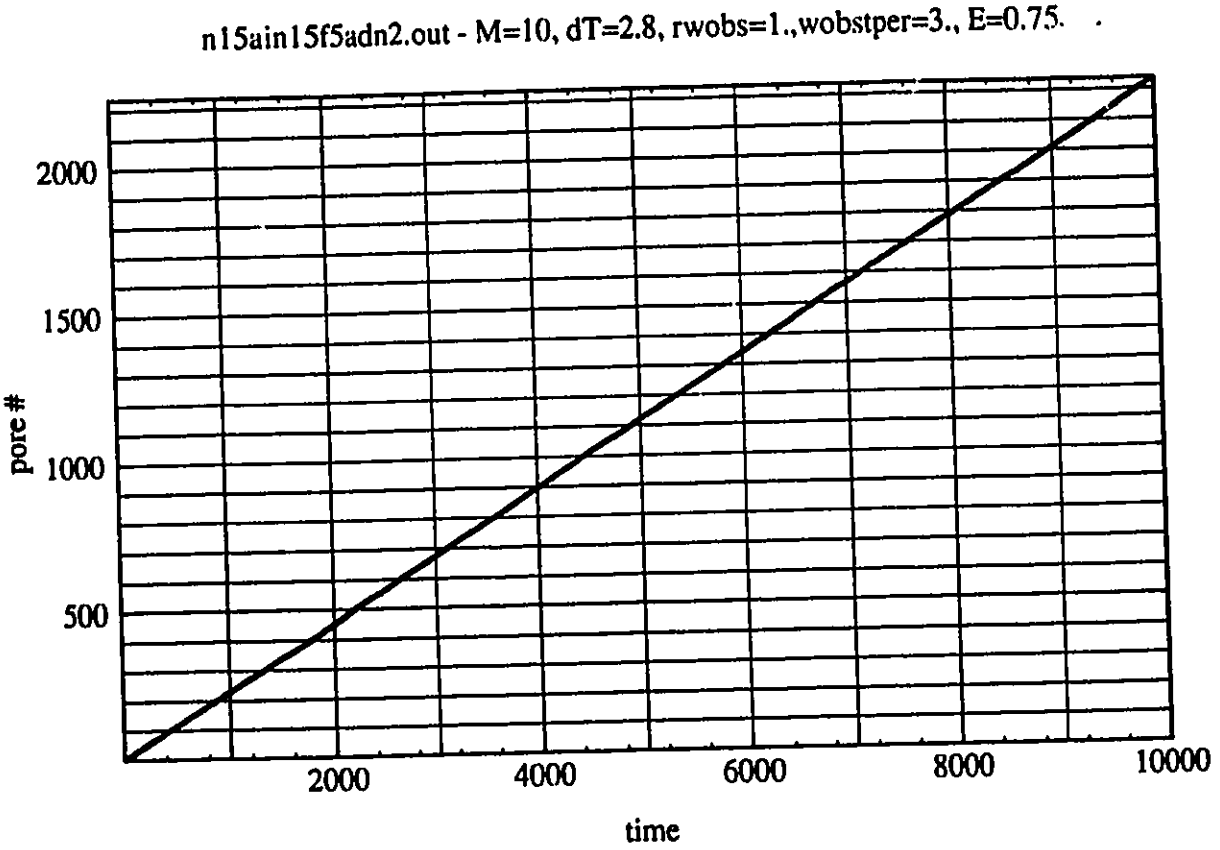

Fig. 4.34 - Position of centre-of-mass $y_{cm}(t)$ vs. time τ for a M=10 bead chain with a field intensity ε=0.75. The distance between pores is 3 units as given by the periodicity of the wall obstacles.

4.4.4 Effect of molecular size M on FAEM.

Table 4.8 gives a series of results for different molecular sizes and for three different field intensities: ε=0.01<ε_{crit}, ε=0.025≤ε_{crit} and ε=0.05≥ε_{crit}. The mean trapping time $\langle\tau_{trap}\rangle$ is a very strong function of the molecular size for the lower field intensity; Fig. 4.33 shows that our results agree with the exponential dependence predicted by Eqs. (122)-(123). However, $\langle\tau_{trap}\rangle$ is a weak function of the electric field strength for the intermediate field regime because the latter is just below the critical field intensity where the loss of entropy is exactly compensated by the gain in (electric) potential energy. Figure 4.33 also shows these data points. Finally, the trapping time $\langle\tau_{trap}\rangle$ becomes essentially independent of molecular size M when the field exceeds the critical field intensity since the Boltzmann factor (Eq. (122)) then exceeds unity (the channels do not restrict the motion anymore). This is the free-draining limit where the velocity is not a function of molecular size.

Finally, it should be noted that in the low field case, where the trapping time is molecular-size dependent, the standard-deviation of the mean trapping time is huge. This clearly indicates that this mechanism cannot be used to separate molecules of different sizes: the different populations of molecules would just overlap too much. This is in agreement with experimental results which show extreme band broadening in the entropic trapping regime in gels.[42]

Of course, the limited number of trial runs and the limited run times make our analysis semi-quantitative at best. However, our results are in agreement with our simple model of entropic trapping.

---

[42] Pascal Mayer and Guy Drouin (unpublished results).

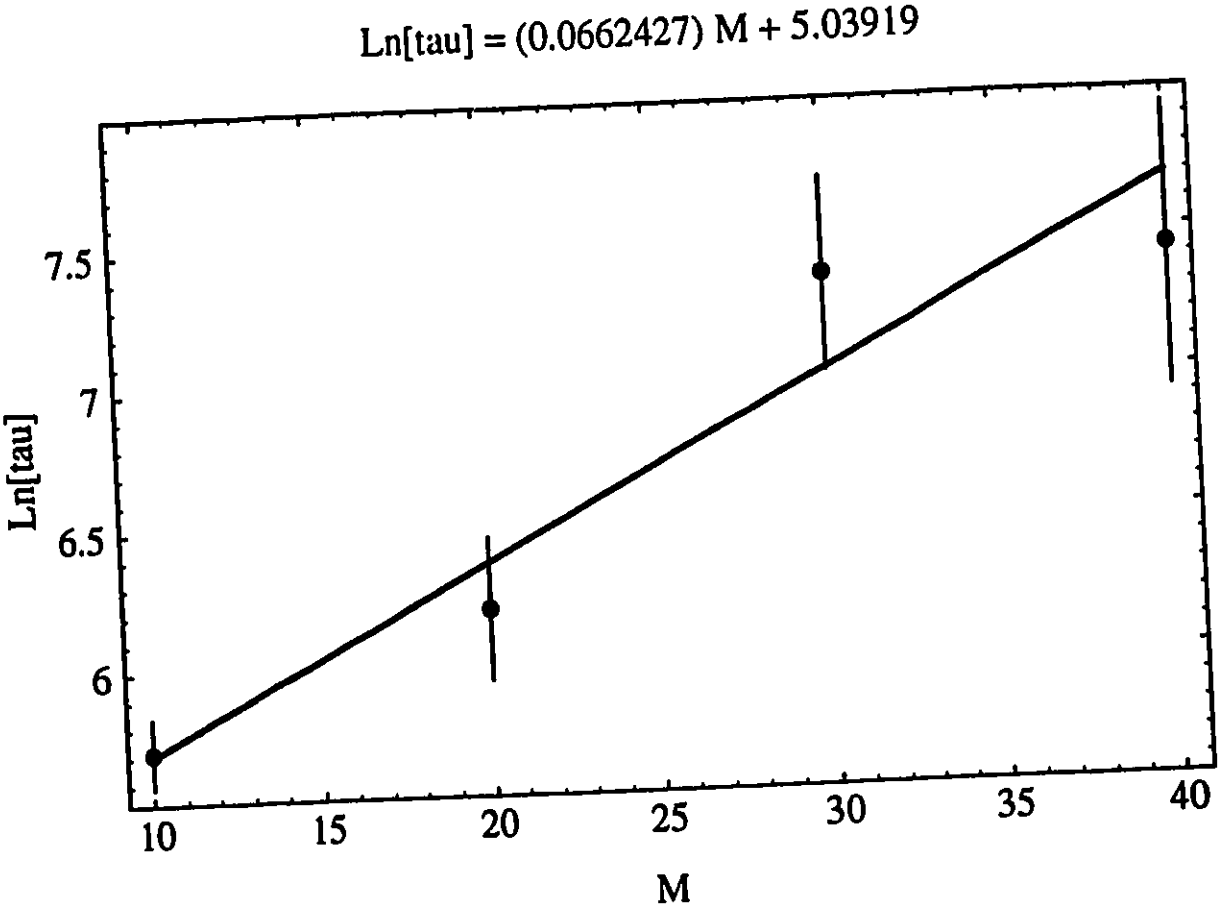

Fig. 4.35 - Here, we verify the scaling law for the mean trapping time $\langle \tau_{trap} \rangle$ as a function of molecular size M for the low-field regime ε=0.01 as given by Eqs. (123 and 122).

e=0.01:

#beads M	10 (τ_{sim}=19700)	20 (τ_{sim}=5117)	30 (τ_{sim}=10000)	40 (τ_{sim}=10000)
#trans	63	7	5	3
$\langle\tau_{trap}\rangle$	303(38)	493(125)	1578(550))	1684(857)
#trans$_+$	46	6	5	3
$\langle\tau_{trap}\rangle_+$	415(38)	575(170)	1578(550))	1684(857)
#trans$_-$	16	0	0	0
$\langle\tau_{trap}\rangle_-$	978(199)	N.A.	N.A.	N.A.
v_{cm}	0.00359()	0.00443()	0.001582	0.001547
mobility μ	0.359()	0.443()	0.1582	0.1547

e=0.025:

#beads M	10 (τ_{sim}=10000)	20 (τ_{sim}=10000)	30 (τ_{sim}=10000)	40 (τ_{sim}=10000)
#transitions	26	14	13	8
$\langle\tau_{trap}\rangle$	348(44)	525(152)	577(149)	897(252)
#trans$_+$	21	13	13	8
$\langle\tau_{trap}\rangle_+$	430(67)	565(160)	577(149)	897(252)
#trans$_-$	4	0	0	0
$\langle\tau_{trap}\rangle_-$	1949(790)	N.A.	N.A.	N.A.
v_{cm}	0.00488()	0.00350()	0.00446()	0.003058
mobility μ	0.1952	0.1402	0.1785	0.1223

e=0.05:

#beads M	10 (τ_{sim}=10000)	20 (τ_{sim}=10000)	30 (τ_{sim}=8543)	40 (τ_{sim}=10000)	50 (τ_{sim}=24320)
transitions	57	39	32	43	90
$\langle\tau_{pore}\rangle$	175(21)	255(36)	258(30)	231(29)	267(21)
#trans$_+$	55	39	32	32	90
$\langle\tau_{trap}\rangle_+$	181(25)	255(36)	258(30)	231(29)	267(21)
#trans$_-$	1	0	0	0	0
$\langle\tau_{trap}\rangle_-$	7114	N.A.	N.A.	N.A.	N.A.
v_{cm}	0.01693	0.01243	0.01088	0.01365	0.01131
mobility μ	0.3387	0.2485	0.2177	0.2731	0.2263

Table 4.8 - The effect of molecular size on the migration process. The field strengths were e=0.01, 0.025, and 0.05. The tube diameter was d_T=2.8 and the channel diameter was d_C=0.8.

Chapter 5

Conclusion

Our Brownian Dynamics algorithm can simulate both linear and nonlinear polymers, including polyelectrolytes such as DNA, under a wide range of conditions such as high electric fields, confined media, interactions with obstacles and pores, etc.

The integration scheme we used is an innovation permitting the algorithm to integrate accurately while maintaining efficiency. A dynamically self-adjusting time increment permits smooth integration even under high stresses. The maximum grain of the integration is specified by a maximum jump-size constraint λ and a maximum time step $\Delta\tau_{max}$. The time increment attempts to increase in time to permit the program to use as large a time increment as permissible (up to the set maximum time increment $\Delta\tau_{max}$); this increases the efficiency drastically. The accuracy part of the integration scheme is more subtle. Having a self-regulating time increment may cause a bias in the system; large Langevin forces tend to breach more constraints (e.g., the maximum jump size constraint λ or spring overstretching) by inducing more stress into the system. In such cases, the algorithm would reduce the time increment accordingly; hence, the algorithm would use smaller time increments for larger stochastic (Langevin) forces. The consequence of this bias is to effectively "cool" the system; the system then behaves as if the temperature is lower than it should otherwise be. It was demonstrated that this predicament can be avoided by requiring Langevin forces to experience *approximately* the same time increment

on the average. To this end, we proposed a geometrically increasing time increment characterized by maximum time increment $\Delta\tau_{max}$ and a damping parameter m; the evolution rate of the time increment decreases with m and the maximum grain of integration is set by the maximum time increment $\Delta\tau_{max}$.

The damping parameter m plays an vital role in the accuracy of the integration scheme. Below a certain critical value, $m_{crit}=1000$, cooling begins to manifest while above m_{crit} the statistics prove to be devoid of this cooling bias. Moreover, it was concluded that there is little penalty, with regards to CPU time, to increase m to a value substantially above m_{crit}, even by one or two orders of magnitude! We found that the maximum time increment, $\Delta\tau_{max}$, can be set to some conveniently large value (e.g., $\Delta\tau_{max}=0.5$) with much gain in the way of integration speed. However, if pursued to extreme values the integration becomes too grainy, and the frequency of spring over-stretching (the maximum spring extensions is $\langle(\Delta r)^2\rangle_{max}=1$) causes the simulation to slow down. Except for a slight increase in the value of $\langle(\Delta r)^2\rangle$ (and related statistics) due to the graininess, there is no noticeable effect on overall simulation accuracy w.r.t. the choice of $\Delta\tau_{max}$.

After carefully benchmarking the program, by verifying that the simulated statistics under Rouse-like conditions reproduce the results predicted by the Rouse model (which are analytical), we proceeded to investigate the effects of confining walls. Again, the resulting statistics were compared with known scaling results and were shown to agree quantitatively.

We next applied the algorithm to the study of simple electrophoretic collisions. Here, four separate regimes were identified: (1) The chains are initially in free drift. (2) At the onset of the collision process, there is a stacking period where band dispersion is substantially reduced. Unfortunately, this is followed by (3) an unstacking or escape regime where there is a rapid onset

of diffusion (this effect was overlooked in a recent study by Volkmuth et al. (1994)). Finally, (4), there is an asymptotic regime beyond which the polyelectrolytes are no longer interacting with the obstacle which produced the collision and where they relax to equilibrium conformations. We provide a simple analytical calculation describing the escape process of the third regime. The simulation results corroborate our theoretical estimates in the experimentally relevant limit of large molecular sizes M and high fields ε. It was found that isolated collisions are disastrous w.r.t. the resolution of electrophoretically migrating molecular bands. In the near future, we will investigate the physics behind migration through filters (which may involve multiple, simultaneous collisions) by placing many obstacles in ordered and random conformations so that we can compare our simulations with experimental results (such as those obtained by Volkmuth et al. (1994) or in traditional gel electrophoresis experiments).

Finally, we investigated the onset of the entropic trapping regime. These investigations are, to our knowledge, the first to deal with the compounding effects of electric fields ε w.r.t. molecular size M within a simple system where scaling arguments apply; moreover, we are the first to introduce the notion of a critical field analytically and verify its manifestation with simulations. These scaling arguments were substantiated semi-quantitatively by our simulations. Unfortunately, for the low field case, where the trapping time is molecular-size dependent, the variance on the trapping time is so large as to render this process useless for separation purposes.

Detailed follow-up studies which will include the effects of random surface roughness and pulsed fields (and stochastic resonance) on polymeric systems (e.g., stars, rings, etc.) are planned for a supercomputer recently granted to G. W. Slater (U. Ottawa) and six other professors (U. de Sherbrooke and U. de Montréal) where our algorithm will be reprogrammed to run in parallel.

Appendix A

Macromol. Theory Simul. 3, 695–704 (1994)

Construction of approximate entropic forces for finitely extensible nonlinear elastic (FENE) polymers

Gary W. Slater, Sylvain J. Hubert, Grant I. Nixon*

Department of Physics, University of Ottawa, P.O. Box 450, Station A, 150 Louis Pasteur, Ottawa, Ontario, Canada K1N 6N5

(Received: November 8, 1993; revised manuscript of January 12, 1994)

SUMMARY:

When the stress applied to a Rouse-like polymer chain is large enough, one must use anharmonic entropic spring forces in order to keep the chain contour length from increasing to unphysical values. Although one can derive "exact" equations relating the spring extension to the entropic force produced by a finitely extensible non-linear elastic (FENE) random-walk polymer, such expressions are usually of little interest because their complexity would entail large evaluation times in numerical studies by computer. Moreover, these expressions can rarely be used directly in analytical studies. In this article, we describe a systematic method to construct analytically simple yet numerically accurate expressions to relate the entropic force to the extension of an entropic spring for a random-walk polymer chain in arbitrary dimension $d \geq 2$. These expressions are modified Pade approximants which yield the correct asymptotic behaviours in both the small and large extension limits. It is shown that the well-known Warner empirical approximation is but a limiting case (for infinite dimensions).

Introduction

The relationship between the end-to-end distance of an ideal, freely jointed polymer chain and the entropic force pulling its ends together is used in many theoretical studies of polymer properties and their dynamics. The standard harmonic approximation leads to simple analytical results in the case of the Rouse model[1] and, consequently, it has been used extensively. However, there are many situations where it is inadequate. For example, the study of chain fracture in extensional flow requires the use of a force-law characteristic of finitely-extensible polymer chains[2]. Another example is provided by the study of polymers in shear flows which requires the use of finitely extensible nonlinear elastic (FENE) dumbbells[3,4] or bead spring models[5] (see also the discussion by Bird and Öttinger[6]). FENE potentials are also used for molecular dynamics simulations of polymer melts[7].

Recently, the study of DNA gel electrophoresis has led to the development of numerous computer simulation algorithms[8], some of which were based on a Brownian dynamics approach. In the latter case, an entropic force-law must be used to represent the tension in the link between consecutive electrically charged "beads". Harmonic "springs" were shown to produce unphysical molecular stretching in the presence of relatively low-intensity electric fields[9]. Smith et al.[10] used a simple anharmonic force-law, while Noolandi et al.[11] used the exact anharmonic force-law for three-dimensional random-walk polymer chains (i.e., without excluded volume effects; see Eq. (7) below). In the last two cases, one also could have used the force-law

 CCC 1022-1344/94/$03.00

for a one-dimensional polymer chain (see Eq. (4) below) since the DNA molecule was forced to move along the axis of a narrow tube. Lately, analytical models of DNA stretching during electrophoresis also made use of anharmonic force-laws[12-14].

The use of anharmonic force-laws in analytical studies usually leads to untractable mathematics because of the complicated nature of the resulting expressions. In simulation studies, these force-laws must be inverted numerically, which is very time-consuming. Tabulating the force values may help reduce the numerical problem, but this method leads to instabilities when the stress is very large (the difference between two consecutive tabulated forces may become extremely large for large polymer extensions).

In a recent simulation study of DNA capillary gel electrophoresis in two dimensions[15], we had to generate a table for the anharmonic force-law (which required the inversion of a ratio of modified Bessel functions); however, because of the instability problems mentioned above, we also had to use an analytical approximation for large extensions. Our investigation of Warner's approximation[16] indicated that it is exceedingly inaccurate for low-dimensionalities, even for moderate spring extensions. In three dimensions, for example, the relative error is more than 33% for extensions above 80% (see our Fig. 1); for two dimensions; the relative error already exceeds 50% at 80% extension. We therefore devised a method to systematically construct rational approximations to the exact anharmonic force-laws for arbitrary dimensionality $d \geq 2$. These approximations are remarkably accurate, both for small *and* large spring extensions, and can be computed very efficiently in computer simulation programs. Moreover, we can also construct rational approximations that can be integrated analytically to give the distribution function for the end-to-end distance of the anharmonic polymer chain; this can greatly help when one analyzes the results of computer simulations.

This article describes our method along with presenting a few typical results. Our approach also leads to better understanding of the assumptions behind Warner's approximation and offers alternative force-laws for analytical and numerical studies of polymers under large stresses. Of course, this method is general and may also be used to construct approximations to many other complicated functions whose asymptotic behaviours are known.

The general entropic spring

The procedure used to determine the relation between the entropic force $f(r)$ and the distance r between the ends of a polymer chain (without excluded volume effects, hydrodynamic effects or internal energy contributions) is well-known[17]. As a simple example, in one dimension (1D), each of the N polymer segments forming the entropic spring may possess but one of two possible projections along the force axis. The single-segment partition function is therefore given by

$$Z_{d=1} = e^{+f_s} + e^{-f_s} = 2 \cosh f_s \tag{1}$$

where the scaled force f_s is defined as

$$f_a = \frac{fa}{k_B T} \tag{2}$$

Here, f is the force "applied to" the ends of the entropic spring and a is the segment length. Since the N segments are mutually-independent (this is the stress ensemble), the average projection of the end-to-end spring vector on the force axis is given by:

$$r = k_B T \frac{\partial \ln Z_d^N}{\partial f} \tag{3}$$

Using Eqs. (1) and (3), we obtain:

$$r_{d=1} = Na \tanh f_a \tag{4}$$

This is a familiar expression of statistical mechanics analogous to what is obtained in spin-1/2 models of paramagnetism. It is fairly easy to invert Eq. (4) to obtain $f(r)$. Note that the maximum spring extension is $r_{max} = Na$, as required.

For $d > 1$, the same procedure can be used but one must project the segment vectors on the force axis. The one-segment partition function for d dimensions can be calculated using hyper spherical coordinates (see Eq. (8.431.3) of ref.[18] for the solution to the integral)

$$Z_d \sim \int_0^\pi e^{f_a \cos\theta} [\sin\theta]^{d-2} \, d\theta = C f_a^{-(d/2-1)} I_{d/2-1}(f_a) \tag{5}$$

where C is a constant and I_s is a modified Bessel function of the first kind of order s. Eqs. (3) and (5) yield directly (using Eq. (8.486.6) of ref.[18])

$$R = \frac{r}{Na} = \frac{I_{d/2}(f_a)}{I_{d/2-1}(f_a)} \tag{6}$$

where we have introduced the reduced end-to-end distance $R = r/r_{max} = r/(Na)$. This result is general (i.e., it is good for all dimensions $d \geq 1$) as can be easily verified. For instance, Eq. (4) is recovered for $d = 1$ and the $d = 3$ result is correctly found to be[17]:

$$R = \coth(f_a) - \frac{1}{f_a} \tag{7}$$

This is the well-known Langevin function. However, Eq. (6) cannot be inverted analytically (to give $f_a(R)$ instead of $R(f_a)$). In the next section, we will describe a systematic method to construct simple yet accurate rational approximations which can replace the time-consuming numerical inversion of Eq. (6); these approximations will preserve the original asymptotic behaviour of $f_a(R)$ for both limits $R \to 0$ and $R \to 1$.

Rational approximations

Series expansions

The Taylor series expansion of Eq. (6) about $f_a = 0$ is:

$$R = \frac{f_a}{d} - \frac{(f_a/d)^3}{1 + 2/d} + \frac{2(f_a/d)^5}{(1 + 2/d)(1 + 4/d)} - \frac{(5 + 12/d)(f_a/d)^7}{(1 + 2/d)^2(1 + 4/d)(1 + 6/d)} + - \ldots \tag{8}$$

Keeping only the first term of the expansion leads to the simple harmonic approximation

$$\frac{f_s}{d} = R \quad \text{or} \quad f = \frac{dk_B T}{Na^2} r \tag{9}$$

where Na^2 is the mean-square end-to-end distance $\langle r^2 \rangle_{harm}$ for a harmonic entropic spring. This is the approximation used in most low-deformation calculations and it allows for exact analytical results in the case of the Rouse model of polymer relaxation[1]. The other expansion terms in Eq. (8) embody the anharmonic effects; however, truncating the series would lead to major problems in the presence of large forces since the extension would then diverge. Therefore, in principle, we must invert the infinite series, not a truncated one. In numerical studies, we must solve Eq. (6) numerically for f_s given a (mean) extension R.

The series expansion for the force $f_s(R)$, obtained from the algebraic inversion of Eq. (8), is:

$$\frac{f_s}{d} = R + \frac{R^3}{1+2/d} + \frac{(1+8/d)R^5}{(1+2/d)^2(1+4/d)} + \frac{(1+14/d+120/d^2)R^7}{(1+2/d)^3(1+4/d)(1+6/d)} + \ldots \tag{10}$$

Again, truncating the series would lead to incorrect asymptotic behaviour since the entropic force would then fail to diverge at full extension ($R = 1$).

To construct our rational approximations, we will be using the following asymptotic expansion for the modified Bessel function (Eq. (9.7.1) of ref.[19]):

$$I_s(f_s) = \frac{e^{f_s}}{\sqrt{2\pi f_s}} \cdot \left[1 - \frac{4s^2 - 1}{8f_s} + \frac{(4s^2-1)(4s^2-9)}{2!(8f_s)^2} - \ldots \right] \tag{11}$$

When the extension R approaches its maximum value (unity), the scaled entropic force f_s becomes very large and we can use the first two terms on the right hand side (rhs) of Eq. (11) to obtain the following asymptotic behaviour:

$$\frac{f_s}{d} \approx \frac{1 - 1/d}{2(1-R)} \quad \text{for} \quad R \to 1^- \tag{12}$$

We note that this expression applies only for $f_s > 0$ and $d > 1$ (the case $d = 1$ is a limit case that will not be treated further in this article). Our goal is to construct rational approximations to Eq. (10) that will reproduce the series expansions to high order as well as yield the correct asymptotic behaviour as given by Eq. (12).

Infinite dimensions

It is interesting to note that Eq. (10) simplifies greatly as d becomes very large (all coefficients then approach unity):

$$\frac{f_s}{d} = \frac{R}{1-R^2} \quad \text{for} \quad d \to \infty \tag{13}$$

Curiously, this is precisely Warner's empiricial approximation [6]. It reduces to Eq. (9) in the harmonic limit (small R's), agrees with Eq. (12) when R is close to unity and d is large, and diverges for $R \to 1$ as expected. Warner's expression may therefore be regarded as a large-d approximation. Moreover, Eq. (13) also results from the simplest possible Pade approximant (see Eq. (14) below). This last observation would suggest that we should investigate higher order Pade approximants in order to construct more accurate approximations for finite dimensionalities. From Eqs. (8) – (10), (12) and (13), it is evident that the "natural variables" are in fact R, f_a/d and $1/d$.

When Eq. (13) is used for finite dimensionalities, as is often the case, the entropic force is overestimated by a factor that reaches a maximum value of

$$(f_{a,\text{Warner}} - f_{a,\text{exact}})/f_{a,\text{exact}} = 1/(d-1) \quad \text{at} \quad R = 1$$

as obtained from Eqs. (12) and (13). Again, we see that Warner's approximation is in fact a large-d approximation (its maximum error vanishes for $d \to \infty$), but it leads to an overestimation by as much as 100% for $d = 2$ and 50% for $d = 3$ (curves a and b in Fig. 1).

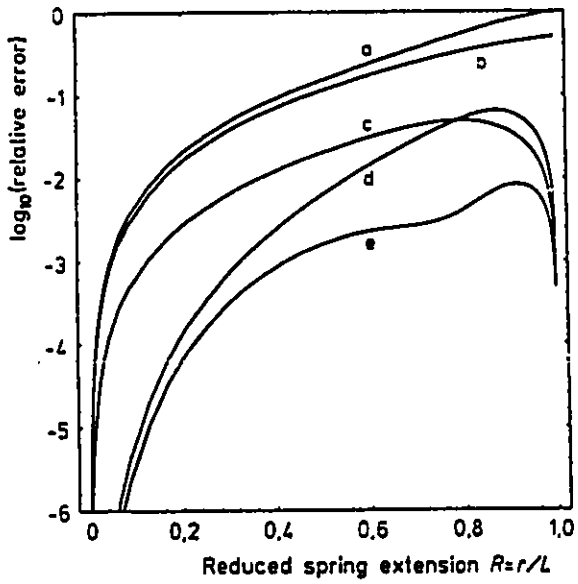

Fig. 1. Logarithm of the magnitude of the relative error (which is defined by $|1 - f_a(\text{approximation})/f_a(\text{exact})|$) made in evaluating the scaled entropic force $f_a(R)$ vs. (scaled) spring extension $R = r/L$ for various approximations. The top two curves use Warner's approximation, Eq. (13), for (a) $d = 2$ and (b) $d = 3$ dimensions. The next two curves use the modified Pade approximant ModPade (R, d, 1, 2; 3, 2), as given by Eq. (18), for (c) $d = 2$ and (d) $d = 3$ dimensions, respectively. The bottom curve (e) uses the modified Pade approximant ModPade (R, d, 3, 4; 7, 4), as given by Eq. (17), for $d = 3$. The modified Pade approximants are much more accurate than Eq. (13), especially for extensions larger than 50%. Note that the error vanishes at both limits of the interval

Although other approximation schemes can be used, Pade approximants[20,21] possess many advantages: they are easy to construct; they lead to the exact behaviour (including the slope) when the argument is close to zero; they can be evaluated easily and efficiently, as they are comprised of polynomials; and, they can be readily modified to exhibit the correct asymptotic behaviour, as we will now demonstrate.

Modified Pade approximants for $f_s(R)$

We will denote Pade (R, d, i, j) as being a Pade approximant where a ratio of polynomials of order i (for the numerator) and j (for the denominator) replaces the rhs of Eq. (10). For example, the simplest non-trivial approximant is

$$\frac{f_s}{d} \approx \text{Pade}(R, d, 1, 2) = \frac{R}{1 - \dfrac{R^2}{1 + 2/d}} \tag{14}$$

This expression provides a better approximation to the "exact" result given by Eq. (10) for R not too close to unity, and it also reduces to Eq. (13) for large d. However, unlike Eq. (13), it does not diverge for $R = 1$; instead, the maximum spring length is now increased to $R_{max} = (1 + 2/d)^{0.5}$. In fact, all Pade approximants show a similar displacement of the maximum spring extension. One can "correct" for this affliction by adding an extra term of the form $A \cdot R^k$, with $k \geq j$ (this is necessary to minimize the effect of this term on the precision of the resulting expression for small values of R) and

$$A = -\text{Denominator}[\text{Pade}(R = 1, d, i, j)] \tag{15}$$

to the denominator of the expression. This will ensure that the resulting expression for $f_s(R)$ diverges as $R \to 1$. Excellent results are obtained with the simple choice $k = j$, i.e., when we correct the last term of the denominator of the original approximant.

Finally, the resulting rational approximation does not exhibit the correct asymptotic behaviour for R close to unity. This can be remedied by adding a term $B \cdot R^m$, with $m \geq i$, to the numerator, where (Den and Num stand for Denominator and Numerator, respectively):

$$B = \frac{d - 1}{2d} \cdot \lim_{R \to 1} \left[\frac{\text{Den}[\text{Pade}(R, d, i, j)] + A \cdot R^k}{1 - R} - \text{Num}[\text{Pade}(R, d, i, j)] \right] \tag{16}$$

The exponent m can be chosen to minimize the error since B is not a function of m. We recommend using even integers for the (denominator) exponent k and odd integers for the (numerator) exponent m to preserve the parity properties of the original expression. We denote these modified Pade approximants as ModPade $(R, d, i, j; m, k)$.

An excellent alternative to Eq. (13) is thus given by the expression

$$\frac{f_e}{d} = \text{ModPade}(R, d, 3, 4; 7, 4) = R \cdot \left[\frac{1 + \dfrac{(1 - 12/d)R^2 + (14/d^2 - 24/d^3)R^6}{(1 + 6/d)(1 + 2/d)}}{1 - \dfrac{(18/d)R^2 + (1 - 10/d + 12/d^2)R^4}{(1 + 6/d)(1 + 2/d)}} \right] \quad (17)$$

This relation is considerably more accurate than Eq. (13), as can be seen readily from Fig. 1 (curve e). For $d = 3$, the maximum relative error is less than 0,85% (which is attained at $R = 0{,}92$) over the whole range of spring extensions, and it reduces to zero for both $R = 0$ and $R = 1$. In fact, one can construct expressions of any desired degree of accuracy by using larger orders $(i, j; m, k)$. Remarkably, all these approximations reduce to Eq. (13) for large values of d, an indication that this method of constructing approximate force laws retains all the salient features of the original expression.

In some instances, what is needed is an accurate approximation, to be used in the integrand of some expression, that will keep the integral analytical. One should then use an expression of the form ModPade$(R, d, i, j \leq 4; m = \text{odd}, k = 2 \text{ or } 4)$.

Sample applications

Numerical expressions

When using an expression like Eq. (17) in a numerical study, better results are obtained if it is re-written such as to minimize the number of multiplications and divisisons. However, simpler (although slightly less accurate) expressions can also be used. For example, the simplest and most efficient modified Pade approximant we can construct is ModPade$[R, d, 1, 2; 3, 2]$, which yields:

$$f_e(R) = \frac{dR - R^3}{1 - R^2} = R\frac{d - R^2}{1 - R^2} \quad (18)$$

The last expression contains only one square root (to get R from R^2), 2 products/divisions and 2 subtractions. It can thus be used whenever excellent accuracy is required, especially for large spring extensions. For $d = 2$ and $d = 3$, Eq. (18) gives a maximum relative error of 6,5% (at $R = 0{,}875$) and 4,9% (at $R = 0{,}800$), respectively (see curves c and d in Fig. 1).

For $d = 3$ dimensions, the more precise Eq. (17) can be rewritten as the continued division

$$f_e(R) = R \cdot \left[R^2 + R^2 + 12 + \cfrac{53}{R^2 - \dfrac{273}{53} + \dfrac{1\,760/2\,809}{R^2 - 45/53}} \right] \quad (19)$$

This expression contains only one square root (to get R from R^2), 3 products/divisions and 6 additions/subtractions, and shows a maximum error of less than 1%; this is indeed a numerically efficient and accurate force-law.

The distribution function and the mean equilibrium spring length

The mean-square equilibrium spring length may easily be computed provided one knows the distribution function for the end-to-end distance of the chain. The latter is a function of the spring force potential, which can be obtained using the modified Pade approximant and integrating $f(R)$ with respect to R. Using Eq. (18), we get:

$$\frac{U(R)}{k_B T} = \mathcal{N} \int_0^R dR' f_a(R') = \frac{N}{2}[R^2 + (1-d)\ln(1-R^2)] \tag{20}$$

The probability distribution function is therefore given by

$$p(R)_{[\text{Eq.(18)}]} = \frac{R^{d-1} e^{-\frac{U(R)}{k_B T}}}{\int_0^1 R^{d-1} e^{-\frac{U(R)}{k_B T}} dR} = C(N) R^{d-1} [1-R^2]^{N\cdot(d-1)/2} e^{-NR^2/2} \tag{21}$$

where $C(N)$ is a numerical constant. When $R \ll 1$, this expression reduces to the Gaussian distribution function $p(R) = C' R^{d-1} \exp[-dNR^2/2]$, as it should. Interestingly, this FENE distribution function is a modified Gaussian distribution which is defined only for $R \in [0, 1]$ and provides zero probability for $R = 1$. Higher order modified Pade approximants lead to similar distribution functions; e. g., in $d = 3$, Eq. (17) leads to

$$p(R)_{[\text{Eq.(17)};\, d=3]} \sim R^2 \cdot \left[\frac{1-R^2}{\left(1-\frac{1}{5}R^2\right)^{5/2}}\right]^N e^{-N\cdot(6R^2+R^4/2)} \tag{22}$$

which exhibits the same general properties as Eq. (21) but is much more precise.

The mean-square end-to-end distance of the chain can be calculated from the distribution function using the following dimensionless integral:

$$\langle R^{2j}\rangle = \int_0^1 dR\, R^{2j} p(R) \tag{23}$$

In general, this has to be evaluated numerically. The distribution function given by Eq. (21), however, leads to an analytical solution, namely

$$\langle R^{2j}\rangle_{[\text{Eq.(18)}]} = \frac{\Gamma\left[\frac{2+d-N+Nd}{2}\right]\Gamma\left[\frac{d}{2}+j\right]}{\Gamma\left[\frac{2+2j+d-N+Nd}{2}\right]\Gamma\left[\frac{d}{2}\right]} \cdot \frac{M\left(j+\frac{d}{2}; \frac{2+2j+d-N+Nd}{2}; \frac{-N}{2}\right)}{M\left(\frac{d}{2}; \frac{2+d-N+Nd}{2}; \frac{-N}{2}\right)} \tag{24}$$

where $M(a; b; z) \equiv {}_1F_1(a; b; z)$ is Kummer's confluent hypergeometric function. The harmonic (Gaussian) approximation gives (the integral then extends to infinity)

$$\langle R^{2j}\rangle_{\text{harmonic}} = \left(\frac{2}{Nd}\right)^{j} \frac{\Gamma\left[j + \frac{d}{2}\right]}{\Gamma\left[\frac{d}{2}\right]} \tag{25}$$

while Warner's approximation yields $p_{\text{Warner}}(R) = C(N)R^{d-1}(1 - R^2)^{Nd/2}$ and

$$\langle R^{2j}\rangle_{\text{Warner}} = \frac{\Gamma\left[j + \frac{d}{2}\right]}{\Gamma\left[\frac{d}{2}\right]} \cdot \frac{\Gamma\left[\frac{2 + d + Nd}{2}\right]}{\Gamma\left[\frac{2 + 2j + d + Nd}{2}\right]} \tag{26}$$

All these approximations reduce to the harmonic approximation for $N \gg 1$ because the anharmonic terms are then negligible. However, our modified Pade approximants converge more quickly towards the harmonic limit; for example, for $d = 3$ and $N = 10$, $\langle R^2\rangle_{\text{harmonic}} = 1/10$, while $\langle R^2\rangle_{[\text{Eq.(18)}]} = 1/11{,}19$ and $\langle R^2\rangle_{\text{Warner}} = 1/11{,}67$.

For $d = 2$ and $N = 5$, $\langle R^2\rangle_{\text{harmonic}} = 1/5 = 0{,}200$, Eq. (24) gives $\langle R^2\rangle_{[\text{Eq.(18)}]} = 0{,}159$, while $\langle R^2\rangle_{\text{Warner}} = 1/7 = 0{,}143$; these values must be compared with the "exact" result $\langle R^2\rangle_{\text{exact}} = 0{,}161$ (obtained from numerical integration using Eq. (6) and the procedure described in Eqs. (20)–(22)). The accuracy achieved from Eq. (24), i.e., −1,25% error, is remarkable considering the simplicity of our approximations and the ease of calculation. This is to be contrasted with the −11,3% error for Warner's approximation. As expected, anharmonic springs are substantially stiffer than are harmonic springs, and Warner springs are far too stiff. Equation (21) also allows for the calculation of other chain properties.

Conclusion

In this short paper, we have described a systematic way to construct a series of approximations of the equations governing the stretching of anharmonic, finitely extensible polymers in arbitrary dimension $d \geq 2$ in the stress ensemble. The method is based on the use of Pade approximants to replace the exact expression, which is the inverse of the ratio of two modified Bessel functions, for small values of its argument. Such approximants, however, do not exhibit the correct asymptotic behaviour characterizing a chain of maximum contour length. In order to extend the range (or accuracy) of these approximants to large values of the argument (the spring extension), we proposed to modify them with simple terms which, while having no inordinate effect on the accuracy for small arguments, make them reproduce to the correct asymptotic behaviour. Our results demonstrate marked improvement over the Warner approximation which, in effect, turns out to be but a limiting case, accurate only for large dimensionalities d.

Our approximations are analytically simple as well as numerically efficient because they are merely comprised of polynomials. In principle, our method permits the construction of approximations of any required degree of accuracy. With the correct choice of polynomial orders, the corresponding distribution functions and mean square end-to-end distances can be obtained analytically. Therefore, we believe that our approximations provide interesting alternatives to Warner's approximation for either numerical or analytical studies.

Other functions can also be represented by modified Pade approximants if their asymptotic behaviour is known. At this time, we are working on the entropic force in the strain ensemble where the exact solution, known as the Treolar result[22], is very difficult to use in practice. A recent article by Glatting et al. offers a new approach to this problem[23].

The sample calculations presented in this paper were performed using Mathematica, a system for symbolic and numerical applications. Our Mathematica commands are available upon request.

This work was supported by a *Research Grant from the Natural Sciences and Engineering Research Council (NSERC) of Canada* to GWS, and by a *NSERC Undergraduate Research Scholarship* to SJH.

1) M. Doi, S. F. Edwards, *"The Theory of Polymer Dynamics"*, Oxford, NY 1986
2) H. R. Reese, B. H. Zimm, *J. Chem. Phys.* 92, 2650 (1990)
3) J. W. Rudisill, P. T. Cummings, *Rheol. Acta* 30, 33 (1991)
4) B. Z. Dlugogorski, M. Grmela, P. J. Carreau, *J. Non-Newtonian Fluid Mech.* 48, 303 (1993)
5) J. M. Kobe, J. M. Wiest, *J. Rheol.* 37, 947 (1993)
6) R. B. Bird, H. C. Öttinger, *Ann. Rev. Phys. Chem.* 43, 371 (1992)
7) K. Kremer, G. S. Grest, *J. Chem. Phys.* 92, 5057 (1990)
8) For a review of the field, see M. Burmeister, L. Ulanovsky, Eds., *"Methods in Molecular Biology"*, vol. 12, Totowa, N.J. 1992
9) E. O. Shaffer II, M. Olvera de la Cruz, *Macromolecules* 22, 1351 (1989)
10) S. B. Smith, C. Heller, C. Bustamante, *Biochemistry* 30, 5264 (1991)
11) J. Noolandi, J. Rousseau, G. W. Slater, C. Turmel, M. Lalande, *Phys. Rev. Lett.* 58, 2428 (1988)
12) H. A. Lim, G. W. Slater, J. Noolandi, *J. Chem. Phys.* 92, 709 (1990)
13) S. B. Smith, L. Finzi, C. Bustamante, *Science* (Washington, D.C., 1883-) 258, 1122 (1992)
14) A.-D. Défontaines, J.-L. Viovy, *Electrophoresis* 14, 8 (1993)
15) G. I. Nixon, G. W. Slater, to be submitted
16) H. R. Warner, Jr., *Ind. Eng. Chem. Fundam.* 11, 379 (1972)
17) J. H. Weiner, *"Statistical Mechanics of Elasticity"*, Wiley, NY 1983, p. 246
18) I. S. Gradshteyn, I. M. Ryzhik, *"Table of Integrals, Series and Products"*, Academic, NY 1980
19) M. Abramowitz, I. A. Stegun, *"Handbook of Mathematical Functions"*, Dover, NY 1965
20) R. L. Burden, J. D. Faires, A. C. Reynolds, *"Numerical Analysis"*, 2nd edition, Prindle, Weber & Schmidt, Boston 1981
21) W. H. Press, S. A. Teukolsky, *Comput. Phys.* 6, 82 (1992)
22) P. J. Flory, *"Statistical Mechanics of Polymer Chains"*, John Wiley & Sons, New York 1989
23) G. Glatting, R. G. Winkler, P. Reineker, *Macromolecules* 26, 6085 (1993)

References

Abramowitz, M.; and Stegun, I. A. *Handbook of Mathematical Functions*, Applied Mathematics Series, Volume 55, Washingon: National Bureau of Standards (1964); reprinted by Dover Publications, New York (1968).

Allen, M. P.; and Tildesley, D. J. *Computer Simulation of Liquids*, Oxford University Press, Oxford (1987).

Binder, K.; and Heermann, D.W. *Monte Carlo Simulation in Statistical Physics - An Introduction* (Second Corrected Edition), Springer Series in Solid-State Science 80, Springer-Verlag, Berlin (1992).

Burlatsky, S.; and Deutch, J. *Influence of Solid Friction on Polymer Relaxation in Gel Electrophoresis*, Science **260**, 1782-1784 (1993).

Ceperley, D.; Kalos, M. H.; and Lebowitz, J. L. *Computer Simulation of the Static and Dynamic Properties of a Polymer Chain*, Macromolecules, 14, 1472-1479 (1981).

de Gennes, P. G. *Scaling Concepts in Polymer Physics*, Cornell University Press, Ithaca (1979).

de Gennes, P. G. Introduction to Polymer Dynamics (Lezioni Lincee), Cambridge University Press, Cambridge (1990).

des Cloizeaux, J.; and Jannink, G. *Les Polymères en Solutions: leur Modélisation et leur Structure*, Les Éditions de Physique, Les Ulis Cedex, France (1987).

Deutsch, J. M.; and Madden, T. L. *Theoretical studies of DNA during gel electrophoresis*, J. Chem. Phys. **90** (4), 15 February 1989.

Deutsch, J. M.; and Reger, J. D. *Simulation of highly stretched chains using long-range Monte Carlo*, J. Chem. Phys. **95** (3), 1 August 1991.

Doi, M. and Edward, S.K. *The Theory of Polymer Dynamics*, International Series of Monographs on Physics • 73 , Oxford University Press, Oxford (1986).

Duke, T. A. Monte Carlo reptation model of gel electrophoresis: Steady state behavior, J. Chem. Phys. **93**, 9049-9061 (1990).

Ermak, D. L. and McCammon, J. A. *Brownian dynamics with hydrodynamic interactions*, J. Chem. Phys. **69**, 1352-1360 (1978).

Flory, P. J. *Statistical Mechanics of Chain Molecules*, Interscience, New York (1969).

Gradshteyn, I. S.; and Ryzhik, I. M., *Table of Integrals, Series, and Products*, Corrected and Enlarged Edition, Academic Press, San Diego (1980).

Gurriieri, S.; Rizzarelli, E.; Beach, D.; and Bustamante, C. *Imaging of Kinked Configurations of DNA Molecules Undergoing Orthogonal Field Alternating Gel Electrophoresis by Fluorescence Migration*, Biochemistry **29**, 3396-3401 (1990).

Harrington, M. G.; Lee, K. H.; Bailey, J. E.; and Hood, L. E. *Sponge-like electrophoresis media: Mechanically strong materials compatible with organic solvents, polymer solutions and two-dimensional electrophoresis*, Electrophoresis **15**, 187-194 (1994).

Heermann, D. W., *Computer Simulation Methods in Theoretical Physics (Second Edition)*, Springer-Verlag, Berlin (1990).

Hoagland, D. A. and Muthukumar, M. *Evidence for Entropic Barrier Transport of Linear, Star, and Ring Macromolecules in Electrophoresis Gels*, Macromolecules **25**, 6696-6698 (1992).

Johnson, J. A. Y. *Dynamics of a Flexible Polymer Chain in Steady Shear Flow: The Rouse Model*, Macromolecules **20**, 103-116 (1987). Original reference is Kramers, H. A. Physics 7(4), 284 (1940).

Knuth, D. E. *The Art of Computer Programming*, Second Edition, Volume 2 / *Seminumerical Algorithms*, Addison-Wesley, Reading, Massachusetts (1981).

Kranbuehl, D. E.; Eichinger, D.; and Verdier, P. H. *Simulation Studies of Excluded Volume Effects on Polymer Chain Dynamics in Several Nonlattice Models*, Macromolecules **24**, 2419-2427 (1991).

Luckey, J. A. and Smith, L. M. *Optimization of Electric Field Strength DNA Sequencing in Capillary Gel Electrophoresis*, Anal. Chem. **65**, 2841-2850 (1993).

Lumpkin, O. J.; Dejardin, P.; and Zimm, B. H. *Theory of gel electrophoresis of DNA*, Biopolymers **24**, 1573-1593 (1985).

Mayer, P.; Slater, G. W.; and Drouin, G. *Exact behaviour of single-stranded DNA electrophoretic mobilities in polyacrylamide gels*, Applied and Theoretical Electrophoresis **3**, 147-155 (1993).

Munk, P. *Introduction to Macromolecular Science*, Wiley - Interscience, New York (1989).

Muthukumar, M. *Entropic barrier model for polymer diffusion in concentrated polymer solutions and random media*, Journal of Non-Crystalline Solids **131-133**, 654-666 (1991).

Nixon, G. I. and Slater, G. W. *DNA Electrophoretic Collisions with Single Obstacles*, Phys. Rev. E., in print (1994).

Olvera de la Cruz, M.; Deutch, J. M.; and Edward, S. F. *Electrophoresis in strong fields*, Phys. Rev. A **33**, 2047-2055 (1986).

Rudnick, J. and Gaspari, G. *The Shapes of Random Walks*, Science (USA) **237**, 384-389 (24 July 1987).

Schwartz, D. C.; and Koval, M. *Conformational dynamics of individual DNA molecules during gel electrophoresis*, Nature **338**, 520-522 (1989).

Shaffer II, E. O.; and Olvera de la Cruz, Monica *Dynamics of Gel Electrophoresis*, Macromolecules **22**, 1351-1355 (1989).

Slater, G. W.; and Drouin, G. *Le Projet du génome Humain en quête d'Innovations Technologiques*, Interface, 15-22, (Mai • Juin 1991).

Slater, G. W.; Hubert, S. J.; and Nixon, G. I. *Construction of approximate entropic forces for finitely extensible nonlinear elastic (FENE) polymers*, Macromol. Theory Simul. **3**, 695-704 (1994).

Slater, G. W.; and Noolandi, J. *New Biased-Reptation Model for Charged Polymers*, Phys. Rev. Lett. **55**, 1579-1582 (1985).

Volkmuth, W. D.; Duke, T.; Wu, M. C.; Austin, R. H.; and Szabo, A. *DNA Electrodiffusion in a 2D Array of Posts*, Phys. Rev. Lett. **72**, 2117-2120 (1994). See also Volkmuth, W.D., Austin, R. H. Nature **358**, 600-602 (1992).